Channel Response Assessment for the Upper Blackfoot

Grant Agreement No. RRG-08-1296

by

Denine Schmitz
Land Resources and Environmental Science
Montana State University

Jessica Mason
Department of Civil Engineering
Montana State University

Matt Blank
Western Transportation Institute and Department of Civil Engineering
Montana State University

Joel Cahoon
Department of Civil Engineering
Montana State University

A report prepared for the

Montana Department of Natural Resources and Conservation

December 1, 2010

DISCLAIMER

ACKNOWLEDGEMENTS

The authors would like to thank the Montana Department of Natural Resources and Conservation for providing a large portion of the funding for this project and for supporting this work. The Helena National Forest staff provided invaluable tours, data, and history of the site. Montana Water Center provided the initial financial support for the pilot project from which this work stemmed. Montana Department of Environmental Quality (DEQ) made available data and communication documents that made this project possible. The Clark Fork Coalition provided background information and contact lists that proved to be invaluable to understanding the complex nature of natural and political environments, and wrote a letter of support to secure funding. Special thanks to Selby's of Bozeman, Montana, for providing the GPS unit and training; Seth Mason for assistance with field work; David Bowers of the Montana DEQ; and Senator David Lewis (R-SD 42) for providing legislative guidance and writing a letter of support for securing funding.

TABLE OF CONTENTS

LIST OF TABLES

LIST OF FIGURES

EXECUTIVE SUMMARY

This report presents research activities and results for a study performed on Mike Horse Dam (MHD) and nearby streams and watersheds in Western Montana (see Figure 1). Streams included in the study were Mike Horse Creek, Beartrap Creek, Anaconda Creek, and the Upper Blackfoot River. The study began with field data collection in 2007. Data collection continued through 2008. Data analyses and report preparation were completed in 2009 and 2010.

The purpose of the research was to investigate the response of vegetation, stream channels, and watershed characteristics to pre-dam mining activities, dam construction (erected in 1941), dam operation, dam failure flood (breach) event in 1975, and the post-breach period. Reclamation activities, largely focusing on removal of contaminated soils and sediments, are currently underway at the dam and in adversely affected stream channels and are anticipated to continue for at least the next decade.

MHD is located 24 kilometers east of Lincoln, Montana, in the Upper Blackfoot Mining Complex (also known as the Heddleston Mining District). Mike Horse Dam creates an impoundment on Beartrap Creek, a headwater tributary to the Upper Blackfoot River. This portion of the Upper Blackfoot River watershed is heavily forested, mountainous terrain 1,600–2,300 meters above sea level. Average annual precipitation is roughly 46 centimeters, most of which falls as snow. The Upper Blackfoot River is a water source to residents in the greater Lincoln area and the watershed is a resource to anglers, hunters, and other recreationists.

We estimated the breach flood event using three independent approaches—1) modeled flow using paleohydrology and step-backwater techniques, 2) empirically derived regional estimates of peak annual discharge, and 3) hydrograph records. Using these techniques, we estimated a flood flow of 11.5 m^3/s for Mike Horse Creek and Beartrap Creek, 15.2 m^3/s for Anaconda Creek, and 26.7 m^3/s for the Upper Blackfoot downstream of the confluence of Beartrap and Anaconda creeks. These estimates are very similar to the 100-year flow estimated using regional regression equations.

We acquired aerial photos of the study area for 1938, 1964, 1978, 1995, and 2005 to analyze changes in channel form and vegetation. We georeferenced and mosaiced the 1938, 1964 and 1978 photos using the 1995 images as the target layers. We identified floodplain extent using the modeled flood path, changes in riparian vegetation extent, and changes in upland vegetation density and horizontal structure. We limited our interpretation to canopy vegetation because it was visible on all aerial photos and indicative of major changes to the riparian landscape. Watershed characteristics were developed for each site using terrain analyses of 10 m digital elevation models (DEMs).

We stratified the vegetation data into three reaches. The Anaconda reach extended from the upstream-most transect on Anaconda Creek to the Anaconda–Beartrap confluence. The Beartrap reach extended from the MHD to the Anaconda–Beartrap confluence. The Upper Blackfoot reach extended from the Anaconda–Beartrap confluence to the downstream-most transect. We analyzed the point observation data in a regression environment to detect relationships between riparian canopy type distribution and watershed characteristics related to hillslope hydrology and network organization. We used Generalized Linear Regression because it is nonparametric, suitable for binomial data (presence/absence), accommodates categorical data, and has adequate goodness of fit measures.

We saw the largest change in canopy distribution on Beartrap and Upper Blackfoot in 1978, three years after the dam failure flood. Our data from 1995 and 2005, in addition to ground surveys in 2007, indicate little recovery has taken place in the 32 years since the flood. However, we provided evidence of active relationships to watershed-scale processes in the Beartrap and Upper Blackfoot reaches. The response of the Beartrap and Upper Blackfoot reaches to dam construction and mining-related activities indicated increased bare ground and fragmentation of riparian vegetation following the lifting of MHD in 1941 and its failure in 1975. The response of the Beartrap and Upper Blackfoot reaches to the dam failure flood was catastrophic. Similar responses were observed following the Pattengail Dam failure flood in 1927. In Pattengail Creek, 90 years later, riparian vegetation has not returned due to marked channel downcutting and coarse substrate resulting from the breach. The Mike Horse study area will likely experience a similar fate without ongoing active restoration. It should be pointed out that active removal of contaminated sediments and restoration of natural channel and floodplain processes is currently being implemented.

A companion study, performed by Jess Mason, was also completed during this project. This study modeled the effect of discharge events, including the 10-, 25- and 100-year recurrence intervals, to assess the potential for sediment transport from the mine-impacted wetland in the Upper Blackfoot Mining Complex. There has been substantial work to assess and remediate the impact of the Upper Blackfoot Mining Complex on aquatic resources by Helena National Forest, Montana Department of Environmental Quality, and the mining company, ASARCO. Until recently, however, the wetland complex has largely been omitted from environmental assessments. This companion study is included as Appendix A.

1. INTRODUCTION

This report presents research activities and results for a study performed on MHD and nearby streams and watersheds in Western Montana (see Figure 1). Streams included in the study were Mike Horse Creek, Beartrap Creek, Anaconda Creek, and the Upper Blackfoot River. The study began with field data collection in 2007. Data collection continued through 2008. Data analyses and report preparation were completed in 2009 and early 2010. The purpose of the research was to investigate the response of vegetation, stream channels, and watershed characteristics to pre-dam mining activities, dam construction (erected in 1941), dam operation, dam failure flood (breach) event in 1975, and the post-breach period. Reclamation activities, largely focusing on removal of contaminated soils and sediments, are currently underway at the dam and in adversely affected stream channels and are anticipated to continue for at least the next decade.

The report describes the study site and its characteristics. Background information including a summary of relevant literature is discussed. The next section describes research methods, followed by a presentation of results and a discussion. The last section of the report provides a summary of the research with a focus on relevant results.

A companion study, performed by Jess Mason, was also completed during this project. The study modeled the effect of discharge events, including the 10-, 25- and 100-year recurrence intervals, to assess the potential for sediment transport from the mine-impacted wetland in the Upper Blackfoot Mining Complex (UBMC). There has been substantial work to assess and remediate the impact of the UBMC on aquatic resources by Helena National Forest (HNF), Montana Department of Environmental Quality (MTDEQ), and the mining company, ASARCO. Until recently, however, the wetland complex has largely been omitted from environmental assessments. This companion study is included as Appendix A.

1.1. Site Information

MHD is located 24 kilometers east of Lincoln, Montana, in the UBMC (also known as the Heddleston Mining District). MHD creates an impoundment on Beartrap Creek, a headwater tributary to the Upper Blackfoot River. This portion of the Upper Blackfoot River watershed is 1,600–2,300 meters above sea level, and is located in heavily forested, mountainous terrain. Average annual precipitation is roughly 46 centimeters, most of which falls as snow. The Upper Blackfoot River is a water source to residents in the greater Lincoln area and the watershed is a resource to anglers, hunters, and other recreationists (Hydrometrics Inc. and Blackfoot Challenge 2003).

The ecology of the region is typical of Montana's Rocky Mountains. Upland vegetation is primarily lodgepole (*Pinus contorta*), Engelmann spruce (*Picea engelmannii*), Douglas fir (*Pseudotsuga menziesii*), and subalpine fir (*Aibes lasiocarpa*), while grasslands dominate valley bottoms. Riparian vegetation is composed of quaking aspen (*Populus tremuloides*), Bog birch (*Betula glandulosa*), thin leaf alder (*Alnus incana*), and Drummond's willow (*Salix drummondiana*) (Vandeberg 2005).

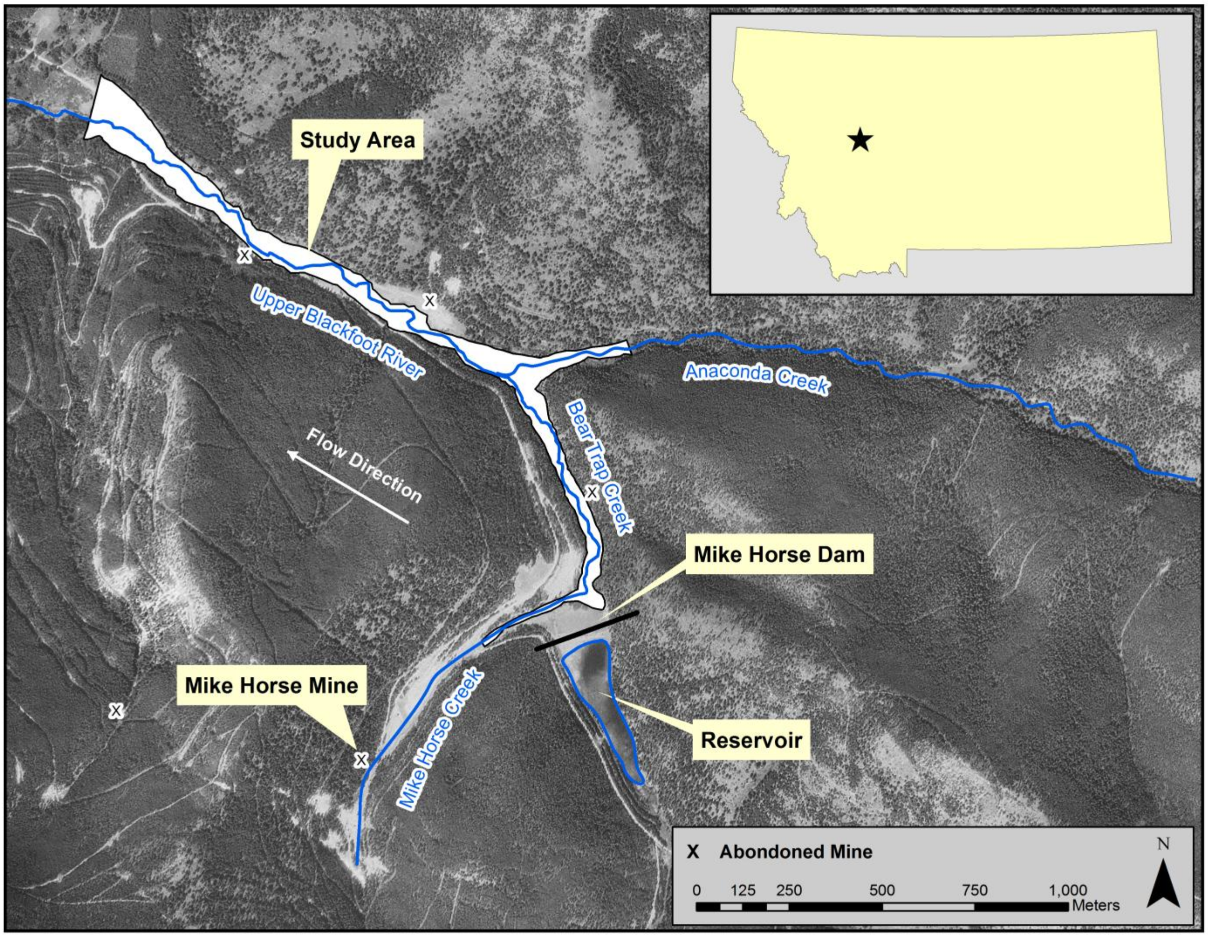

Figure 1: Site Map of Study Area.

Portions of the watershed occur in federally designated grizzly bear and gray wolf recovery areas. Bald eagles, peregrine falcons, and whooping cranes may also be seen in the area (Hydrometrics Inc. 2005). The Blackfoot watershed supports 12 native fish species (Montana Fish Wildlife and Parks 2006). Bull trout (*Salvelinus confluentus*) are listed as threatened under the Endangered Species Act and westslope cutthroat trout (*Oncorhynchus clarki lewisii*) are listed as a species of special concern within the state of Montana. The study area is 16 kilometers upstream of Landers Fork, a designated “core area” for bull trout (US Fish and Wildlife Service 2002).

Upland soils are composed of Typic Cryoboralfs and Typic Cryoboralfs-Typic Cryochrepts Complexes with 40% to 80% angular rocks. Clay accumulations are common in subsoils. Soil textures are variable, and mostly range from silty loams to extremely gravelly, cobbly sandy loams (Hydrometrics Inc. 2005).

1.2. History of Mining and Dam Breach

The MHD was formed in two phases. First, mining activities in the 1940s deposited lead, silver, and zinc mine tailings from Mike Horse Mine across Beartrap Creek on United States Forest Service (USFS) land. In 1975, a rain on snow event caused flow to overtop and breach MHD. Contaminated sediment from the dam and impoundment were deposited on and along the Beartrap Creek and Upper Blackfoot River floodplains. This event created a “moonscape” devoid of the once lush riparian vegetation. During the second phase of construction, an earthfill dam with a pipe spillway was constructed across the eroded opening in 1975 and raised in 1980. A recent evaluation of the dam concluded that the structure is unstable due to an inadequate spillway, detectible seepage flow, and erosion from piping inside the structure (US Forest Service 2005). USFS began stream restoration in late 2007, and is currently leading a cleanup effort that will partially or completely remove MHD (US Forest Service 2006).

The study area is part of a Comprehensive Environmental Cleanup and Responsibility Act (CECRA) facility. However, CECRA requirements do not address restoration. In 2002, USFS entered into an agreement with ASARCO (the current patent owner) to “control and contain” contaminants that threaten human and environmental health on public lands as they relate to the MHD and the tailings impoundment. This goal will require restoration of several stream reaches and monitoring long-term impacts along the entire segment.

1.3. Background

The Upper Blackfoot watershed has experienced three documented changes in flow regime—natural flow regime, dam construction, and dam breach. A fourth flow regime change, dam hazard reduction, began in 2007. Common understanding in river ecology and geomorphology holds that channel and floodplain landforms, riparian vegetation, and aquatic habitats are dynamic in space and time. The Blackfoot River watershed plans used resources dating from 1979 (after the breach) to characterize the watershed and design restoration of active channels. Vandeberg (Vandeberg 2005) mapped bankfull channel changes downstream of MHD from 1963 (before breach), 1979, and 1995 aerial photos. Ecological response to flow regime changes extends beyond the bankfull channel, and often beyond visible floodplains. Further, these studies have delineated channels using the morphology-based Rosgen stream classification scheme (Juracek and Fitzpatrick 2003). To date, little assessment of process-based channel and floodplain response has been made. And, ecological response to dam construction in 1941 remains undescribed. Combined with these studies, the long-term ecologic and geomorphic responses to changes in flow regime can be explained and will likely aid future dam hazard reduction and restoration activities.

There have been substantial studies on the water quality, sediment quality and dam stability in the streams directly adjacent to Mike Horse Dam. However, the temporal and spatial aspects of these studies are limited. Streams are a product of local and watershed-scale processes operating on short and long time periods. A gap remains in understanding the dynamic nature of the impacted segment, which can be filled by assessing historical changes in vegetation and the watershed structure. Restorative action on the MHD began in late summer 2007. Gathering channel response potential information prior to decommissioning Mike Horse Dam will maximize the assessment of historic ecological response and potentially guide restoration strategies.

1.3.1. Restoration Potential

The restorative potential of dam removal on ecosystem function depends on the reversibility of the ecological effects of the dam. The initial effect of dam removal is the reestablishment of the natural flow regime, sediment dynamics, and longitudinal connectivity between upstream and downstream reaches (Bednarek, 2001). In a restored natural flow regime, vegetation recruitment, species diversity, and successional processes within riparian areas will increase with time. Restored sediment dynamics can increase channel and floodplain development, water quality and nutrient cycling, all of which ecologists can detect in riparian plant communities (Shafroth et al. 2003) and biogeochemistry (Stanley and Doyle, 2002). Thus, by removing a dam, managers can restore the vertical, lateral, and longitudinal gradients that drive ecological processes along a stream.

The ranges of channel and floodplain environmental gradients, as they affect riparian vegetation, are wider under natural flow regimes than they are under regulated flow regimes. Vertical gradients affect plant composition directly through changes in water table elevations (Stromberg et al., 1996), but indirectly through changes in water depth during floods (Bendix, 1994). Lateral gradients incorporate several environmental conditions such as soil moisture and other properties (Nilsson, 1987), depth to water table (Stromberg et al., 1996), flow hydraulics (Simon and Rinaldi, 2006), and floodplain and valley geomorphology (Piegay et al., 2000; Steiger and Gurnell, 2003). Along longitudinal gradients, flow hydraulics vary with valley and reach geomorphology (Grant and Swanson, 1995) and, therefore, influence plant community composition.

Additionally, when restorationists restore natural sediment dynamics by removing a dam there will be short-term changes to sediment dynamics. The effect of releasing sediment stored in reservoirs is channel incision; adding sediment to sediment-starved downstream channels and floodplains results in burial of aquatic species habitats. The aquatic and riparian communities will be negatively impacted by the abrupt change in flow and sediment dynamics. However, most sediment responses to dam removals and failures are short-term and on the order of days or weeks to a few years (Winter, 1990; Department of Urban and Regional Planning [DURP], 1996), and vary with discharge (Pizzuto, 1994). By the same token, many aquatic and riparian species are adapted to, and at times require, sediment pulses (Junk et al., 1986). Over a short time, fish spawning habitat, macroinvertebrate habitat, and water quality will likely improve (Iversen et al., 1993; Bushaw-Newton et al., 2002; Stanley et al., 2007). In addition to these benefits, by removing dams we run the risk of permanently losing species that have adapted to lentic, cold water, and low sediment environments (Catalano et al., 2001). Importantly, in order to realize the restoration potential of dam removal on a system, managers need to document the ecological functions and traits lost due to the dam and its operations as well as the ability of the system to respond to the removal, as intended.

1.3.2. Sediment Management

The sediment management method used in dam removal has great influence over the short- and long-term geomorphic, chemical and ecological effects (Bednarek, 2001; Pizzuto, 2002; Burroughs, 2007). Sediment in the empty reservoir can be removed naturally, mechanically, or stabilized in place. Natural sediment removal allows the natural processes of erosion, deposition, floodplain development and channel evolution to distribute reservoir sediments with subsequent flood events. These processes occur as a result of base level lowering (Schumm et al., 1984) and depend on dam, reservoir, river, substrate, and watershed characteristics. Mechanical sediment removal entails dredging the reservoir sediments (once drained) and using them elsewhere, such as in road bases, filling in open pits and construction foundation materials (Shuman, 1995). Stabilizing sediments occurs through capping with concrete (or equivalent) or vegetation. Both mechanical removal and stabilization reduce short-term effects on upstream and downstream reaches and inhibit invasive plant establishment on newly eroded or deposited surfaces (Winter, 1990).

1.3.3. Dam Removal Versus Dam Failure

Engineered removals are done at base flow (including breach to bed level, partial removal, or full removal), and the structure is either completely or partially dismantled down to the original channel bed level and transported offsite. In the Lake Mills drawdown experiment (Glines Canyon Dam, Port Angeles, WA), a notched method allowed controlled drainage of the large reservoir (Grant, 2004). If natural sediment removal is chosen, a small to moderate amount of the reservoir sediment is transported with drainage (Winter, 1990; DURP, 1996). Then, during subsequent floods, varying amounts of sediment are removed depending on flood size and sediment composition (Winter, 1990; DURP; 1996; Doyle et al., 2003b). Short-term data show that channel adjustments will likely mimic base level lowering (Shumm et al., 1984; Doyle et al., 2003b) and vary with dam, river, and watershed attributes. Additionally, vegetation responses may tend toward weedy species due to the timing of the disturbance (Dukes and Mooney, 1999). These weedy species may have a founder’s effect and inhibit native species establishment (Middleton, 1999).

Conversely, dam failures (natural or human dams) generally occur at peak flow. The large flows have the capacity to transport more volume and larger-sized sediments. While some failures are explosive, resulting in flash floods, many failures occur slowly due to piping, overtopping, or partial rupture, causing slow drainage over a period of days to weeks (Costa and Schuster, 1988; Cenderelli and Wohl, 2001, 2003; Butler and Malanson, 2005). Differences in flood peaks from natural dam failures are controlled by dam characteristics and failure mechanisms (Costa and Schuster, 1988) similar to human dam removals. Ecologically, draining reservoirs (natural or human) at peak flow has the highest potential to benefit upstream and downstream riparian and aquatic plant communities. In the western United States, cottonwood, alder, and willow species release seed at about the time of peak flow, increasing their probability of landing on moist, wet sediment, germinating, and surviving to reproductive age (Mahoney and Rood, 1998). Further, some wetland species have adapted to reproducing during anaerobic conditions at specific times during the growing season (Middleton, 1999; Mitsch and Gosselink, 2000). Also, some aquatic communities have adapted to sediment pulses during peak flows (Catalano et al., 2001), and once established, these natives have a higher chance of resisting non-native invasions. Thus, an analysis of natural flow regime of a potential dam removal setting and the adaptations of native species to that regime can inform restoration goals.

1.3.4. Paleohydrology

Paleohydrology is the study of past or ancient floods where paleoflood stage indicators are used to estimate peak flows (Baker, 1987). Where dams have failed or have been removed with natural sediment removal, subsequent flood events transport sediment downstream, creating fluvial deposits of sediment and wood, as well as scour zones and vegetation scars on the floodplain. While paleohydrology is generally applied to Holocene floods (100 – 10,000 years), Jarrett (1990) estimated the peak discharge from the 1976 Big Thompson flood near Loveland, Colorado using a combination of paleohydrology and regional flood frequency estimates. Wohl (1995) applied these techniques in ungaged streams in Nepal where hydrologic data are sparse or untraceable. We can use this technique to estimate peak flows and their paths following dam removal. In addition, where we need to understand the ecological responsiveness of a stream system prior to setting restoration goals, we can apply paleohydrology to estimate peak flows and assess the ecological response.

2. OBJECTIVES

Floodplain ecosystem function up and downstream from the MHD is the product of centuries of natural variation in hydrology followed by decades of human changes in flow regime. Because recorded history extends over a century for the Mike Horse Mine area, there is an opportunity to assess floodplain topographic and riparian vegetation responses to past changes in flow regime. Through this assessment, changes in floodplain topography and riparian vegetation distribution may be attributed to specific events through an investigation of historical aerial photos and relicts of past floods. This information can be used to characterize the response potential of each reach in the floodplain area. To achieve the long-term goal of a fully functioning riparian system in the Upper Blackfoot watershed, an assessment of past ecological response to the Mike Horse Dam and the 1975 breach event was performed. The overarching goal of the project was to assess the ecological response potential of floodplains associated with MHD.

Objective 1 – Determine the channel response potential of different stream reaches.

Objective 2 – Estimate the peak flow caused by the 1975 dam breach event.

Objective 3 – Determine the vegetative response of riparian communities along different stream reaches.

Objective 4 – Predict areas of high and low risk to impacts of dam hazard reduction for use in a monitoring program.

3. METHODOLOGY

Several methods were used to achieve the objectives of this study. The first part of this section describes the hydrologic characterization, followed by a description of the methods used for aerial photo interpretations. The method section ends with a description of watershed characteristics and the vegetation study.

3.1. Hydrologic Characterization

We estimated the breach flood event using three independent approaches: 1) modeled flow using paleohydrology and step-backwater techniques; 2) empirically derived regional estimates of peak annual discharge (Parrett and Johnson 2004); and 3) hydrograph records.

3.1.1. Modeled Flow Using Paleohydrology

We estimated peak discharge by combining paleoflood hydrologic techniques with a step-backwater model (Cinderelli and Wohl 2001). Flood modeling was done using the Hydrologic Engineering Center River Analysis System (HEC-RAS) version 4.0. Several reaches were used to build the hydraulic model. Mike Horse Creek and Beartrap Creek were modeled as Upper Blackfoot River Reach 1. Anaconda Creek was modeled as Anaconda Reach 1, and the Upper Blackfoot River downstream of the confluence of Beartrap Creek and Anaconda Creek was modeled as Upper Blackfoot River Reach 2. Table 1 shows some basic characteristics of these reaches. This approach combines two independent data sources to arrive at the best possible estimate of the historic flood environment—flood stage indicators (FSIs) and nonflooded surfaces. FSIs include fluvial sediment deposits, woody debris piles, and scour zones. Nonflooded surfaces exhibit undisturbed vegetation and changes in substrate.

Table 1: Summary of reach characteristics for hydraulic model.

Study Reach	**Reach Elevation**	**Drainage Area**	**Reach Length**	**Average Gradient**	**Initial Channel n[a]**	**Initial Overbank n[a]**
	M	**km^2**	**m**			
Anaconda Creek Reach 1	1626.1	7.5	144.84	0.045	0.036	0.067
Upper Blackfoot River Reach 1	1626.4	5.2	335.86	0.090	0.06	0.088
Upper Blackfoot River Reach 2	1596.3	14.2	370.20	0.065	0.052	0.07

[a]Determined from method described by Arcement and Schneider (1989).

Peak stage determination is a critical component to estimating historic peak discharge (Pruess, Wohl et al. 1998). The accuracy of FSIs and nonflooded surfaces for estimating peak flows is susceptible to several uncertainties (Jarrett and Tomlinson 2000). FSIs tend to underestimate peak discharge. High water marks tend to accurately indicate peak stage; however, they can be ephemeral (Jarrett and Tomlinson 2000). Nonflooded surfaces tend to overestimate peak discharge.

Boundary conditions are necessary to initiate the calculation of the water surface using the step-backwater technique. We assumed the flow was subcritical during the flood event. Flow during extreme flood events in natural channels is primarily subcritical with locally supercritical flow (Jarrett 1984; Trieste and Jarrett 1987). Our downstream boundary was selected at a cross section far enough downstream from the area we were estimating flood extents that the model would be able to converge to a single water surface profile, and so that the effect of the boundary condition on the predicted elevations was minimized. Energy losses in the step-backwater method include losses due to roughness elements in the channel and floodplain as well as losses due to expansion and contraction of the flow. During extreme flood events, there is significant energy loss caused by turbulence and sediment/debris transport. Therefore, the flow resistance coefficient (represented as Manning's n) must account for the total energy loss due to channel and floodplain roughness, turbulence, and sediment/debris transport.

Initial roughness coefficients for the channel and overbank areas were determined using methods described by Arcement and Schneider (1989) and checked using roughness charts by Chow (1959).

In order to maximize the accuracy of the peak discharge estimate and to account for the uncertainties previously described, we estimated a range of flood stages by bracketing the upper and lower limits of the flood environment at each of several cross sections in the stream channels. The lower elevations of nonflooded surfaces and high water marks served as the upper limits and the highest elevations of FSIs served as the lower limits. We varied discharge and channel and floodplain roughness estimates to achieve the best estimate of the peak flood event. The "best match" was the combination of discharge and roughness that minimized the average error, calculated as the average of the difference between the predicted water surface and the upper and lower limits at each cross section, across the entire modeled reach. Table 2 shows the initial and final roughness estimates for the model.

Table 2: Initial and final estimates of channel and overbank roughness.

Study Reach	**Cross Section**	**Initial Channel n**	**Adjusted Channel n**	**Initial Overbank n**	**Adjusted Overbank n**
Anaconda Creek Reach 1	3	0.034	0.036	0.067	0.067
	2	0.034	0.036	0.067	0.067
	1	0.034	0.036	0.067	0.067
	0.5	0.034	0.036	0.067	0.067
Upper Blackfoot Reach 1	12	0.038	0.038	0.033	0.040
	11	0.038	0.038	0.033	0.040
	10	0.077	0.038	0.113	0.040
	9	0.077	0.038	0.113	0.040
	8	0.077	0.069	0.102	0.088
	7	0.077	0.060	0.102	0.088
	6	0.077	0.060	0.102	0.088
	5	0.077	0.030	0.102	0.088
	4	0.077	0.050	0.102	0.088
	3	0.077	0.020	0.102	0.088
	2	0.077	0.050	0.102	0.088
	1	0.077	0.090	0.102	0.090
	0.5	0.077	0.035	0.102	0.070
Upper Blackfoot Reach 2	17	0.052	0.040	0.078	0.070
	16	0.052	0.052	0.078	0.070
	15	0.052	0.035	0.078	0.070
	14	0.052	0.052	0.078	0.070
	12	0.052	0.035	0.078	0.070
	11	0.052	0.094	0.078	0.070
	10	0.052	0.097	0.078	0.070
	9	0.052	0.052	0.078	0.070
	8	0.052	0.052	0.078	0.070
	7	0.052	0.052	0.078	0.070
	6	0.052	0.052	0.078	0.070
	5	0.052	0.052	0.078	0.070
	4	0.052	0.052	0.078	0.070
	3	0.052	0.052	0.078	0.070
	2	0.052	0.052	0.078	0.070
	1	0.052	0.052	0.078	0.070

In general, we placed cross sections for modeling at locations that had gradually varied flow characteristics, and paid attention to points of floodplain constriction and expansion along the length of each study reach (see Figure 2). At each cross section, we surveyed breaks in slope, banks, channel margins, and channel thalwegs using a total station and a survey grade GPS.

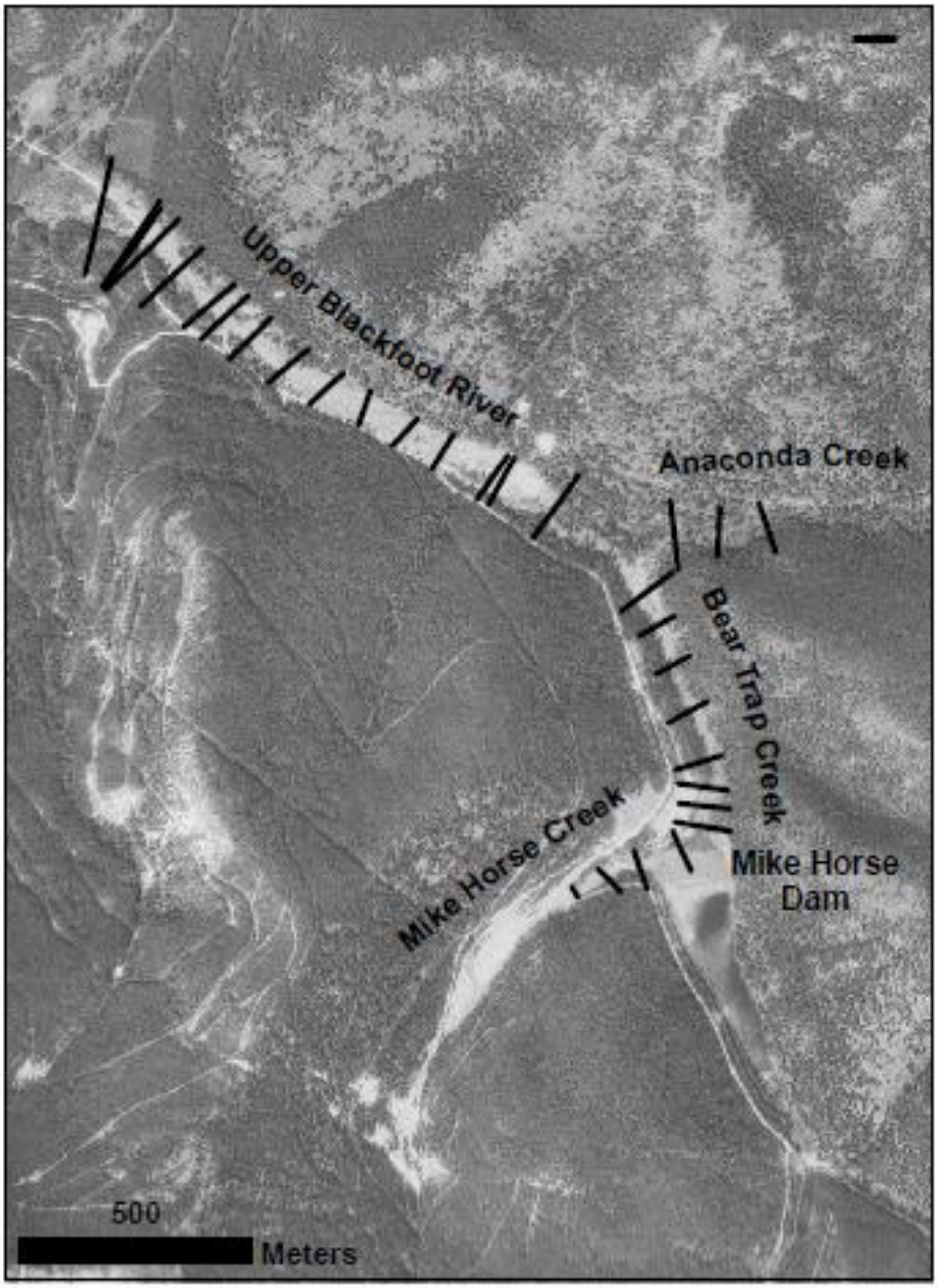

Figure 2: Map showing locations of channel cross sections (shown as bold lines) used for flood modeling. Note: **The flood modeling reaches were as follows: Upper Blackfoot Reach 1 encompassed both Mike Horse and Beartrap Creek; Upper Blackfoot Reach 2 encompassed the Upper Blackfoot River downstream of Anaconda Creek; and Anaconda Creek Reach 1 encompassed Anaconda Creek only.

3.1.2. Regional Estimates

We used empirically derived, regional estimates as a second estimate of peak discharge. Parrett and Johnson (2004) developed regression models for hydrologic regions in Montana, Wyoming, Idaho and Canada based on channel geometry. We estimated peak discharges for 100-year floods based on the active channel width for each reach and the drainage area at the study point.

3.1.3. Hydrograph Records

We analyzed hydrograph records as a third estimate of peak discharge. The nearest USGS gage, No. 12340000, is located at Bonner, Montana.

3.2. Aerial Photo Processing

We acquired aerial photos of the study area for 1938, 1964, 1978, 1995, and 2005. This offered the best possible data for assessing riparian vegetation before dam construction in 1955, before and after dam failure in 1975, and before dam removal in 2008. We downloaded 1995 and 2005 orthophotos from the Montana Natural Resource Information System web site. We ordered the 1964 and 1978 scenes from the Aerial Photography Field Office in Salt Lake City, UT. Lastly, we purchased the 1938 images from the National Archives Reproductions Administration.

We georeferenced and mosaiced the 1938, 1964 and 1978 photos using the 1995 images as the target layers. We chose points close to the floodplain to reduce distortion due to topographic relief (Hughes, McDowell et al. 2006). Using between 6 and 15 hard and soft control points, we produced georeferenced images with root mean square errors between 2.36 and 4.90. RMS values are dimensionless measures of the difference between control points on the control photo (1995 digital orthoquad quadrangle) and the georeferenced image (scanned image). While we cannot assign a distance measure to RMS values, we can choose control points that minimize RMS values as an indication of best fit (ESRI 2005). We transformed images using a first order polynomial transformation to allow scaling, stretching, shifting, and rotating. We applied no bending or wrapping. We mosaiced all scenes from a given year, then clipped the images to the study area.

3.3. Aerial Photo Interpretation

We identified and delineated channel location and sinuosity for each photo year. We calculated sinuosity using valley length and channel length.

We identified floodplain extent using the modeled flood path, changes in riparian vegetation extent, and changes in upland vegetation density and horizontal structure. We limited our interpretation to canopy vegetation because it was visible on all aerial photos and indicative of major changes to the riparian landscape. While understory vegetation is disturbance-dependent, its analysis was not possible using the historic aerial photos. We delineated floodplain cover for each photo at the same scale (1:1000) to maintain the same level of accuracy between years. Several photos were difficult to interpret due to lengthy shadows and low quality photo resolution. Based on ground-truthed photos of riparian vegetation patches, we identified areas dominated by coniferous, deciduous, and herbaceous vegetation and bare ground. Coniferous patches were dominated by *Abies engelmanii*, *Pinus contorta*, and standing dead conifers. Deciduous patches were dominated by *Populus trichocarpa* (black cottonwood), *Alnus incana* (thin leaf alder), *Salix* spp. (willow species) and *Acer glabrum* (Rocky Mountain maple). Man made developments such as roads, structures, ditches, and the dam were also delineated. Then, based on texture, pattern, and distribution of vegetation patches and man made developments, we delineated the entire extent of the identified floodplain.

3.4. Data Collection

3.4.1. Riparian Vegetation

We dissolved the riparian vegetation polygons from each photo year to acquire the number of patches for each canopy type present at each photo year. Along each hydrology transect, we made point observations of riparian canopy type every 10 meters for each photo year. The total area, number of patches, and point observations for each canopy type were exported for statistical analysis.

3.4.2. Watershed Parameters

Watershed characteristics were developed for each site using terrain analyses of 10 m digital elevation models (DEMs) (see Table 3). Sites were located on DEMs at the most downstream cells. Site elevations were taken directly from DEMs. Watersheds were delineated and clipped using ArcGIS 9.2 HydroTools data model. This approach used topography to define stream networks and riparian areas. Hydrologic watershed variables were based on stream networks derived based on a threshold contributing area of 5 hectares and a D8 flow algorithm (Tarboton 2008).

Table 3: Watershed variables (properties) defined at each transect.

Physical Property	**Description of Variable**
Drainage Area at Site	area draining in to stream at the site
Elevation above Riparian Area	the average difference in elevation between grid cells in the upslope drainage area and grid cells in the riparian zone
Site Elevation	elevation of the most downstream point in a site
Stream Network Elevation	the average elevation of all stream grid cells upstream of the site
Subcatchment Size	the average contributing area of all grid cells draining into the site
Upslope Basin Elevation	the average elevation of all grid cells draining into the riparian zone, including stream cells
Upslope Basin Gradient	the average slope of all grid cells draining into the riparian zone, including stream cells

Hydrologic variables were chosen to represent hillslope influences on riparian groundwater processes, network organization and fluvial dynamics. Each characteristic was calculated for individual DEM grid cells in the drainage area of each site. Subcatchment size represents the distribution of drainage area throughout the catchment of a site lending insight into network structure (McGlynn, McDonnell et al. 2003). Upslope basin elevation and gradient indicate the degrees of influence that distributed elevation and gradient have on watershed processes. Stream network elevation represents the influence of distributed elevation on hydraulic parameters affecting fluvial processes. We define the riparian zone geographically as the area within 3 m above the stream channel following flow paths toward the stream (McGlynn, Gooseff et al. 2003). The elevation above the riparian area, therefore, is the elevation of the watershed minus that of the stream and riparian areas and represents the influence of hillslope processes on the riparian zone.

3.5. Analysis Methods

We stratified the vegetation data into three reaches. The Anaconda reach extended from the upstream-most transect on Anaconda Creek to the Anaconda-Beartrap confluence. The Beartrap reach extended from the MHD to the Anaconda-Beartrap confluence. The Upper Blackfoot reach extended from the Anaconda-Beartrap confluence to the downstream-most transect.

We conducted summary statistics on riparian vegetation canopy types for each photo year. These included counts and sums. The number of polygons represents a count of discrete areas delineated as supporting dominant riparian vegetation of the stated canopy type. Area indicates the number of square meters of a given canopy type. The number of points indicates the number of point observations made at 10-meter intervals along hydrology transects.

We analyzed the point observation data in a regression environment to detect relationships between riparian canopy type distribution and watershed characteristics related to hillslope hydrology and network organization. We chose Generalized Linear Regression because it is nonparametric, suitable for binomial data (presence/absence), accommodates categorical data, and has adequate goodness of fit measures. See Austin et al. (1990) for a detailed discussion of using GLMs to test the importance of environmental variables (continuous and categorical). We constructed GLMs for every combination of photo year, canopy type, and significant watershed variable for a total of 300 univariate models. We identified functional models as those with predictors with an alpha level of 0.1 or less. We assessed functional model performance using maximum deviance explained for the least number of degrees of freedom used. We compared the predicted "present" values with a probability greater than 0.5 with the observed values to calculate a percent accuracy. We constructed multivariate models from functional univariate models. We chose the best models based on the statistical significance of predictors in the model, maximum deviance explained, and highest prediction accuracy.

4. RESULTS

4.1. Hydrologic Characterization

The majority of FSIs were located along Beartrap Creek closer to the dam. No FSIs were identified along Mike Horse Creek or Anaconda Creek. FSIs were identified along the Upper Blackfoot downstream of the confluence of Beartrap Creek and Anaconda Creek (see Figure 3). Figure 4 includes photos of the stream channel up- and downstream of the dam.

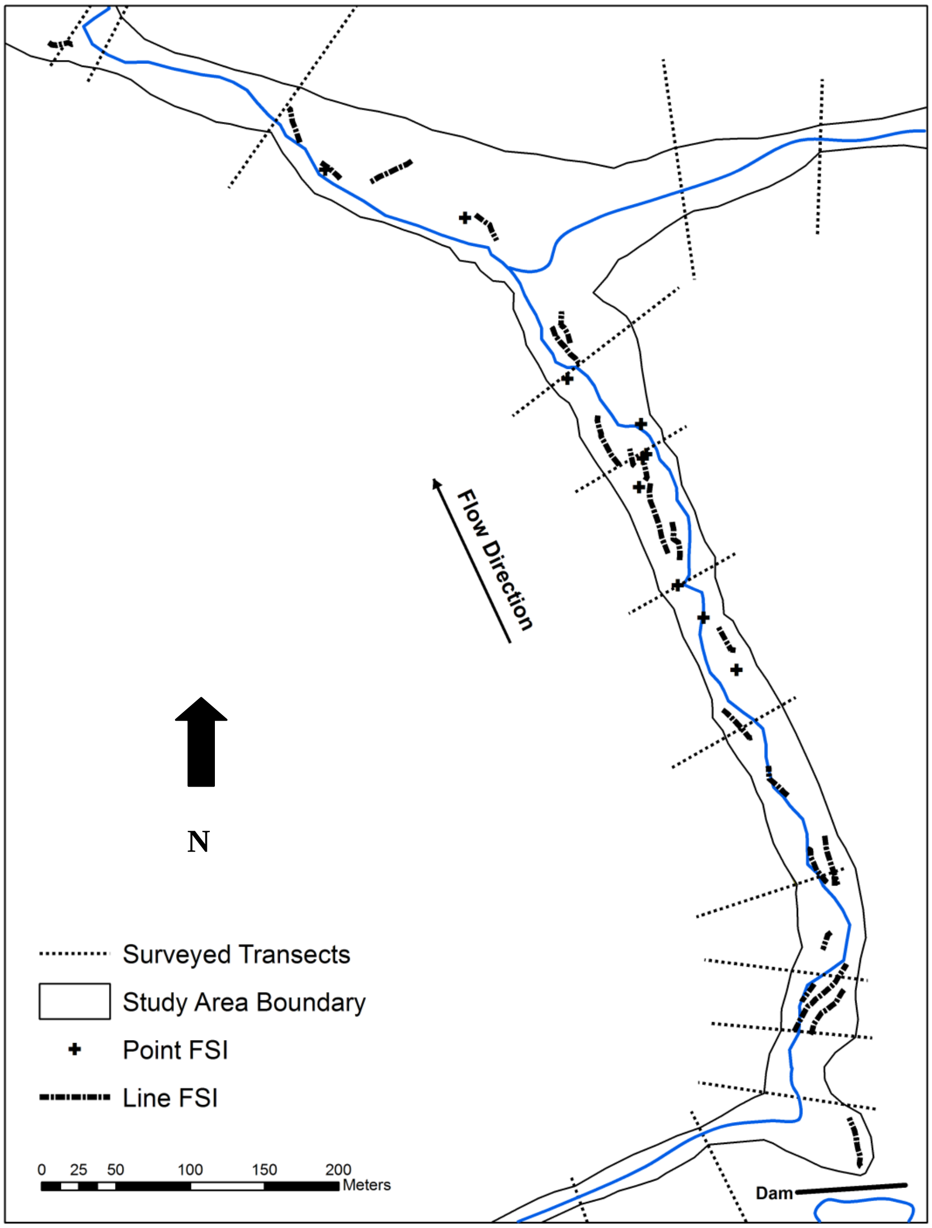

Figure 3: Location of FSIs in study area.

We estimated a flood flow of 11.5 m^3/s for Mike Horse Creek and Beartrap Creek combined (Upper Blackfoot Reach 1), 15.2 m^3/s for Anaconda Creek and 26.7 m^3/s for the Upper Blackfoot (Upper Blackfoot Reach 2 downstream of confluence of Beartrap and Anaconda).

The extent of the modeled flood water is shown in Figure 5 (north part of study area) and Figure 6 (south part of study area). Two figures were used to show the flood extents because when shown as only one figure the details are lost.

Figure 4: Photo of dam face and of downstream channel. Both photographs were taken in the upstream direction.

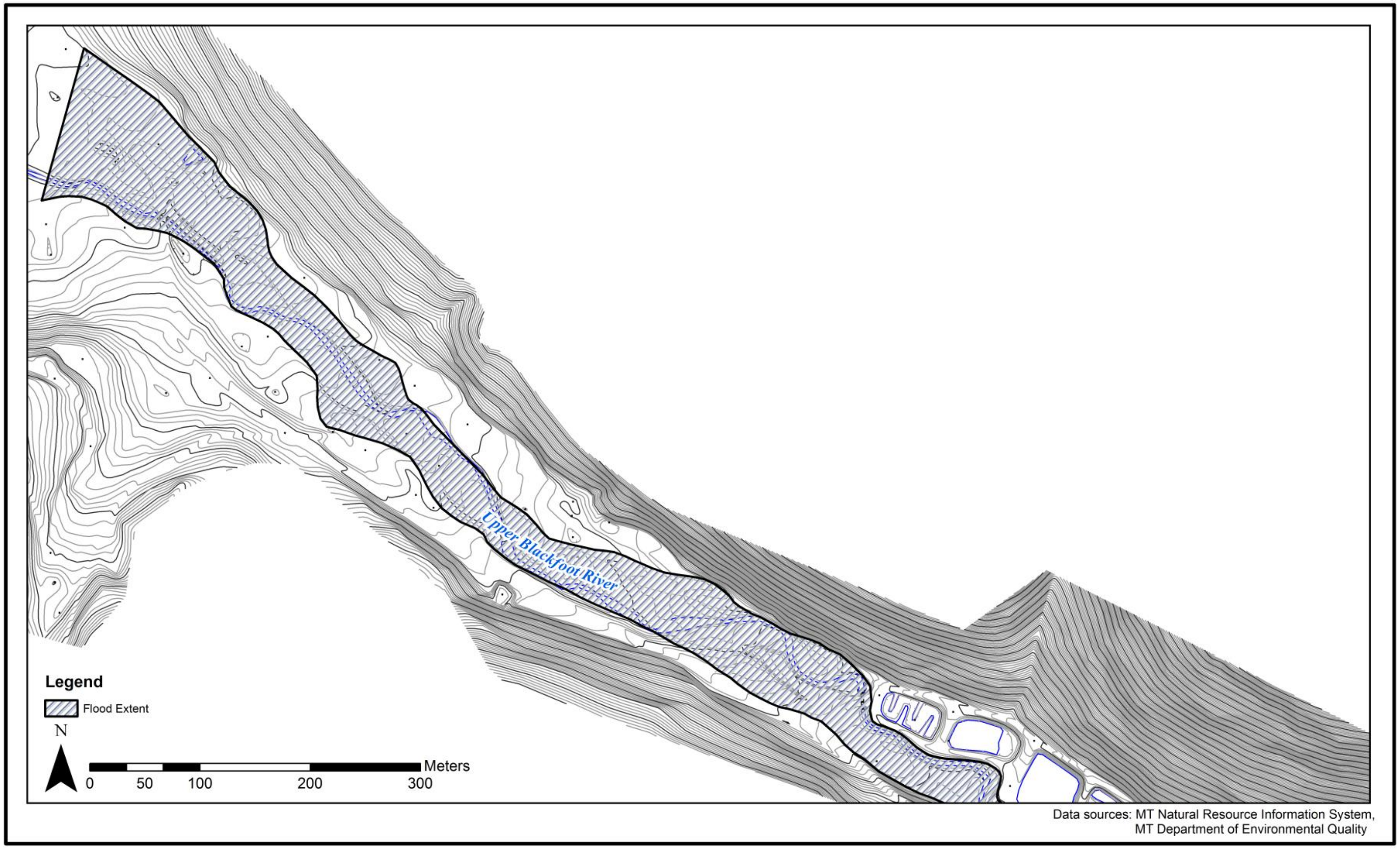

Figure 5: Map shows the estimated extents of flooding for the north part of the study area.

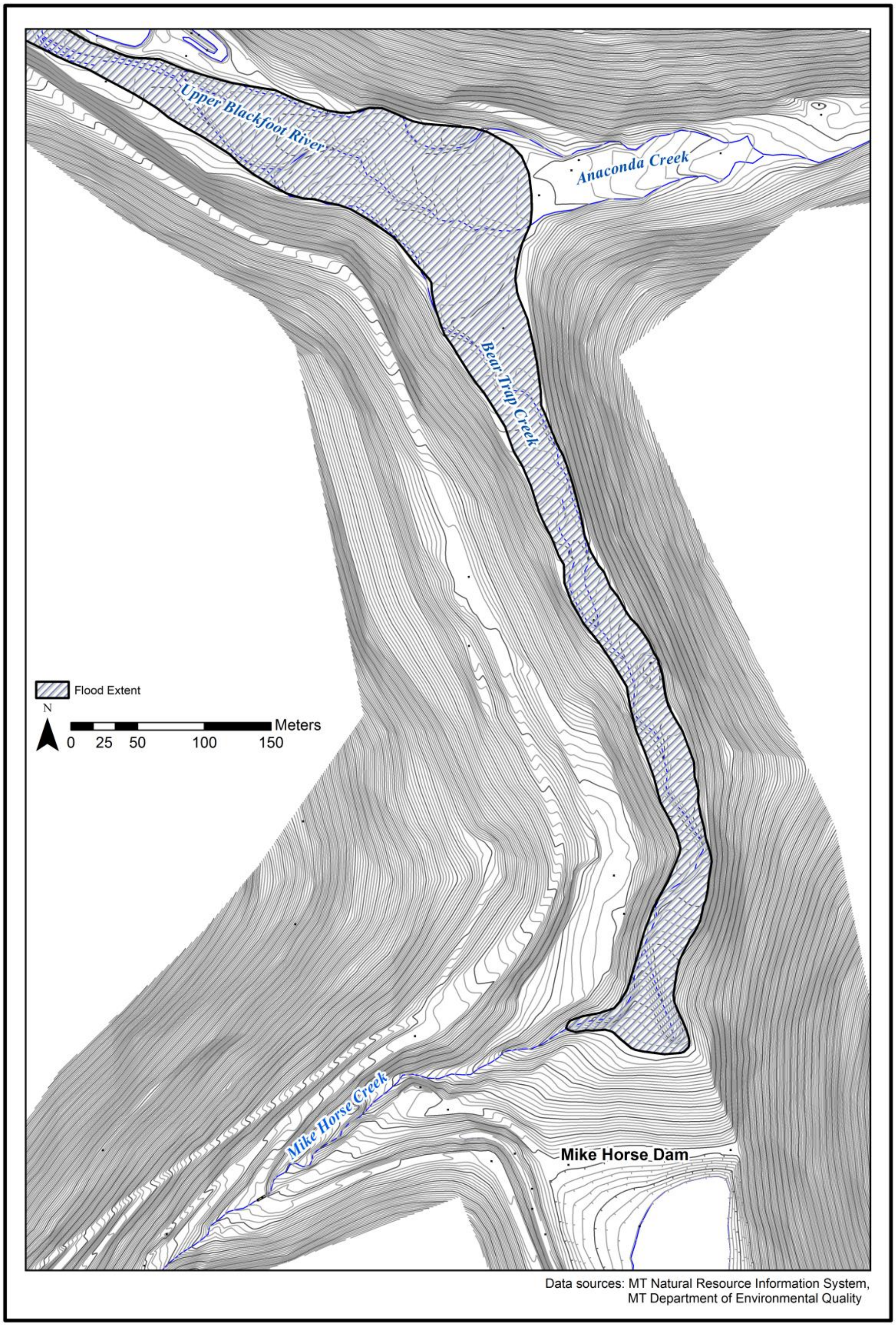

Figure 6: Map shows the estimated extents of flooding for the south part of the study area.

Using the regional regression equations, the 100-year flood for Mike Horse Creek and Beartrap Creek was 11.2 m^3/s. The 100-year flood was estimated at 14.9 m^3/s for Anaconda Creek, and 23.4 m^3/s for the Upper Blackfoot River.

4.2. Vegetation Response

4.2.1. Canopy Type Changes

In order for our techniques to detect the ecological response of the riparian plant communities to Mike Horse Dam (MHD) construction and failure, the communities had to either survive or develop since the events of 1955 and 1975, respectively. We are also careful to note the influence of mining-related events and activities that occurred before, during and after MHD construction. The major drivers of riparian vegetation in this basin include floods, development, mining, and their correlates. Therefore, our results are biased toward those processes active within and influential on the valley bottom between photo years, in addition to watershed characteristics that affect these processes. Also, our techniques necessarily incorporate plant communities that occurred along the valley margins, which include a substantial amount of upland plant communities. Thus, because of the sheer magnitude of the 1975 dam failure flood, our results will include an unusual amount of upland plant communities for a riparian study.

4.2.2. Reference Data

Anaconda Creek served as a reference reach for two reasons. First, the impacts due to mining were vastly limited compared to the Beartrap and Upper Blackfoot reaches. Second, it was not impacted by the dam breach flood in 1975. However, to avoid collecting data from two different channel types, we only laid three transects on Anaconda Creek. This limited our statistical power.

The data collected from the 1938 photos also served as a reference for detecting changes. At this point, there had been mining activity in the basin for at least 40 years, although the extent and intensity was limited due to the difficulty in transporting large volumes to distant smelting facilities. Thus, the channel geomorphology, riparian vegetation distribution, and watershed function was largely intact at the time of the 1938 photo. We analyzed for reference data the 1938 photos of the Anaconda, Beartrap, and Upper Blackfoot reaches, as well as all additional photos for the Anaconda reach. We tested the data from the 1964, 1978, 1995, and 2005 photos of the Beartrap and Upper Blackfoot reaches for changes due to dam construction and dam failure flood.

4.2.3. Temporal Distribution

Once we stratified the data into three reaches and omitted the confluence area, we assessed the aerial and point data for detectible differences between years. We assessed 16,400 m^2 of floodplain at 22 points along 3 transects on the Anaconda reach. For Beartrap, 49,200 m^2 of floodplain at 49 points along 8 transects. For Upper Blackfoot, 127,600 m^2 of floodplain at 149 points along 13 transects. Coniferous species composed the dominant canopy type for all years along all reaches, except for 1978 on Anaconda when deciduous species dominated riparian vegetation (see Figure 7).

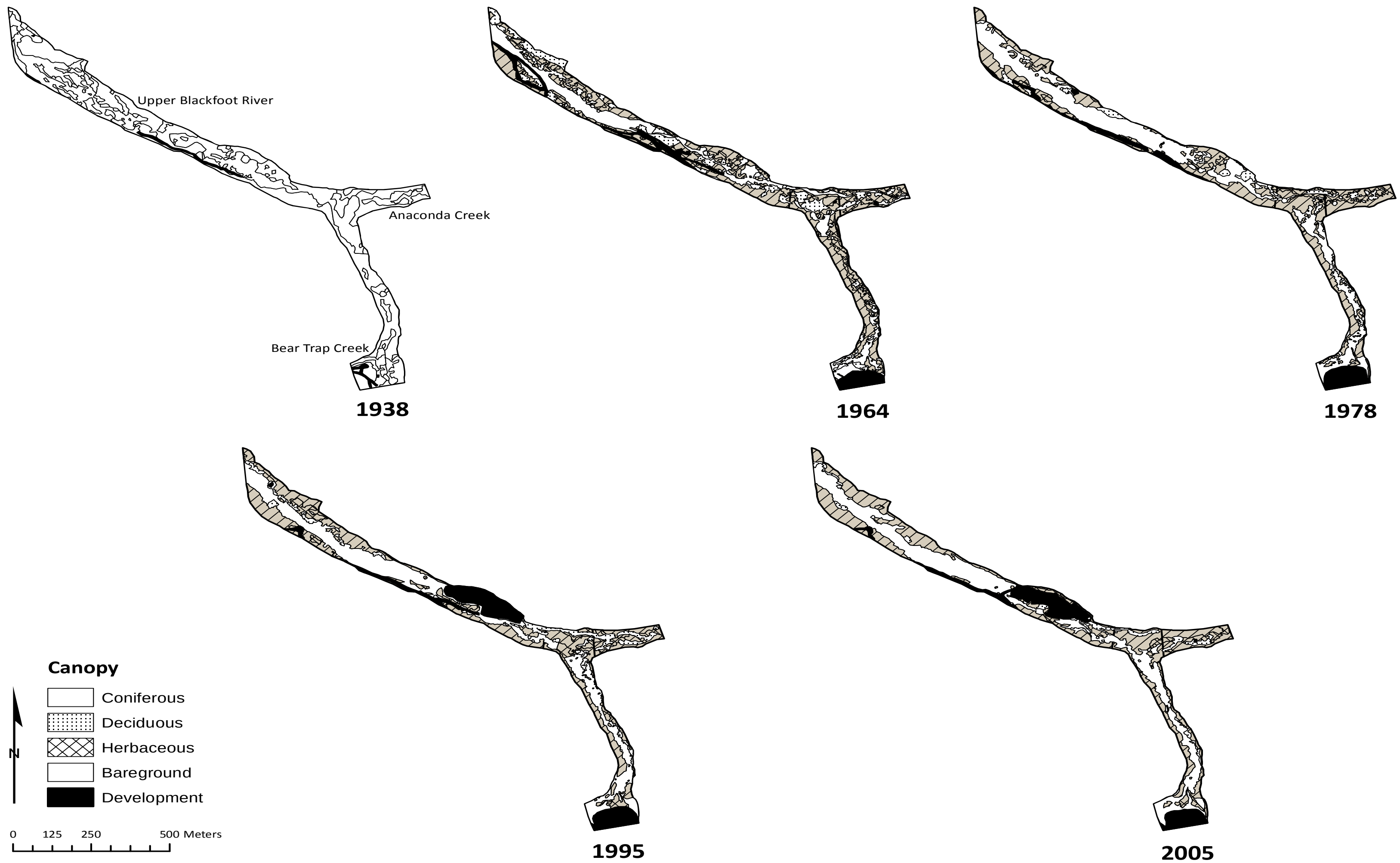

Figure 7: Vegetation changes for Anaconda, Beartrap and Upper Blackfoot reaches.

4.3. Preconstruction 1938

Mining activity started in the basin around 1889. Upstream of the study area along Mike Horse Creek, the Sterling Mining and Milling Company constructed the Mike Horse Mill in 1919 and continued operations until the late 1920s. The mine sat idle for over a decade until Mike Horse Mining and Milling leased it in 1938. Miners deposited mine tailings from the mine along Beartrap Creek directly upstream of the study area. Eventually, they pushed the creek to the east side of the valley to prevent it from eroding the tailings piles (US Forest Service 2006). We observed evidence of this activity in the 1938 photos and expect that it increased the sediment load passing through the Beartrap and Upper Blackfoot study reaches. Thus, we presume that the riparian vegetation in 1938 had responded to both natural processes and anthropogenic activities associated with mining. However, we found no weather or stream gage data for this period to characterize the natural events leading up to the study period.

From the 1938 photo, we measured channel sinuosity of the entire study area as 1.165. This is consistent with the channel gradient, narrow valley, and cobble substrate setting of the region.

We interpreted the 1938 photo to show the highest amount of coniferous, deciduous, and herbaceous cover as well as total cover for Beartrap and Upper Blackfoot reaches for the study period. From the number of polygons and the distribution of canopy cover, we determined that patches of vegetation in all three reaches were most contiguous and at maximum extent for all three reaches in 1938 compared to the rest of the study period (Figure 7 and Figure 8). Despite the upstream mining activities at the time, we suggest that the riparian area maintained significant function. Consequently, we used data from 1938 to provide context for interpreting changes in the later photos.

We observed high amounts of coniferous, deciduous, and herbaceous cover in Anaconda (Figure 8). We delineated few polygons, yet all with high amounts of aerial cover. Coniferous canopy was dominant in terms of aerial cover and number of point observations. However, the number of polygons was evenly distributed among coniferous, deciduous, and herbaceous canopy types. Hansen and others (1995) presented riparian vegetation data typical of the region and setting that is consistent with our Anaconda data from 1938. From this data we suggest that little mining activity occurred along this reach in 1938 and the floodplain vegetation was structurally intact and functional.

Along the Beartrap reach, we delineated a high proportion of coniferous aerial cover, half that amount in deciduous cover, and half in herbaceous cover (see Figure 8). However, we observed only a few polygons of each. We collected a high number of point observations of coniferous and deciduous canopy in 1938. This suggests that the riparian vegetation at this time provided some amount of ecological function such as flood energy dissipation, sediment trapping, and fish habitat (Vaghti 2003). From the amount of deciduous canopy present, we suggest that the channel sinuosity at the time decreased the channel slope and provided suitable conditions for deciduous species such as *Populus trichocarpa* (black cottonwood). We believe it is possible that the bare ground present in 1938 indicates that mining activity was impactful during this time by increasing the sediment load. A flood event could account for the bare ground patches. But, climate and gage data are absent for the period prior to 1940.

Given the wider valley of the Upper Blackfoot reach compared to that of Beartrap, we expected a higher proportion of deciduous canopy cover and point observations. As with the other reaches, we determined that floodplain vegetation patches were mostly contiguous and quite large based on the number of polygons in conjunction with the aerial cover of coniferous, deciduous, and herbaceous cover. We do not have sufficient climate and stream gage data to attribute the bare ground to a recent flood event or solely to mining-related activity. Because these data supported our assumption that the riparian zone was functional in 1938, we continued with our analysis using the 1938 data as reference.

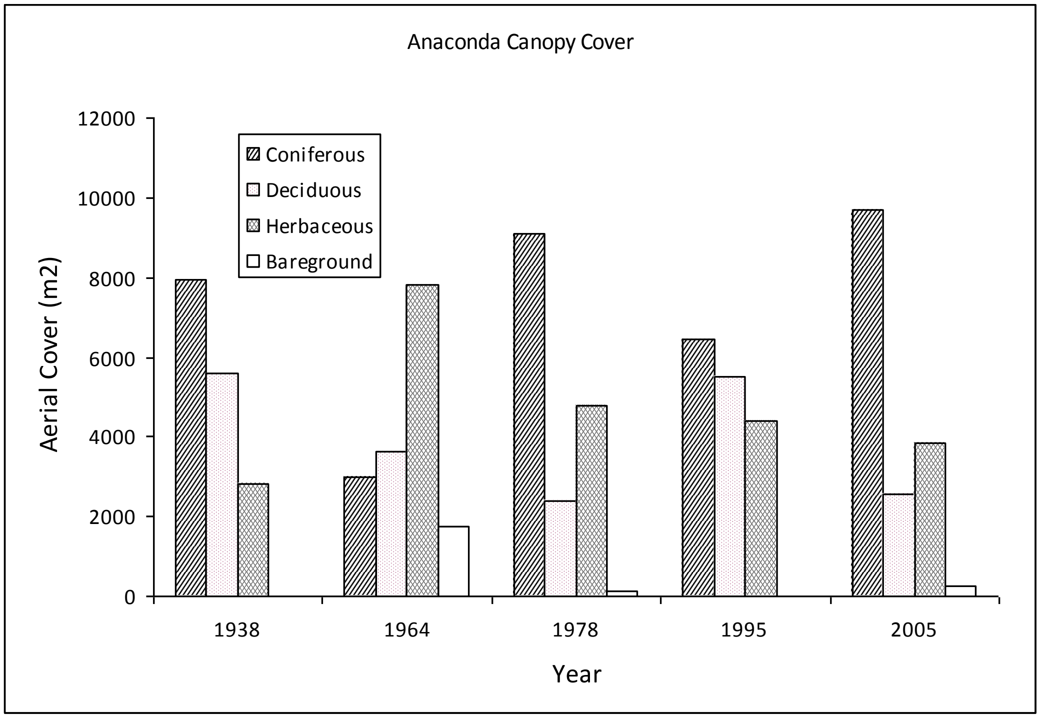

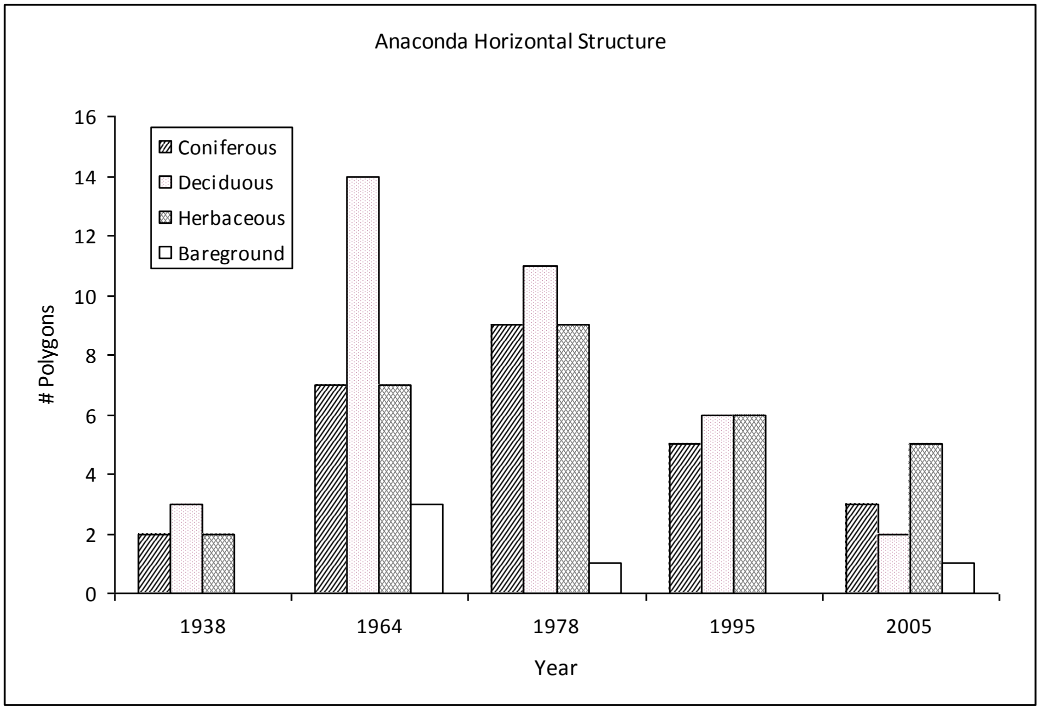
Anaconda Horizontal Structure
Polygons
Coniferous
Deciduous
Herbaceous
Bareground
0
2
4
6
8
10
12
14
16
1938
1964
1978
1995
2005
Year

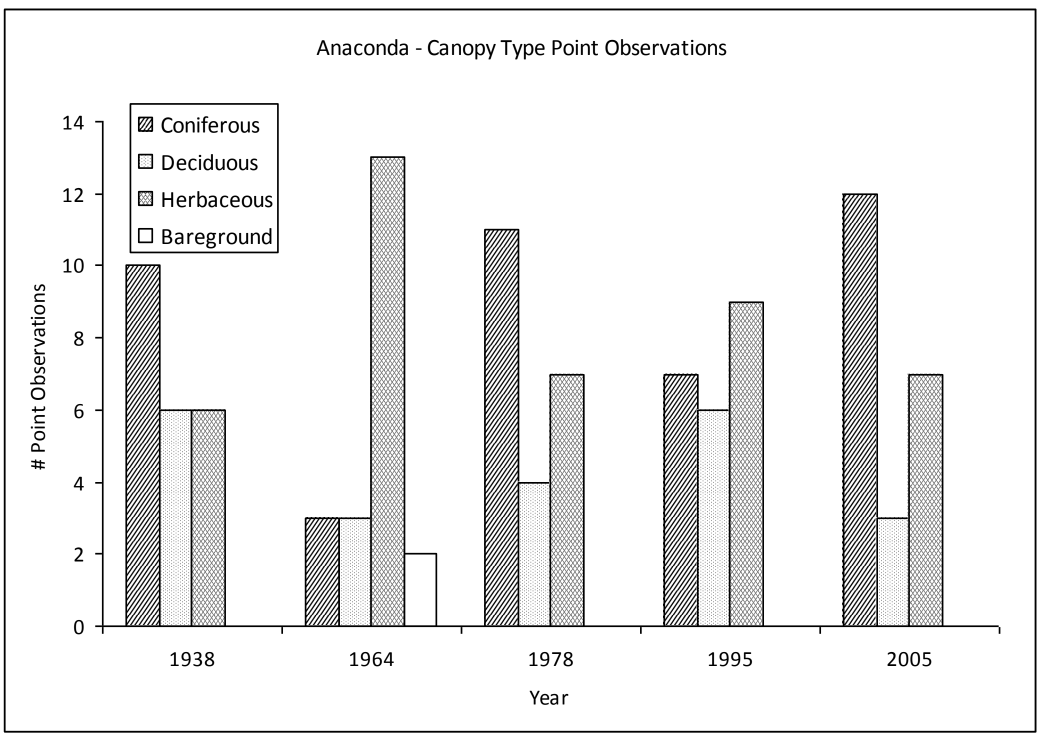
Anaconda - Canopy Type Point Observations
Point Observations
Coniferous
Deciduous
Herbaceous
Bareground
0
2
4
6
8
10
12
14
1938
1964
1978
1995
2005
Year

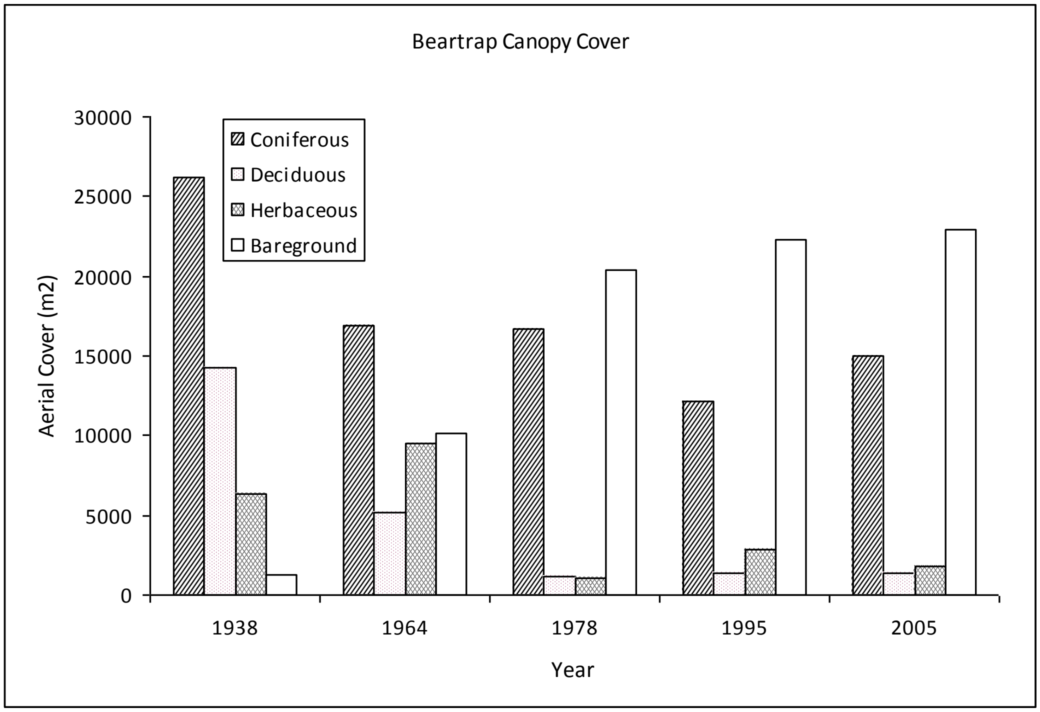
Beartrap Canopy Cover
Coniferous
Deciduous
Herbaceous
Bareground
Aerial Cover (m2)
30000
25000
20000
15000
10000
5000
0
1938
1964
1978
1995
2005
Year

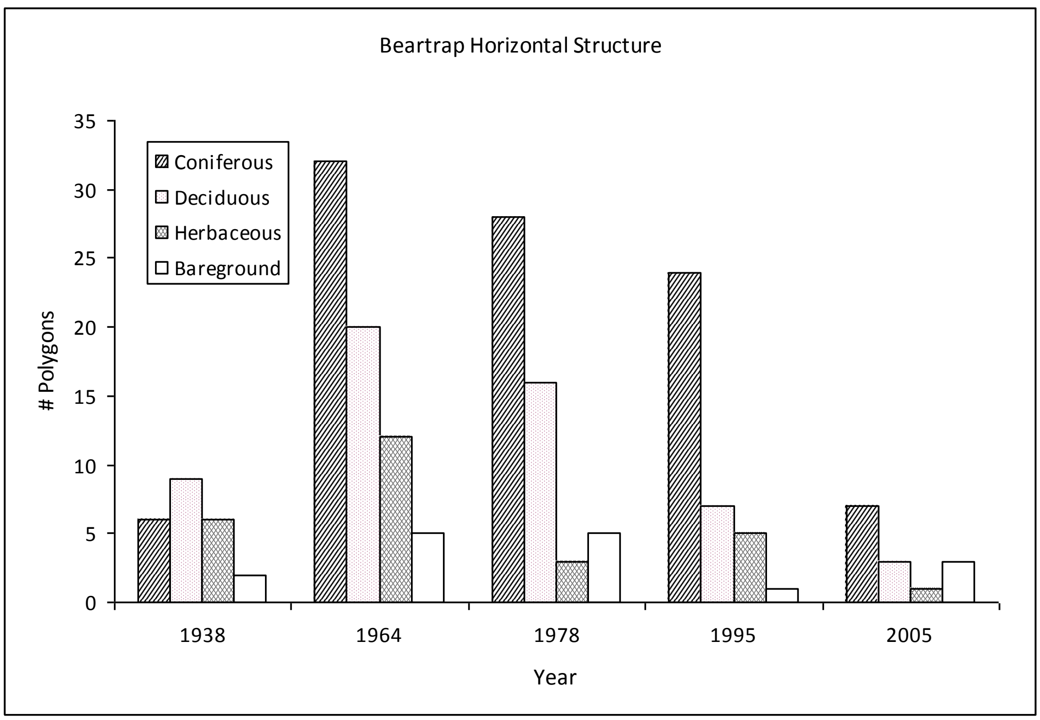
Beartrap Horizontal Structure
Coniferous
Deciduous
Herbaceous
Bareground
Polygons
35
30
25
20
15
10
5
0
1938
1964
1978
1995
2005
Year

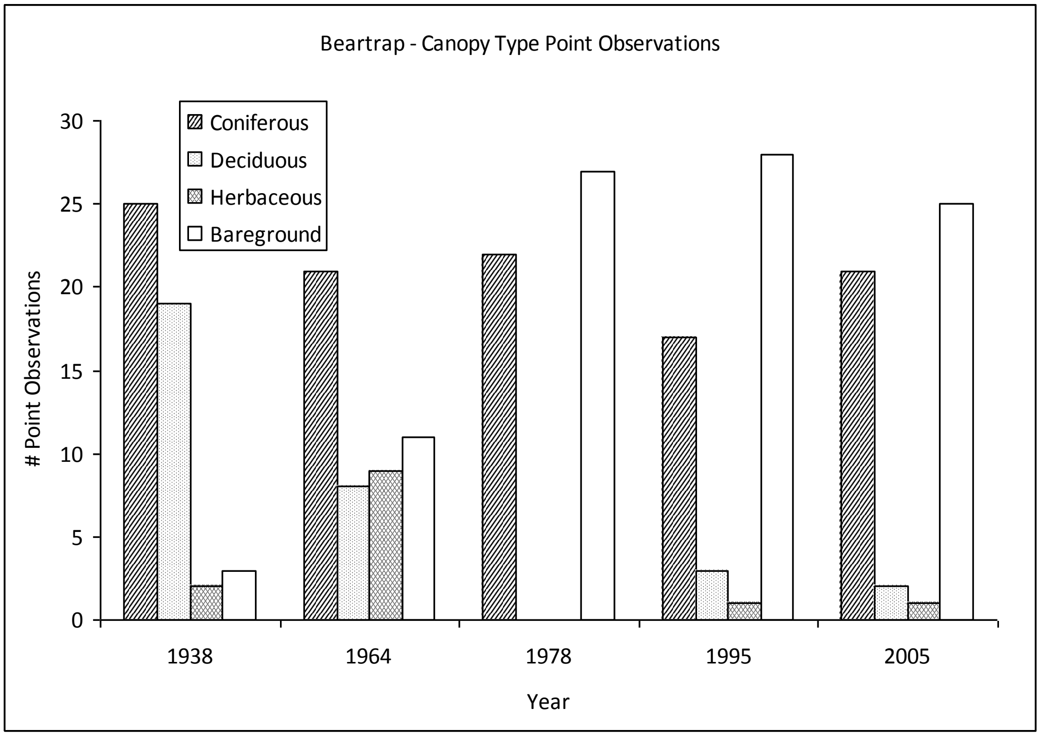
Beartrap - Canopy Type Point Observations
Coniferous
Deciduous
Herbaceous
Bareground
Point Observations
0
5
10
15
20
25
30
1938
1964
1978
1995
2005
Year

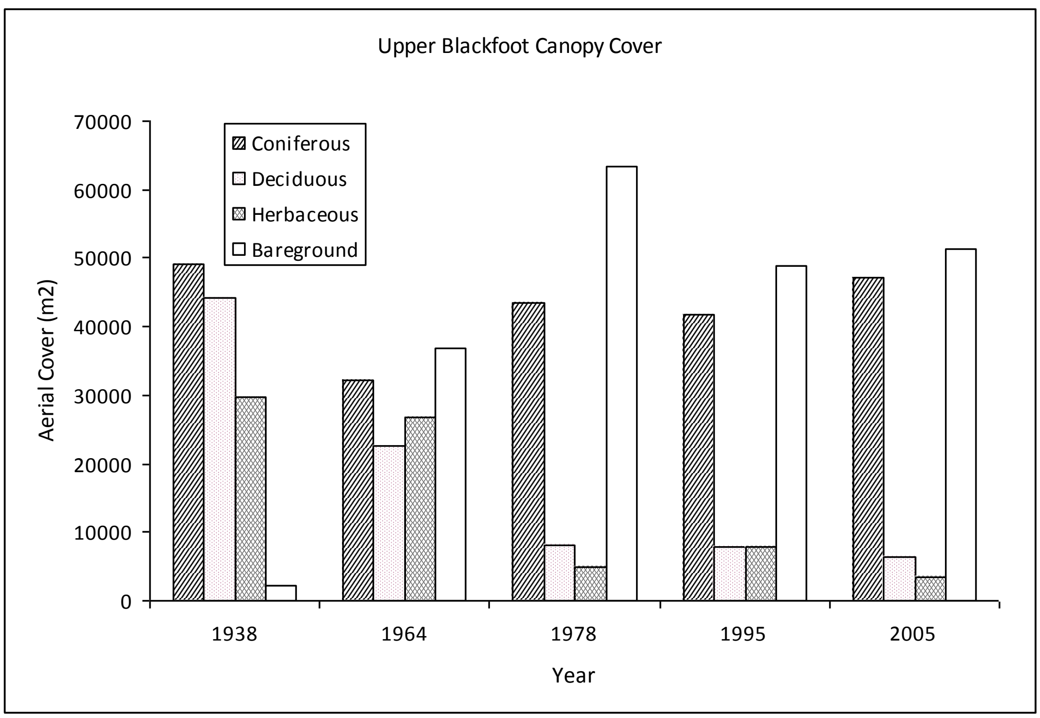
Upper Blackfoot Canopy Cover
Coniferous
Deciduous
Herbaceous
Bareground
Aerial Cover (m2)
0
10000
20000
30000
40000
50000
60000
70000
1938
1964
1978
1995
2005
Year

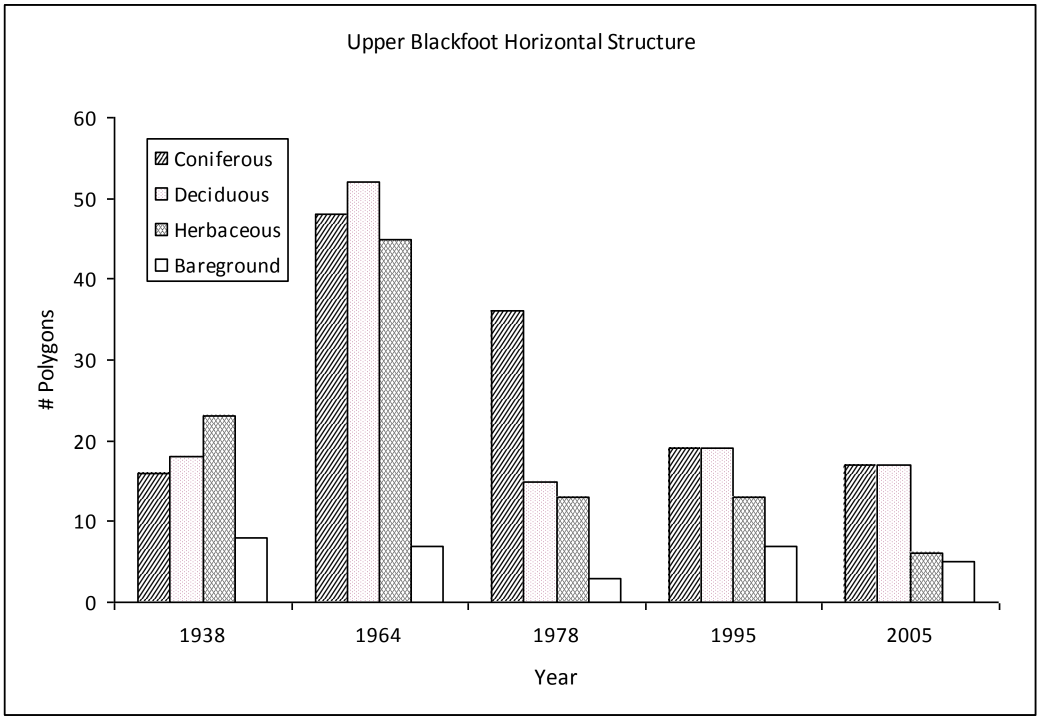

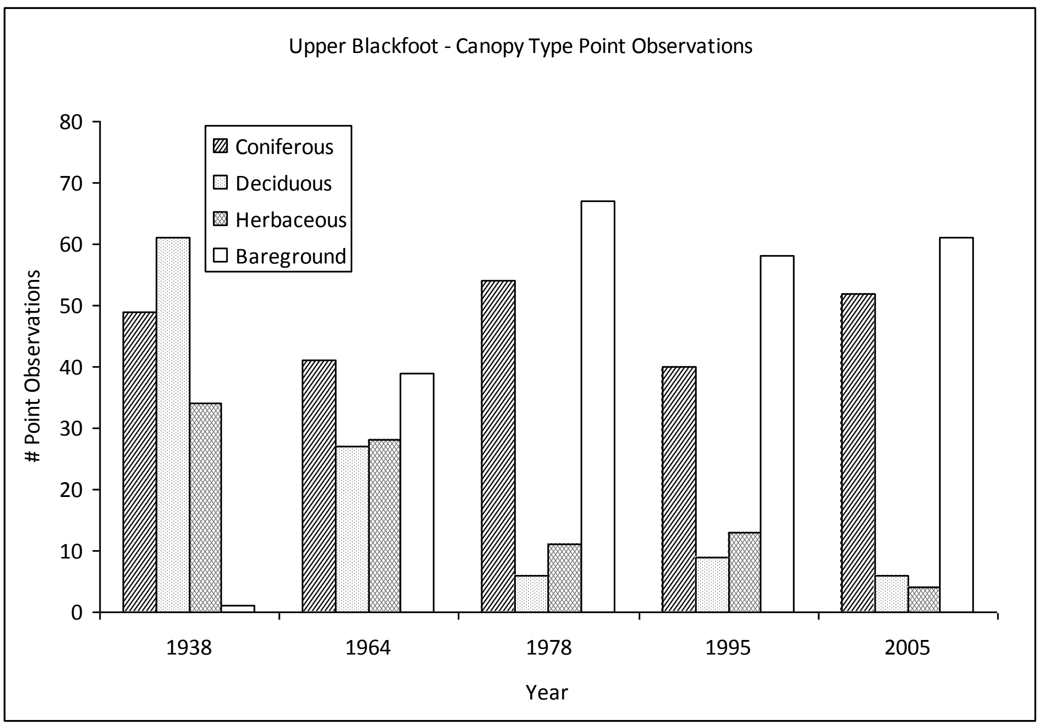

Figure 8: Changes in canopy cover and number of polygons indicate a trajectory from contiguous to fragmented to overly simplified.

4.4. Postconstruction 1964

Mike Horse Mining and Milling (later purchased by ASARCO) constructed the MHD to form a settling impoundment between 1941 and 1953 (US Forest Service 2007). USFS (2007) reports that under normal flows, the earthen dam released water in the form of seepage. In 1964, workers cut an emergency spillway around a clogged outflow to conduct flows of a high runoff event. The Bonner, Montana, stream gage (USGS 1234000), over 100 miles downstream, registered the event as one of the highest on record (see Figure 9). We observed the effects of this high flow event, as well as those of mining activity, on the downstream floodplain vegetation in the 1964 image.

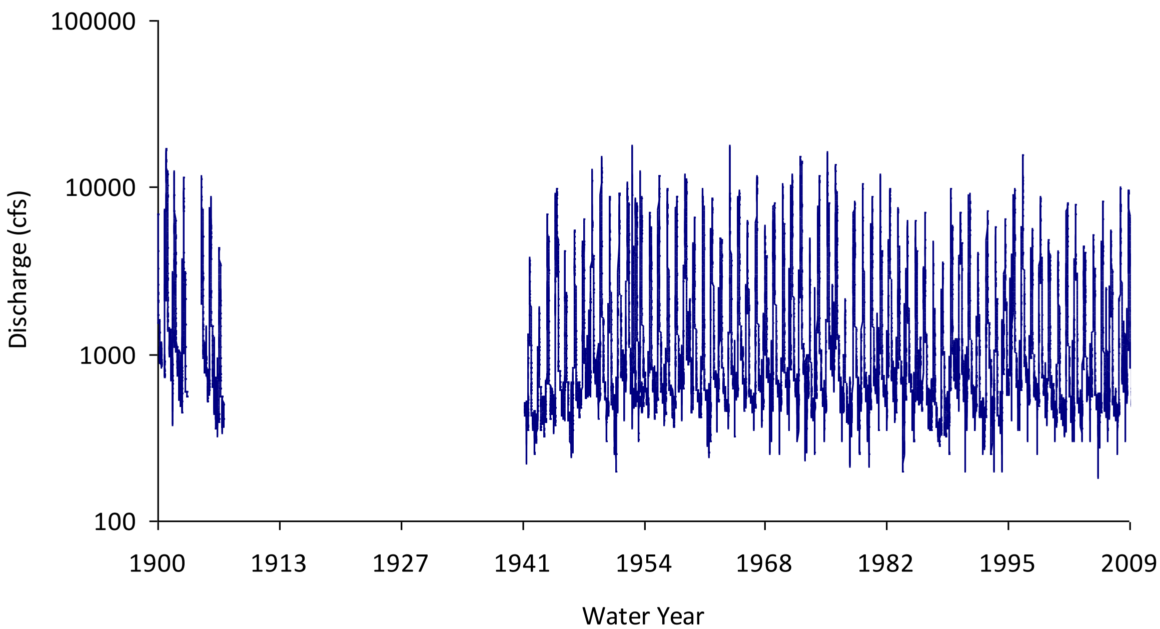

Figure 9: Hydrograph from USGS Gage No. 12340000 downstream of study area near Bonner, Montana.

Anaconda supported diverse canopy composition in 1964 and underwent significant changes since 1938. We observed a four-fold increase in the number of patches from 1938 to 1964. Interestingly, we assessed more deciduous cover than any other canopy type (Figure 8). In contrast, we detected a shift in dominance from coniferous and deciduous cover in 1938 to herbaceous in 1964. Similarly, in the point observation data, we observed that the majority of point locations shifted to herbaceous canopy: 22.7% from coniferous and 18.2% from deciduous (Table 4). Fragmentation of wooded areas combined with increased bare ground and herbaceous patch sizes is characteristic of early response to a major disturbance.

In Beartrap, we observed dominance of coniferous cover and number of polygons, but we saw more bare ground points of observation in the 1964 photo (Figure 8). We assessed that 10% of the deciduous points changed to herbaceous and another 10% changed to bare ground since 1938 (Table 5). We expected coniferous species cover to surpass other canopy types in number and extent given the confined valley and steeper slope of the Beartrap reach. We attributed the great amount of bare ground created since 1938 to the 1964 flood, which occurred a few months prior to the photo. The USFS reported headcutting along the emergency spillway cut on the east abutment to pass the high spring runoff of the year (US Forest Service 2007). We surmised that the flows from the 1964 flood were sufficiently powerful to scour vegetation from the east side of the floodplain. Consequently, the number of bare ground patches increased in size more than in number. Conversely, the coniferous, deciduous, and herbaceous patches shrunk and increased in number. We observed the most contiguous patch of coniferous on the west side of the Beartrap reach.

We measured relatively even proportions of coniferous, deciduous, herbaceous, and bare ground cover in the Upper Blackfoot reach in 1964 (Figure 8). We saw a parallel response to the Beartrap reach in that the number of patches of coniferous, deciduous, and herbaceous cover drastically increased compared to that of bare ground. As we saw in Beartrap, the number of point locations we observed as bare ground increased substantially. Primarily, we detected changes in point locations to bare ground from coniferous, deciduous, and herbaceous (Table 6). We suggest that the 1964 flood event is the likely driver of these changes, as well. However, we note that the extent of the changes is less in the Upper Blackfoot than in the Beartrap reach due to the wider valley width. This possibly allowed the flood energy to dissipate and drop sediment. Riparian species such as *Populus trichocarpa*, *Alnus incana*, and *Acer glabrum* are quite resilient to burial (Youngblood, Padgett et al. 1985; Hansen, Pfister et al. 1995; Walford, Jones et al. 2001).

We align the pattern of decreased woody species patch size and increase in patch number, combined with the increase in bare ground and herbaceous cover with that of other riparian areas in the region following large flood events (e.g. Baker and Walford 1995; Hawkins, Bartz et al. 1997). It is likely that mining-related activities have contributed to a decreased resilience of the riparian zone in the study area through increased sedimentation, altered hydrology, and reduced understory cover. While we cannot discount the role of mining-related activities on the changes we observed on these three reaches, we point to the 1964 flood event as the major driver of the increase in patchiness and shift in canopy dominance.

Table 4: Canopy changes for the Anaconda reach.

	1938-1964	1964-1978	1978-1995	1995-2005
Coniferous-Deciduous	9.1%	0.0%	18.2%	0.0%
Coniferous-Herbaceous	22.7%	0.0%	9.1%	0.0%
Coniferous-Bare ground	4.5%	0.0%	0.0%	0.0%
Deciduous-Coniferous	0.0%	9.1%	4.5%	9.1%
Deciduous-Herbaceous	18.2%	0.0%	4.5%	4.5%
Deciduous-Bare ground	4.5%	0.0%	0.0%	0.0%
Herbaceous-Coniferous	4.5%	18.2%	4.5%	13.6%
Herbaceous-Deciduous	0.0%	9.1%	0.0%	0.0%
Herbaceous-Man made	4.5%	0.0%	0.0%	0.0%
Bare ground-Coniferous	0.0%	4.5%	0.0%	0.0%
Bare ground-Deciduous	0.0%	4.5%	0.0%	0.0%
Manmade- Coniferous	0.0%	4.5%	0.0%	0.0%
No Change	*32%*	*50%*	*59%*	*73%*
Total Change	*68.2%*	*50.0%*	*40.9%*	*27.3%*

Table 5: Canopy changes for the Beartrap reach.

	1938-1964	1964-1978	1978-1995	1995-2005
Coniferous-Deciduous	10.2%	0.0%	4.1%	0.0%
Coniferous-Herbaceous	8.2%	0.0%	0.0%	0.0%
Coniferous-Bare ground	8.2%	10.2%	10.2%	4.1%
Deciduous-Coniferous	14.3%	6.1%	0.0%	2.0%
Deciduous-Herbaceous	10.2%	0.0%	0.0%	0.0%
Deciduous-Bare ground	10.2%	10.2%	0.0%	2.0%
Herbaceous-Coniferous	4.1%	4.1%	0.0%	2.0%
Herbaceous-Bare ground	0.0%	14.3%	0.0%	0.0%
Bare ground-Coniferous	0.0%	2.0%	4.1%	8.2%
Bare ground-Deciduous	2.0%	0.0%	2.0%	2.0%
Bare ground-Herbaceous	0.0%	0.0%	2.0%	2.0%
No Change	*33%*	*53%*	*78%*	*78%*
Total Change	*67.3%*	*46.9%*	*22.4%*	*22.4%*

Table 6: Canopy changes for the Upper Blackfoot reach.

	1938-1964	1964-1978	1978-1995	1995-2005
Coniferous-Deciduous	8.2%	2.1%	0.0%	0.0%
Coniferous-Herbaceous	3.4%	1.4%	3.4%	0.0%
Coniferous-Bare ground	4.8%	4.1%	5.5%	1.4%
Coniferous-Man made	2.1%	0.0%	8.2%	0.7%
Deciduous-Coniferous	8.9%	7.5%	2.1%	2.1%
Deciduous-Herbaceous	10.3%	2.1%	0.0%	0.0%
Deciduous-Bare ground	12.3%	6.2%	0.7%	3.4%
Deciduous-Man made	2.1%	1.4%	0.0%	0.0%
Herbaceous-Coniferous	4.1%	5.5%	0.7%	3.4%
Herbaceous-Deciduous	2.1%	0.0%	0.0%	0.7%
Herbaceous-Bare ground	8.9%	8.2%	1.4%	4.1%
Herbaceous-Man made	3.4%	2.1%	2.7%	0.0%
Bare ground-Coniferous	0.0%	1.4%	2.7%	3.4%
Bare ground-Deciduous	0.0%	0.7%	4.8%	2.7%
Bare ground-Herbaceous	0.0%	0.7%	2.1%	0.7%
Bare ground-Man made	0.0%	0.7%	5.5%	1.4%
Manmade- Coniferous	0.0%	2.1%	2.1%	1.4%
Manmade-Herbaceous	0.7%	0.0%	0.7%	1.4%
Manmade-Bare ground	0.0%	4.1%	1.4%	1.4%
No Change	*29%*	*50%*	*56%*	*72%*
Total Change	*71.2%*	*50.0%*	*43.8%*	*28.1%*

4.5. Post Dam Failure—1978

In 1975, a rain-on-snow event deposited nearly three inches of precipitation in one day (Rogers Pass 9 NEE weather station, NOAA) and filled the Mike Horse tailings impoundment after clogging a diversion ditch. MHD failed and produced a catastrophic flood that passed through the Beartrap and Upper Blackfoot study reaches and reportedly deposited contaminated sediment for tens of miles downstream (Hydrometrics Inc. and Blackfoot Challenge 2003; Confluence Consulting Inc., DTM Consulting Inc. et al. 2004). ASARCO repaired the breach with a clay core in the breached area, resloped and protected the up- and downslope dam faces, and replaced the spillway (US Forest Service 2007). The Anaconda reach experienced the rain-on-snow runoff event but was spared the added impact of the flows from the dam failure. We evaluated the preceding 10 years of weather data and found them to be high snow years for the region (Figure 10). This would allow floodplain vegetation throughout the study reach to develop multiple canopy layers, stabilize bank and floodplain sediments, and promote the establishment of early to mid-seral plant communities (Johnson 1994; Baker and Walford 1995; Nilsson and Svedmark 2002).

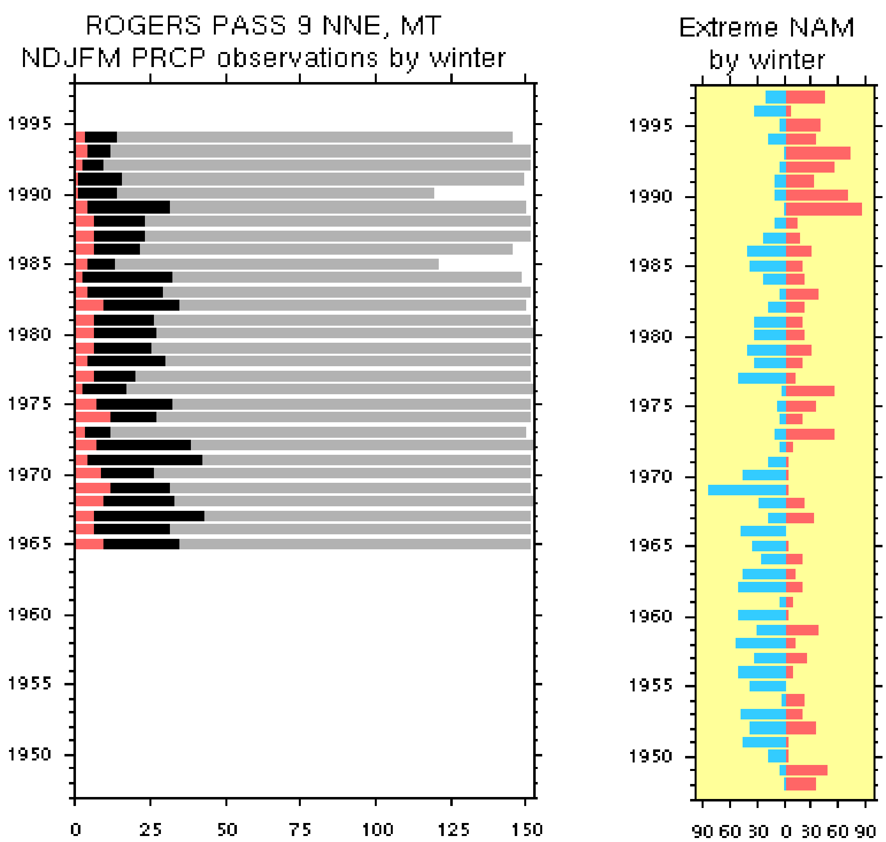

Figure 10: Climate data from Rogers Pass.

We observed an increase in coniferous and a decrease in herbaceous cover and point locations since 1964 along the Anaconda reach (Figure 8). We delineated more polygons of coniferous and herbaceous canopy in the 1978 photo than in the 1964 photo. In addition to detecting a decrease in bare ground cover, we saw a decrease in the number of bare ground polygons. In addition, we observed an 18.2% increase in coniferous canopy in 1978 from herbaceous in 1964, an increase of 9.1% in coniferous from deciduous, and 9.1% increase in deciduous from herbaceous (Table 4). Lastly, we identified a significant loss of bare ground at point locations. Taken in combination, we interpret this pattern to indicate an overall trend toward encroachment of conifer species into the riparian zone. Conifers opportunistically encroach on riparian areas in the absence of recent disturbance. While the rain-on-snow event of 1975 was comparable in magnitude to that of 1964, the Anaconda reach appears to have passed the flows without much damage.

In contrast to the Anaconda reach, we observed a marked decrease in deciduous and herbaceous cover and a corresponding increase in bare ground in the Beartrap and Upper Blackfoot reaches (Figure 8). We delineated fewer polygons in the 1978 photo than in 1964, overall. For all point locations, we interpreted them as either coniferous or bare ground. Expectedly, in Beartrap we assessed changes in point locations as converting to bare ground from coniferous (10.2%), deciduous (10.2%), and herbaceous (14.3%) (Table 5). We observed more dispersed changes in the Upper Blackfoot reach including conversions to bare ground from coniferous, deciduous, and herbaceous canopy at 4.1%, 6.2%, and 8.2%, respectively. We recorded additional conversions from deciduous (7.5%) and herbaceous (5.5%) canopy to coniferous canopy in the Upper Blackfoot reach. We interpret these results to indicate fewer patches of coniferous, deciduous, and herbaceous canopy that are significantly smaller in size, compared to the distribution of riparian canopy in 1964. Further, since 1964 we saw the same number of bare ground patches, but they were substantially larger.

We see a similarity in the patterns of the 1938–1964 and 1964–1978 photo periods, except the latter is more strongly expressed. Figure 8 shows clearly the path of the most powerful flows of dam failure flood. What remains is an upland border of coniferous canopy surrounding a barren floodplain. Schmitz and others (2009) portrayed the same pattern following a catastrophic dam failure flood on Pattengail Creek in Western Montana. During ground-truthing in 2007, we observed boulder-sized sediment deposited as overbank gravel bars. Further, we suggest that the response of the Anaconda reach indicates that it received much lower energy flows than the Beartrap and Upper Blackfoot reaches. In light of this evidence, the response of the riparian vegetation can only be attributed to the dam failure flood of 1975. While we believe that the Anaconda reach could have been used as a reference reach in the context of restoration potential for Beartrap and Upper Blackfoot, the impacts of the dam failure are too great for recovery to occur naturally in our lifetime.

4.6. Recovery from Dam Failure—1995

Following the dam failure, the USFS and State of Montana engaged in regulatory action to clean up the toxic deposits and attenuate any remaining hazard to habitat and downstream residences and towns (US Forest Service 2007). This instigated an ongoing effort to monitor surface and groundwater and to evaluate options for dealing with contaminated sediment. Envirocon, Inc., (1993) conducted a floodplain analysis to identify tailings deposits transported by the dam failure flood that would threaten downstream habitat in the event of a 100-year flood. In addition, researchers pursued opportunities to assess the geomorphology and aquatic habitat condition following the dam failure flood. Spence (1977) and Moore (1992) conducted studies on the aquatic resources following the dam failure flood. Vandeberg (2005) revealed that the trace elements that remain in the floodplain sediment can be reactivated during subsequent high flow events. During the time of the majority of the regulatory actions and environmental analyses, there was a period of low snow years from 1975 to 1988 (Figure 10). The years from 1989 to 1995 were high snow years coupled with moderate runoff (Figure 9).

In Anaconda, we observed an increase in deciduous and herbaceous cover and point observations with corresponding decreases in coniferous values between 1978 and 1995 (Figure 8). Also, we delineated fewer patches of coniferous, deciduous, and herbaceous vegetation in this photo year. We assessed the largest point location changes from coniferous to deciduous canopy (18.2%) and from coniferous to herbaceous canopy (Table 4). Given the increase in colonization of bare ground and increase in structural complexity, we suggest that these data indicate recovery of the Anaconda reach from the 1975 rain-on-snow event.

We detected very little change in canopy cover, number of polygons, or point observations of the four canopy types assessed in the Beartrap and Upper Blackfoot reaches. However, we saw a decrease in number of coniferous polygons that we suggest indicates a minor amount of recovery. Given the extensive reworking of these floodplains with coarse substrate following the dam failure flood, we find the lack of recovery in 20 years reasonable.

4.7. The Need for Restoration—2005

In the 10 years since the last aerial photo assessment, we have no evidence of impactful events along the Anaconda reach. We observed an increase in coniferous cover and number of point observations as well as decreases in the deciduous and herbaceous parameters along the Anaconda reach (Figure 8). Further, the point location changes indicate conversion from deciduous and herbaceous canopy to coniferous (Table 4). The number of polygons of all canopy types decreased, which we interpret as typical riparian habitat succession.

We observed no significant differences in canopy cover, number of patches, or point observations in the Beartrap and Upper Blackfoot reaches since 1995 with one exception. Since 1978, we assessed a decline in coniferous cover in the Beartrap reach. We attribute this decrease to the gradual die-off of coniferous trees following the dam failure flood where they may have succumbed to the trauma of burial, flood scars, toxicity, or being stranded above the water table.

4.8. Watershed Relationships

We tested the watershed variables to identify those with the most explanatory power for each of the study reaches using the point observation dataset. Of the 11 tested (Appendix B), we chose six due to their low correlations and widest distributions among the canopy types and changes in canopy type for each photo period. We found high correlations among watershed variables for each reach. They ranged between 0.826 and 0.999 for Anaconda, 0.854 and 0.999 for Beartrap, and 0.935 and 0.999 for Upper Blackfoot (Appendix C). We detected different relationships between canopy type and watershed variable distribution in the box plots for each photo year for each reach (Appendix D). Likewise, we found similar relationships for canopy type change for each photo year (Appendix E). Ultimately, for GLM analysis we chose to test drainage area (DA), elevation above the riparian area (EARAVG), site elevation (SELEV), stream network elevation (SNEAVG), upslope basin elevation (UBEAVG), and upslope basin gradient (UBGAVG).

4.8.1. Anaconda

In Anaconda, we found significant GLMs for coniferous and herbaceous canopy types (Table 7). For coniferous canopy cover, we discovered four significant GLMs with the 1938 vegetation data and single watershed variables that explained 18.5–21.5% of the deviance and accurately predicted 77.3%. We produced no significant GLMs from the 1964, 1978, 1995, or 2005 coniferous canopy data. For herbaceous canopy cover, we found significant GLMs for the 1938, 1978, and 1995 coniferous dataset. These models explained 11.5–23.6% of the deviance and predicted 77.3–81.8% (Table 7). We found no significant multivariate models using the Anaconda datasets.

In the best performing 1938 coniferous model for Anaconda, we found that decreasing UBEAVG was related to higher probabilities of coniferous canopy cover. We detected similar relationships with SELEV, SNEAVG, and UBGAVG that explained slightly less deviance. We suggest that the influence of low elevation watershed characteristics indicates hillslope hydrology is a driving force behind the coniferous vegetation on the Anaconda valley bottom.

We found significant results in the Anaconda univariate GLMs for the 1938, 1978, and 1995 herbaceous datasets. All of the 1938 models accurately predicted 81.8% of the herbaceous cover, while all of the 1978 and 1995 models predicted 77.3%. We discovered that increasing EARAVG and UBGAVG corresponded with high probabilities of herbaceous cover in 1938, 1978, and 1995. Further, we detected that EARAVG explained the most deviance, but UBGAVG exerted the greatest effects on herbaceous cover.

Table 7: Summary of Best Logistic GLMs for Anaconda.

Cover Type	Year	Predictor	Coefficient	Deviance Explained	Accuracy	Df (residual/null)	AIC
Coniferous	2005	ALL	NS				
	1995	ALL	NS				
	1978	ALL	NS				
	1964	ALL	NS				
	1938	DA	0.00	18.9	77.3	20/21	28.561
		EARAVG	NS				
		SELEV	-0.44	20.4	77.3	20/21	28.125
		SNEAVG	-0.99	18.5	77.3	20/21	28.714
		UBEAVG	-1.55	21.5	77.3	20/21	27.791
		UBGAVG	-61.58	19.9	77.3	20/21	28.285
Deciduous	2005	ALL	NS				
	1995	ALL	NS				
	1978	ALL	NS				
	1964	ALL	NS				

Cover Type	Year	Predictor	Coefficient	Deviance Explained	Accuracy	Df (residual/null)	AIC
	1938	ALL	NS				
Herbaceous	2005	ALL	NS				
	1995	DA	0.00	20.2	77.3	20/21	27.440
		EARAVG	1.35	21.4	77.3	20/21	27.401
		SELEV	0.40	19.2	77.3	20/21	28.050
		SNEAVG	0.97	20.5	77.3	20/21	27.660
		UBEAVG	1.35	18.0	77.3	20/21	28.420
		UBGAVG	57.11	19.6	77.3	20/21	27.920
	1978	DA	0.00	12.6	77.3	20/21	28.050
		EARAVG	1.07	16.1	77.3	20/21	27.080
		SELEV	0.30	11.5	77.3	20/21	28.370
		SNEAVG	0.72	13.0	77.3	20/21	27.900
		UBGAVG	42.21	11.9	77.3	20/21	28.240
	1964	ALL	NS				
	1938	DA	0.00	22.6	81.8	20/21	23.950
		EARAVG	1.32	23.6	81.8	20/21	23.700
		SELEV	0.43	21.7	81.8	20/21	24.180
		SNEAVG	1.00	22.8	81.8	20/21	23.900
		UBEAVG	1.51	20.6	81.8	20/21	24.470
		UBGAVG	60.68	22.1	81.8	20/21	24.080
Bare ground	2005	ALL	NS				
	1995	ALL	NS				
	1978	ALL	NS				
	1964	ALL	NS				
	1938	ALL	NS				

Note: NS indicates model did not meet p-value criteria of 0.1.

4.8.2. Beartrap

In Beartrap, we identified significant relationships between watershed structure and the 1938 deciduous cover and the 1964 herbaceous data (Table 8). We identified UBGAVG as the most influential variable in both groups of models. For 1938, before dam construction, we found that watershed relationships accounted for a small yet significant amount of deviance (6.1–6.9%) and accurately predicted 59.1–67.3% of the deciduous canopy. We detected an identical set of relationships with better performance for the 1964 herbaceous canopy. These results indicate that decreasing network elevation distributions, less steep network gradients, and lower site elevations corresponded with increases in deciduous canopy during times of limited disturbance. We found no significant multivariate GLMs for the Beartrap reach.

Table 8: Summary of best logistic GLMs for Beartrap.

Cover Type	Year	Predictor	Coefficient	Deviance Explained	Accuracy	Df (residual/null)	AIC
Coniferous	2005	ALL	NS				
	1995	ALL	NS				
	1978	ALL	NS				
	1964	ALL	NS				
	1938	ALL	NS				
Deciduous	2005	ALL	NS				
	1995	ALL	NS				
	1978	ALL	NS				
	1964	ALL	NS				
	1938	DA	0.000	6.30	59.180	47/48	65.323
		EARAVG	-0.117	6.10	59.180	47/48	65.459
		SELEV	-0.070	6.90	67.300	47/48	64.916
		SNEAVG	-0.189	6.70	67.300	47/48	65.060
		UBEAVG	-0.117	6.08	59.180	47/48	65.459
Herbaceous	2005	ALL	NS				
	1995	ALL	NS				
	1978	ALL	NS				
	1964	DA	0.000	11.90	81.600	47/48	45.161
		EARAVG	-0.175	11.80	81.600	47/48	45.242

Cover Type	Year	Predictor	Coefficient	Deviance Explained	Accuracy	Df (residual/null)	AIC
		SELEV	-0.106	11.00	81.600	47/48	45.575
		UBEAVG	-0.175	11.76	81.600	47/48	45.242
		UBGAVG	-5.113	12.18	81.600	47/48	45.043
	1938	ALL	NS				
Bare ground	2005	ALL	NS				
	1995	ALL	NS				
	1978	ALL	NS				
	1964	ALL	NS				
	1938	ALL	NS				

Note: NS indicates model did not meet p-value criteria of 0.1.

4.8.3. Upper Blackfoot

We discovered numerous significant univariate and multivariate GLMs for canopy cover in the Upper Blackfoot reach (Table 9 and Table 10). For coniferous canopy, we recorded univariate GLMs for 1964, 1995, and 2005. We identified univariate GLMs for 1964 and 2005 for deciduous canopy. We found univariate GLMs for 1964, 1978, and 2005 for herbaceous canopy. Lastly, we detected univariate GLMs for 1964, 1978, 1995, and 2005 for bare ground. Despite high prediction accuracies of 58.2–92.5%, the majority of the univariate models explained less than 7% deviance. Further, we noticed in virtually all low deviance-explained model groups that UBGAVG had the greatest influence on canopy cover, regardless of type. We explored the multivariate GLMs only to find little deviance explained (3.4–9.4%) and moderate prediction accuracies (57.5–71.9%) (Table 8).

We found univariate models with high prediction accuracies and that explained high amounts of deviance in the herbaceous and deciduous model group. In the herbaceous GLMs, watershed variables explained 21.3–28.73% deviance and accurately predicted 97.2% of the herbaceous cover. Further, while the coefficients were less than 1.0, we identified EARAVG and SNEAVG as the most influential variables of the group. In the deciduous GLMs, watershed variables explained 17.8–21.0% deviance and accurately predicted 95.9% of the deciduous canopy. Notably, we found that UBGAVG, and to a lesser degree SNEAVG, exerted the greatest effect on deciduous cover.

We found different suites of variables in the significant multivariate GLMs, two for coniferous cover and three for bare ground (Table 10). All exhibited low coefficients. For the 1964 coniferous multivariate GLM, we found UBEAVG and SELEV to have opposing influences on coniferous cover in the Upper Blackfoot, positive and negative, respectively. We interpret this model to indicate increasing probabilities of coniferous cover. This model explained 5.1% deviance and accurately predicted 71.9% coniferous canopy. We identified EARAVG and

UBGAVG as significant watershed variables in the 2005 multivariate GLM. The combined effect of decreasing EARAVG and increasing UBGAVG corresponded with increasing probabilities of coniferous cover. The model explained 8.5% deviance and accurately predicted 65.8% coniferous cover. In the 2005 multivariate deciduous GLM, we found decreasing EARAVG combined with increasing SELEV to align with increasing probabilities of deciduous canopy. This model explained 9.35% deviance but only accurately predicted 59.6% deciduous cover.

Table 9: Summary of best logistic GLMs for Upper Blackfoot.

Cover Type	Year	Predictor	Coefficient	Deviance Explained	Accuracy	Df (residual/null)	AIC
Coniferous	2005	SNEAVG	-0.230	6.11	63.010	144/145	182.520
		SELEV	-0.077	5.67	64.383	144/145	183.350
		EARAVG	-0.105	4.63	59.589	144/145	185.330
		UBEAVG	-0.108	4.56	63.010	144/145	185.470
		UBGAVG	-1.892	4.15	64.383	144/145	186.250
		DA	0.000	4.03	64.380	144/145	186.460
	1995	SNEAVG	-0.230	5.68	64.383	144/145	165.710
		SELEV	-0.076	5.27	64.383	144/145	166.420
		EARAVG	-0.109	4.56	64.383	144/145	167.620
	1978	ALL	NS				
	1964	DA	0.000	3.03	71.917	144/145	172.120
		EARAVG	0.077	2.78	71.917	144/145	172.550
		UBGAVG	1.477	2.76	71.917	144/145	172.520
		UBEAVG	0.078	2.60	71.917	144/145	172.800
		SELEV	0.042	1.90	71.917	144/145	174.010
	1938	ALL	NS				
Deciduous	2005	UBEAVG	0.300	21.04	95.890	144/145	43.520
		DA	0.000	21.02	95.890	144/145	43.532
		EARAVG	0.284	20.69	95.890	144/145	43.695
		UBGAVG	5.524	20.57	95.890	144/145	43.754
		SELEV	0.196	19.62	95.890	144/145	44.233
		SNEAVG	0.550	17.85	95.890	144/145	45.119
	1995	ALL	NS				
	1978	ALL	NS				
	1964	SNEAVG	-0.182	3.40	81.506	144/145	139.060
		DA	0.000	2.98	81.506	144/145	139.650
		SELEV	-0.058	2.92	81.506	144/145	139.730

Cover Type	Year	Predictor	Coefficient	Deviance Explained	Accuracy	Df (residual/null)	AIC
		EARAVG	-0.090	2.90	81.506	144/145	139.750
		UBEAVG	-0.092	2.84	81.506	144/145	139.840
		UBGAVG	-1.632	2.70	81.506	144/145	140.040
	1938	ALL	NS				
Herbaceous	2005	EARAVG	0.468	28.73	97.260	144/145	30.133
		UBEAVG	0.381	24.88	97.260	144/145	31.544
		SNEAVG	0.781	23.01	97.260	144/145	32.232
		SELEV	0.227	21.32	97.260	144/145	32.851
	1995	ALL	NS				
	1978	DA	0.000	4.59	92.465	144/145	78.455
		UBGAVG	2.105	4.56	92.465	144/145	78.477
		EARAVG	0.102	4.08	92.465	144/145	78.853
	1964	SELEV	0.056	3.10	80.821	144/145	142.300
		SNEAVG	0.156	2.91	80.821	144/145	142.580
		UBEAVG	0.078	2.57	80.821	144/145	143.060
		UBGAVG	1.414	2.45	80.821	144/145	143.240
		EARAVG	0.073	2.43	80.821	144/145	143.260
		DA	0.000	2.21	80.821	144/145	143.570
	1938	ALL	NS				
Bare ground	2005	DA	0.000	6.54	58.210	144/145	189.470
		EARAVG	-0.121	6.17	58.210	144/145	190.200
		EARAVG	-0.121	6.17	58.210	144/145	190.200
		UBGAVG	-2.297	6.12	58.210	144/145	190.290
		UBEAVG	-0.119	5.64	58.210	144/145	191.250
		SNEAVG	-0.189	4.43	58.210	144/145	193.640
		SELEV	-0.065	4.35	58.210	144/145	193.810
	1995	DA	0.000	1.52	60.273	144/145	197.200
		UBGAVG	-1.091	1.50		144/145	197.240

Cover Type	Year	Predictor	Coefficient	Deviance Explained	Accuracy	Df (residual/null)	AIC
		EARAVG	-0.056	1.48	60.273	144/145	197.270
	1978	DA	0.000	3.26	50.000	144/145	198.850
		UBGAVG	-1.584	3.15	52.000	144/145	199.060
		EARAVG	-0.077	2.74		144/145	199.890
	1964	SNEAVG	-0.134	2.11	73.287	144/145	169.900
		SELEV	-0.042	1.77	73.287	144/145	170.470
	1938	ALL	NS				

Note: NS indicates model did not meet p-value criteria of 0.1.

Table 10: Summary of best multivariate logistic GLMs.

Cover Type	Year	Predictors	Coefficient	Deviance Explained	Accuracy	Df (residual/null)	AIC
Coniferous	2005	EARAVG	-0.514	8.50	65.753	143/145	179.980
		+UBGAVG	0.691				
	1995	SNEAVG	NS				
	1978	ALL	NA				
	1964	UBEAVG	0.656	5.10	71.917	143/145	170.520
		+SELEV	-0.376				
	1938	ALL	NA				
Deciduous	2005	ALL	NS				
	1995	ALL	NA				
	1978	ALL	NA				
	1964	ALL	NS				
	1938	ALL	NA				
Herbaceous	2005	ALL	NS				
	1995	ALL	NA				
	1978	ALL	NS				

Cover Type	Year	Predictors	Coefficient	Deviance Explained	Accuracy	Df (residual/null)	AIC
	1964	ALL	NS				
	1938	ALL	NA				
Bare ground	2005	EARAVG	-0.564	9.35	59.589	143/145	185.890
		+SELEV	0.290				
	1995	DA	0.000	3.35	57.534	143/145	195.540
		+SELEV	0.000				
	1978	DA	0.000	6.32	60.273	143/145	194.690
		+EARAVG	0.000				
	1964	ALL	NS				
	1938	ALL	NA				

5. DISCUSSION

5.1. Temporal Distributions

We sought to detect changes in riparian canopy distribution as they relate to dam construction and dam failure using aerial estimates and point observations. We used the Anaconda reach and the 1938 data from all reaches as a reference reach to varying degrees of success. We found the Anaconda reach to be responsive to the 1964 and 1975 runoff events, in addition to maintaining adequate riparian function throughout the mining era of the region. This was evidenced by an increase in bare ground following the runoff events, followed by expansions of deciduous and herbaceous canopy types. Encroachment of coniferous cover occurred after 10 or more years since that last major disturbance. This follows riparian succession reported elsewhere (Johnson 1994; Baker and Walford 1995; Greco and Plant 2003). Due to the short length of the reach and small number of point observations, we found the utility of the Anaconda reach as a reference to be limited. From the 1938 Beartrap and Upper Blackfoot data, we inferred the presence of riparian function from the few but continuous patches of coniferous, deciduous, and herbaceous patches. Thus, the combination of temporal data from the Anaconda reach and the 1938 Beartrap and Upper Blackfoot data provide a useful context for restoring the Beartrap and Upper Blackfoot reaches to pre-mining functional levels.

We present evidence of impacts due to dam construction, dam failure, and mining-related activities. The response of the Beartrap and Upper Blackfoot reaches to dam construction and mining-related activities indicates increased bare ground and fragmentation of riparian vegetation following the lifting of MHD in 1941 and its failure in 1975. The response of the Beartrap and Upper Blackfoot reaches to the dam failure flood was catastrophic. Schmitz (2009) reported a similar loss of vegetation and increase in bare ground following the Pattengail Dam failure flood in 1927. Ninety years later, riparian vegetation has not returned due to marked channel downcutting and coarse substrate. The Mike Horse study area will likely experience a similar fate without active restoration.

5.2. Watershed Relationships

Network organization and structure, fluvial processes and climate all strongly influence the hydrology of a riparian zone (Bendix 1994; McDonnell, McGlynn et al. 1998; McGlynn and Seibert 2003). All these factors are driven (or influenced in the case of climatic factors) by the topography of the watershed (elevation and position within the watershed) (Wallace and Oliver 1990; Kirkby 1993). We found that UBGAVG was the major variable influencing riparian canopy type in the study area. UBGAVG is an indication of the steepness of the area contributing to a point on a stream. McGlynn and others (2003) described headwater reaches as tending to have steeper contributing areas than reaches lower in the basin. Therefore, residence time of runoff tends to be shorter in steeper watersheds (headwater) than in those with gentler slopes (Beven and Kirkby 1979). We detected other highly influential watershed characteristics, but their effects were not persistent enough to make inferences about specific events. We observed SNEAVG, EARAVG, and SELEV to affect canopy cover distribution in similar ways to UBGAVG. We interpreted these relationships as indicators of steep contributing areas to the Mike Horse study area riparian zones and having the capacity to convey high energy flows during runoff periods.

In the GLM results, there is a trend for coniferous and bare ground canopy to respond in the opposing direction from deciduous cover, in relation to AVG (Table 7, Table 8, Table 9, and Table 10). That is, in a given reach for a given year, if there is a significant relationship between canopy type and UBGAVG, then the relationship of UBGAVG to deciduous cover runs counter to that with coniferous or bare ground. In general, increasing deciduous cover indicates riparian expansion. Coniferous expansion is a sign of upland encroachment, or riparian area constriction. And bare ground suggests recent disturbance such as erosive flows or surface activity. Whether riparian expansion or contraction occurred in a given reach for a given year was quite variable. In some models, riparian expansion aligns with increasing UBGAVG suggesting that increased runoff or the timing of recent runoff periods facilitated deciduous species in the valley bottom. In other models, upland encroachment or bare ground expansion aligned with increasing UBGAVG. This suggests that recent runoff periods conveyed scouring flows or they occurred at times that caused dry floodplain conditions. These circumstances would have created bare ground or allowed coniferous species to thrive.

The relationships detected using logistic regression are significant in that they indicate the consistent influence of steep gradient contributing areas over time, space, and a variety of natural and anthropogenic events. However, the relationships to canopy cover are not consistent enough to infer anything further about the specific events or processes. Thus, we cannot ascribe any patterns of watershed–canopy type relationship to dam construction or dam failure using this dataset at this time.

A watershed dataset constructed with a multi-flow direction algorithm may have produced a stronger signal that regression analysis could detect. Uni-direction flow algorithms like the D8 found in ArcHydro 8.0 are less sensitive than multi-flow direction algorithms because all flow is routed to a single cell (Tarboton 1997; McGlynn and Seibert 2003). Multi-flow direction algorithms more closely resemble spatial patterns of flow that affect riparian hydrology. Repeat analysis with a multi-flow algorithm might provide a more continuous (less discrete) dataset that, in turn, would produce a stronger signal to be detected using GLMs. Additional reference area transects in other tributaries such as Pass and Shave Creeks may provide more watershed–canopy type relationships from which to describe changes in the Beartrap and Upper Blackfoot reaches. However, these data provide the proof of concept for others to conduct watershed analyses aimed at establishing adequate reference data to construct a restoration plan.

6. SUMMARY

Because riparian areas integrate multi-scale factors in space and time, attributing changes to specific events is a difficult task. However, the use of reference data such as the 1938 dataset and the Anaconda datasets allows us to make inferences into cause. We saw the largest change in canopy distribution on Beartrap and Upper Blackfoot in 1978, three years after the dam failure flood. Our data from 1995 and 2005, in addition to ground surveys in 2007, indicate little recovery has taken place in the 32 years since the flood. We provided evidence of active relationships to watershed-scale processes in the Beartrap and Upper Blackfoot reaches. By combining these data with detailed watershed analyses and designs for dynamic channels and floodplains, restoration of riparian function to 1938 levels is achievable.

We feel the summary of this project should be presented relative to the objectives listed in Section 2.0 of this report.

- Objective 1 – Determine the channel response potential of different stream reaches.

The response of the Beartrap and Upper Blackfoot reaches to dam construction and mining-related activities indicates increased bare ground and fragmentation of riparian vegetation following the lifting of MHD in 1941 and its failure in 1975. The response of the Beartrap and Upper Blackfoot reaches to the dam failure flood was catastrophic. Schmitz (2009) reported a similar loss of vegetation and increase in bare ground following the Pattengail Dam failure flood in 1927. Ninety years later, riparian vegetation has not returned due to marked channel downcutting and coarse substrate. The Mike Horse study area will likely experience a similar fate without active restoration.

If contaminated sediments are removed and natural floodplain and channel structure and function are restored using templates like Anaconda, Pass and Shave Creeks, there is a good chance the stream channels will respond and begin to provide natural function and better habitat for aquatic species.

- Objective 2 – Estimate the peak flow caused by the 1975 dam breach event.

We estimated a flood flow of 11.5 m^3/s for Mike Horse Creek and Beartrap Creek combined (Upper Blackfoot Reach 1), 15.2 m^3/s for Anaconda Creek, and 26.7 m^3/s for the Upper Blackfoot (Upper Blackfoot Reach 2 downstream of confluence of Beartrap and Anaconda). These values compared very well with the 100-year flood estimated using the Regional Regression equations.

- Objective 3 – Determine the vegetative response of riparian communities along different stream reaches.

We saw the largest change in canopy distribution on Beartrap and Upper Blackfoot in 1978, three years after the dam failure flood. Our data from 1995 and 2005, in addition to ground surveys in 2007, indicate little recovery has taken place in the 32 years since the flood.

We found the Anaconda reach to be responsive to the 1964 and 1975 runoff events, in addition to maintaining adequate riparian function throughout the mining era of the region. This was evidenced by an increase in bare ground following the runoff events, followed by expansions of deciduous and herbaceous canopy types. Encroachment of coniferous cover occurred after 10 or more years since that last major disturbance. This follows riparian succession reported elsewhere (Johnson 1994; Baker and Walford 1995; Greco and Plant 2003).

- Objective 4 – Predict areas of high and low risk to impacts of dam hazard reduction for use in a monitoring program.

Because the channels in Beartrap Creek and the Upper Blackfoot in the study area are so severely impacted from the 1975 dam breach, we feel there is little risk that the dam hazard reduction will have any adverse effects on them. Any effort to improve natural channel function by removal of contaminated sediments and restoring natural structure and function using templates from Anaconda, Pass and Shave creeks will benefit these stream channels and aquatic organisms.

A monitoring program that incorporates water quality measurements, channel geomorphic characteristics and vegetation surveys conducted at transects located near transects used in this project will allow for detailed pre-hazard reduction to post-hazard reduction comparisons. The number of monitoring transects will depend on the budget for the monitoring program.

Monitoring transects should be placed at locations that capture the entire area between the dam and the most downstream transect in this study. For example, if there is only budget to collect data at three transects, they should be located at the very upstream end of this study near the dam, at the midpoint of the study area, and at the most downstream end of the study area. In addition, at least one transect should be placed in a reference reach like Anaconda to provide a control for data related to changes in a relatively undisturbed stream and channel. The sample size for monitoring should be selected at a sufficient number of transects in both the disturbed (treatment) and relatively undisturbed (control) watersheds like Anaconda to achieve statistical significance.

7. APPENDICES

Appendix A

ASSESSING THE POTENTIAL FOR CONTAMINANTED SEDIMENT
RESUSPENSION FROM A MINE IMPACTED WETLAND

by

Jessica Elyce Mason

A professional paper submitted in partial fulfillment

of the requirements for the degree

of

Master of Science

in

Civil Engineering

MONTANA STATE UNIVERSITY

Bozeman, Montana

May 2009

TABLE OF CONTENTS

LIST OF TABLES

LIST OF FIGURES

LIST OF APPENDICES

Appendix

ABSTRACT

Wetlands associated with Montana hard rock mines play a paradoxical role. The benefit of attenuating flood water and sediment has led to wetlands serving as sinks for metal precipitates and contaminated sediment. However, during high spring runoff or storm events these wetlands may become significant sources of resuspended contaminated sediments and generate potential impacts to downstream recipients. Using a loosely coupled hydraulic model (HEC-RAS) and a GIS, we explored the influence of flood events of varying magnitude on stream hydraulics and sediment mobilization across a wetland complex located in the Blackfoot River near Lincoln, MT. Field survey data provided a topographic template for running the hydraulic model. Spatial interpolation and geostatistical methods were used to create spatially continuous data surfaces for model input parameters (i.e. roughness coefficient, D_{50}), measured contaminant concentrations (As, Cu, Zn, Cd, Pb) for the upper 2 inches of soil, model output parameters (i.e. velocity, water depth), and critical velocity. Combining critical velocity data layers with modeled velocity and contaminant concentration data layers allowed us to identify zones with high contaminant concentrations and a high potential for sediment mobilization in a spatially explicit manner. Sensitivity analysis showed the one-dimensional hydraulic model to be increasingly sensitive to roughness coefficients with increasing discharge. Comparison of modeled stream velocity distributions to measured velocity distributions showed deviations from observed data in shallow near-bank and over-bank areas. Thorough investigation of differences between modeled and measured velocity distributions at a range of flows and across several transects at a given site will help practitioners decide whether or not this approach will be useful and provides an avenue for future flood risk assessment. We conclude that when carefully applied, this approach may be a valuable tool for assessing contaminated sediment mobilization risk in areas where data is limited and/or development of more data intensive models is not feasible.

1.0 INTRODUCTION

1.1 EXECUTIVE SUMMARY

Hydrologic and hydraulic analyses are used by scientists and engineers for environmental and regulatory decisions. The integration of spatial analysis and hydrological modeling by way of geographic information systems (GIS) is becoming an integral component of flood assessment practices. The potential environmental impacts to downstream groundwater, surface water, and sediment quality affect human, aquatic, and riparian resources (Werner 2001). Flood risk assessment calls for a thorough spatial evaluation of a flood event, where risk is defined as the relationship between hazards in the area and the area's vulnerability, and GIS provides a tool for this type of analysis. This study models the effect of discharge events with varying return intervals in order to assess the potential for sediment transport from a mine-impacted wetland in the Upper Blackfoot Mining Complex (UBMC). There has been substantial work to assess and remediate the impact of the UBMC on aquatic resources by Helena National Forest (HNF), Montana Department of Environmental Quality (MTDEQ), and the mining company, ASARCO. Until recently, however, the wetland complex has largely been omitted from environmental assessments.

The benefit of attenuating flood water and sediment has led to some wetlands serving as sinks for metal precipitates and contaminated sediment. However, during high spring runoff or storm events these wetlands may become significant sources of resuspended contaminated sediment. An essential step for mine-impacted wetland and water resource management and conservation is the capability to predict the impacts of floods on wetlands (Thompson et al. 2004b). Combining surface water hydrology and hydraulic modeling with a GIS provides a method for assessing the potential for resuspension of metals from mine-impacted wetlands currently serving as contaminant sinks. This proof-of-concept report details a methodology that authorities may use to judiciously apply remediation efforts to impacted wetlands.

Identifying critical shear stresses for channel and floodplain areas for several flood frequencies provides a relatively straightforward method for assessing the probability of sediment erosion and transport in contaminated floodplain zones. Erosion is a result of increased shear stresses on soil particles on the channel bed and overbank surfaces. Large storm events may cause sediments, typically smaller sediment particles, within a wetland to erode when the critical shear stress is surpassed. Critical shear stress is the maximum unit tractive force a particle can withstand. Metals that are resuspended, adsorbed to sediments, or precipitated behave as any other sediment in a fluvial environment (Gibbs 1973). Therefore, improved understanding and simulation of flood risk analysis will assist water resource managers and restoration practitioners in future remediation efforts. It is hoped that incorporation of the methodology presented in this report into current remediation strategies will benefit downstream recipients of water from the mine-impacted wetland as well as researchers, and state and local organizations concerned with flood prediction, mapping, and risk assessment.

This report evaluated a method for assessing potential contaminant resuspension given a data set that included topography, flow, and sediment parameters. Remediation requires knowledge of the metals distribution and an understanding of the potential for resuspension. We utilized a loosely coupled modeling technique that integrates a one-dimensional hydraulic model (HEC-RAS) and a GIS via an extension, HEC-geoRAS. The selected hydraulic model—HEC-RAS (developed by the U.S. Army Corps of Engineers)—is a widely used model and requires relatively little input data, especially when coupled with digital elevation models (DEM) in a GIS. Due to its relative simplicity and low data requirements when compared to more complicated 2D or 3D hydraulic models, it is believed that this approach is a viable option for assessment of sediment suspension risk. This is an especially attractive approach for large sites where costs prohibit the collection of fine scale spatial data needed to accurately parameterize complex models. The methodology described in this report aims to determine the potential for resuspension of sediments within inundated areas corresponding to various extreme discharge events. Locations in the study area that warrant attention from governing agencies and consultants for possible removal from the dynamic fluvial system are identified.

1.2 BACKGROUND

Risk and mine impacted wetlands

The legacy and future of mining in Montana will likely impact wetlands located downstream from mine adits and tailings piles for generations. The wetland downstream of the McLaren Mine in the Stillwater basin is a prime example. The Stillwater wetland has been assessed for metals distribution and the origin of those metals (Cook 2007; Furniss et al. 1999; Gurrieri 1998). Cook (2007) found that metals concentrations increased with depth in the floodplain due to sediment trapping and decreased with depth in the channel due to annual flushing. August et al. (2002) studied a mine-impacted wetland near Leadville, Colorado and found the wetlands have a finite ability to retain metals and predict they will eventually shift from being a contamination sink to a source. Despite these risks, no hazard assessments of metals-laden wetlands have been conducted to date. Instead, most studies point to these wetlands as sinks that should not be disturbed (e.g. Moore 1992).

The Upper Blackfoot wetland has been studied for several decades. The impact of more than a century of silver, lead, and zinc mining has drawn attention from federal and state officials and research scientists. Spence (1975) inventoried the aquatic biota and water quality before and after a 1975 dam breach that drastically altered water quality in the drainage. The role of the wetlands in attenuating the impact of mine tailings transport during the flood was considered limited. Moore (1992) evaluated aquatic biota upstream and downstream of the wetland ten years later and found that contaminated sediment is transported downstream of the wetland during high flows. This impacts the food web of the drainage through bioaccumulation. Dolhopf, et al. (1988) evaluated the wetland for its ability to remove water borne contamination carried from upstream sources. They estimated that approximately 550 metric tons of iron is deposited in the wetland. The DEQ recently embarked on a damages assessment that includes the wetland (TetraTech 2007). This study will map the distribution of contaminants deposited during the dam breach flood of 1975. Currently, the potential for these contaminants to be resuspended has not been evaluated.

Most of the focus on mine impacted wetlands has been to identify the source of contamination and assign responsibility for damages. Most often these wetlands are sinks for contamination and left in place to protect downstream resources. However, August et al. (2002)

showed that mine impacted wetlands are finite sinks that may eventually become contaminate sources. Helena National Forest (HNF) is currently removing a major source of metals-laden sediment upstream of the wetland (an impoundment and tailings dam); however, there remains a second significant source of surface flow from the Mike Horse Mine adit. Any disturbance to contaminated sediment (natural, remedial, or constructive) will cause metals resuspension as well as alter the biogeochemical environment with an increase in metals mobilization.

Modeling floods and erosion

Extensive research and risk assessment of sites with contaminated sediment typically involves chemical identification and an evaluation of the quantities and location of pollutants. The inherent risk of erosion of contaminated sediment which eventually leads to transport and deposition further downstream requires knowledge of sediment behavior and the hydraulic forces acting on the riverbed (Haag et al. 2001). When contaminated sediments are suspended into the water during erosion, the bioavailability and toxicity levels usually increase generating hazardous conditions for aquatic life and downstream recipients. Forstner (2004) suggests a model for evaluating the mobility of contaminated sediment that incorporates measurements of sediment regions, shear stress, and critical shear stress. Therefore, assessing the environmental impacts of contaminated sediment involves an evaluation of the risk of erosion due to hydraulic forces and potential transport during a flood event.

Intricate analysis and simulation capabilities are available with both hydrologic/hydraulic models and GIS, and the integration of the two provides a powerful tool for scientific researchers and policy makers. The widespread availability of spatially distributed data through GIS has made physically based hydrologic models more useable and spurred the development of hydrologic models that take advantage of these new data. Engineering hydrology has time-tested empirical approaches for hydrologic modeling, and the development of hydrologic models that can better simulate spatially varied hydrology involves a combination of these practices with the data-handling capabilities of GIS and enhanced processing involved with GIS modules (Sui and Maggio 1999). Further development of scaling relationships for spatially distributed hydrologic variables will lead to improved performance of the integrated models. Hydrologic and GIS models, however, have inherently different temporal data representation schemes. The input, storage, and management of time varying data are not adequately facilitated by GIS technology to date. GIS has a rigid spatial-temporal framework that restricts complex hydrological processes; therefore, coupling hydraulic modeling results and GIS becomes an interactive process incorporating uncertainty during information exchange (Ogden et al. 2001; Sui and Maggio 1999).

A variety of software is available that attempts to integrate GIS and hydrologic/hydraulic models. Loose coupling is the most widely used practice by GIS and hydrologic/hydraulic modelers. This technique combines a GIS package and hydrologic/hydraulic modeling programs, such as HEC-1, HEC-2, or STORM, and statistical packages, such as SAS or SPSS. Without a common user interface, data is exchanged between the three packages via a common language or format (ASCII or binary data format) and requires extensive data development, which can be labor intensive and error prone (Ogden et al. 2001; Sui and Maggio 1999).

The majority of robust hydraulic engineering models, including HEC, MIKE 11, and ISIS, incorporate one-dimensional flow routing approaches. Additional flood simulation approaches that accommodate more realistic physical and hydrodynamic conditions in river processes require two- and three-dimensional analysis. One-, two-, and three-dimensional hydraulic modeling approaches incorporate terrain analysis and the calculation of flood extents and depth by means of GIS, and each has advantages and disadvantages for use in flood risk estimates.

Exercising a loosely coupled modeling technique, the one-dimensional HEC-RAS model (U.S. Army Corps of Engineers) has the capability to incorporate georeferenced cross-section data into its model coordinate system for hydraulic analysis through modeling software, such as HEC-geoRAS. Techniques for coupling the results from one-dimensional flow models with a GIS involve geostatistical interpolation, neighborhood analysis, and calculating interception points of water levels in the cross section profile (Werner 2001). For hydraulic modeling of river channels, high resolution digital terrain models (DTM) provide detailed cross-sections for analysis and the location of the channel thalweg, but these are typically only available through land survey data or remote sensing.

One-, two-, and three-dimensional models each have advantages and disadvantages for use in a flood risk assessment. One-dimensional models require cross-sections which do not accurately model topographic changes in water surface elevations between transects. Two- and three-dimensional modeling incorporates a continuous surface to represent complicated river systems and to generate a finite element mesh. Quality point data and information about channel morphology for interpolation of points from cross sections is important where unrealistic surfaces could result from cross section location and spacing, inclusion of points outside the main channel, and interpolations that do not capture the true thalweg. Merwade, Cook et al. (2008) recommend anisotropic techniques that define search neighborhoods and assign weights according to flow direction when working with point measurements. They also propose a method for linear interpolation between cross sections to incorporate information about unmeasured locations. The merging of intricate and accurate channel and floodplain topography produce an accurate terrain model for flood modeling and groundwater/surface water interaction investigations. However, the time and expense involved in collecting such high resolution spatial data may be beyond the scope and budget of many remediation strategies.

Although two- and three-dimensional hydraulic flow models produce descriptive results for flood analysis, they have high computational requirements and labor-intensive data input making them difficult to use for decision support systems. The incorporation of higher dimensions into a hydraulic analysis introduces more uncertainty as the number of assumptions increases. Rapid assessment of flood impacts is most easily completed with a one-dimensional hydraulic model, as two- and three-dimensional models require comprehensive data that may not be readily available for the area of study.

GIS based hydrologic models will likely advance current practices in flood control, flood mitigation, floodplain mapping, and flood insurance studies. A fully integrated hydrologic and GIS based system would apply robust modeling techniques and concepts representing spatial and temporal processes at the same level. GIS provides a powerful tool when coupled with hydrologic/hydraulic models not only for visualization of flood extents and depths but for further analysis of flood damage and risk estimates.

1.3 SITE DESCRIPTION

Location

The UBMC is east of Lincoln, Montana in Lewis and Clark County and is located at the headwaters of the Blackfoot River. The area encompasses several abandoned mines on private property and the National Forest Service (see Figure 1.1). Once mined for silver, zinc, and lead, the mines continue to be a source of contamination to local water-ways. The major individual mines include the Mike Horse Mine, the Anaconda Mine, the Edith Mine, the Paymaster Mine, and the Carbonate Mine. Smaller mines are located within the Blackfoot River drainage. In conjunction with a plugged spillway pipe, a 1975 rain-on-snow event lead to a breach in the Mike Horse tailings impoundment below the Mike Horse Mine. The resulting flood wave washed tailings down the headwaters of the Blackfoot River (Tate et al. 2002). Combined effects from the breach and continuous leaching of acid mine drainage from historic mine sites along tributaries acidified sediments along the floodplain and within a downstream wetland. Within the drainage area, elevations range from 5,200 feet above mean sea level (AMSL) at the marsh system to 7,500 feet AMSL along the continental divide (Figure 1.1).

Hydrology

Several tributaries contribute runoff to the Blackfoot within the UBMC. The confluence of Beartrap Creek and Anaconda Creek form the Blackfoot River. Further downstream, the wetland receives flow from five additional streams (three perennial, two intermittent) during spring runoff, Shaue Creek, Stevens Gulch, Paymaster Creek, Pass Creek, and Meadow Creek. The wetland system initiates just upstream of the confluence of the Blackfoot River and Pass Creek and continues for several miles downstream of the confluence. The total drainage area to the wetland is 14 square miles. Figure 1.1 denotes drainage areas to the study area.

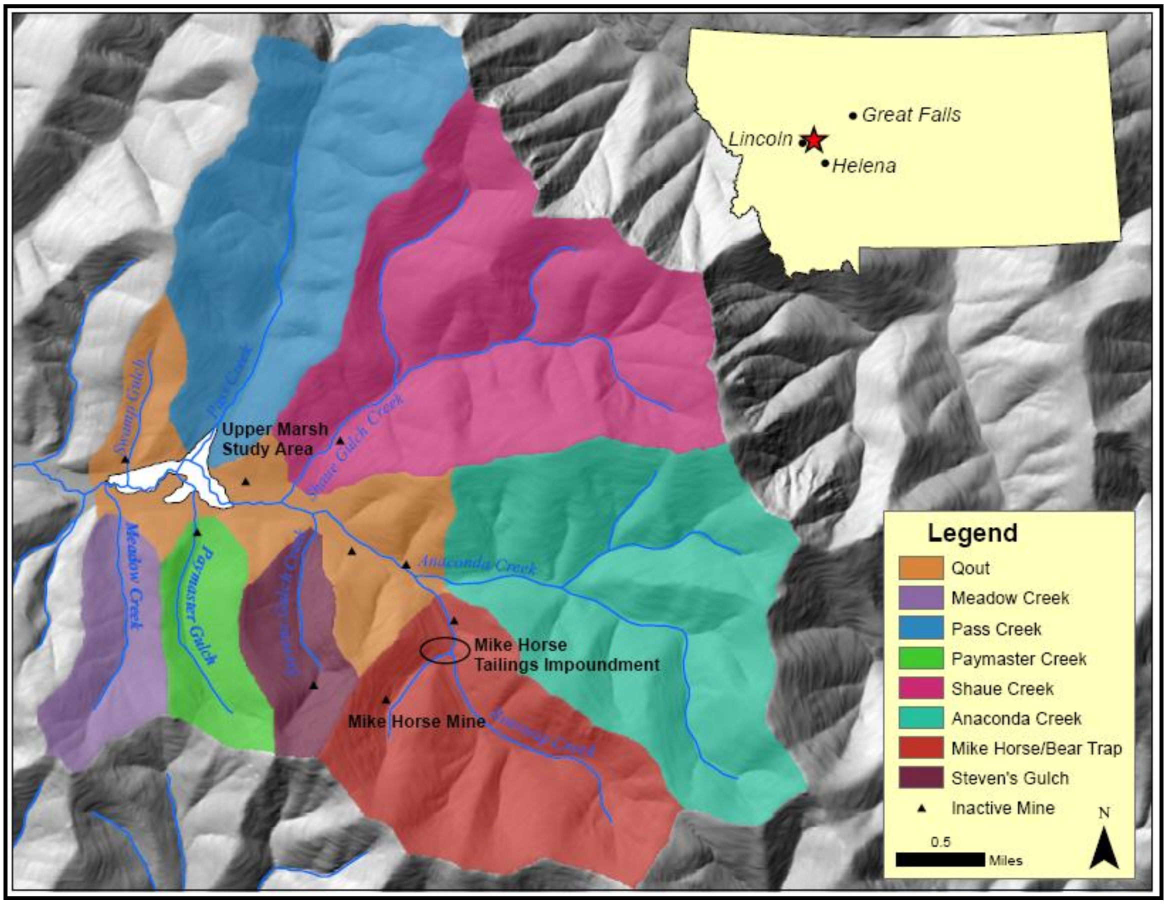

Figure 1.1. The Upper Marsh Study Area (denoted in white above) is located along the Blackfoot River with several upstream abandoned mines acting as sources of heavy metals (Data Source: NRIS, MT DEQ)

Climatic data is recorded at the nearby Rogers Pass Station and Lincoln Ranger Station. Annual precipitation averages are 17.99 inches. The highest annual precipitation in the area was recorded in 1975 (31.4 inches), the year of the tailings impoundment breach. Until the recent draining of the reservoir behind the tailings impoundment, water seeped through the earthen dam and flowed through the overflow pipe during runoff periods maintaining a supply of heavy metals to downstream tributaries.

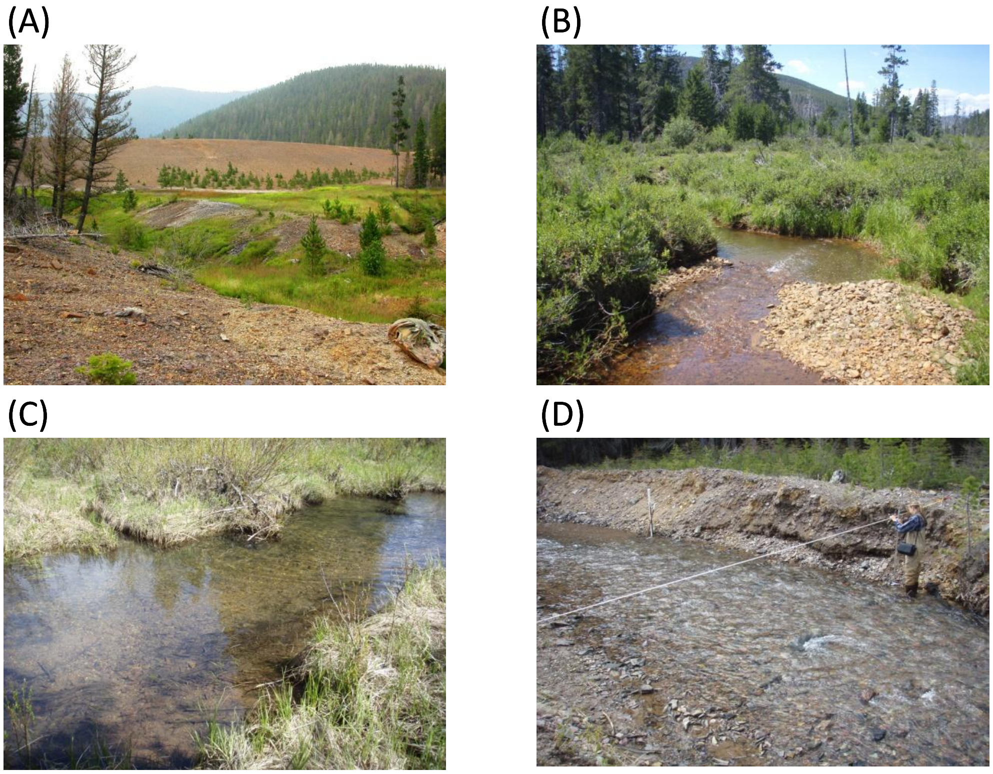

Figure 1.2 (A) The Mike Horse Tailings Impoundment is located upstream of Bear Trap Creek at the headwaters of the Upper Blackfoot River. (B) The upper marsh area is heavily vegetated and serves as a sink for heavy metals along the Blackfoot River. (C) Pass Creek is a tributary to the Blackfoot just upstream of the upper marsh area. (D) Velocity measurements were recorded along reaches to compare to one-dimensional velocity output results.

Vegetation and Ecology

The vegetation of the UBMC is characteristic of the Rocky Mountains with some alterations due to mining activity. The majority of the slopes and transition areas into floodplains are composed of coniferous forest with lodgepole pine, spruce, and Douglas fir. Mountain big sagebrush and fescue grassland dominate drier slopes. Wetland and riparian areas within the study area encompass coniferous and deciduous tree communities as well as shrubs and herbaceous species. The photos represent vegetation coverage in the marsh study area and surrounding drainage areas.

The diverse ecology of the study area provides recovery areas for several species and fish habitat. In the less impacted areas of Anaconda Creek and Shaue Creek, westslope cutthroat trout have been observed.

Geology and Hydrogeology

A mixture of bedrock units are identified within the UBMC, including the Belt Series Spokane Formation, a diorite sill, and Tertiary-age intrusive bodies. Based on well yield tests, low bedrock permeability characterizes the site. Permeability is also restricted due to low recharge areas near the continental divide. Groundwater flows are recharged primarily from snowmelt from higher elevations to alluvial groundwater systems and tributaries. Major flowpaths include secondary fractures, joints, and fault zones.

2.0 Methods and data collection

The goal of this study was the evaluation of a one-dimensional hydraulic model and the production of a hazard probability map that encompassed the potential erosive surfaces for the 10, 25, and 100 year recurrence intervals. The identification of drainage areas assisted with the estimation of flood event discharge values necessary for the hydraulic analysis. A detailed topographic survey provided the foundational data for the hydraulic model. Soil samples collected from various points in the wetland by MT DEQ and during field campaigns provided information on surface roughness and contaminant distributions.

Discharge

Drainage areas (Figure 1.1**)** for each reach were determined with a GIS. Using the methods described by Parrett et al. (2004), the drainage area, basin characteristics, annual precipitation, and active channel width were determined for each reach to estimate discharge events with 2, 10, 25, 50, 100, 200 and 500 year recurrence intervals. Table 2.1 provides results from the regression analysis. Discharge estimates were used to parameterize the hydraulic model.

Velocity and stage measurements were taken in each tributary at the same cross section for thirteen weeks beginning in May and ending in July. Velocity measurements were recorded every 0.5 ft at a depth six tenths from the bed using a Marsh McBirney. Recorded velocity measurements across each surveyed cross section provided parameters for an evaluation of the one-dimensional hydraulic model performance.

Table 2.1 Drainage areas were estimated for each tributary in the study area and discharges for flood events were estimated.

Drainage Area ID	Drainage Area (sq. miles)	2-yr (cfs)	5-yr (cfs)	10-yr (cfs)	25-yr (cfs)	50-yr (cfs)	100-yr (cfs)	200-yr (cfs)	500-yr (cfs)
Anaconda Creek	2.90	13	36	64	129	212	344	538	966
MikeHorse/Bear Trap Creek	1.99	14	37	65	126	200	311	466	784
Shaue Creek	3.28	26	65	109	205	317	485	716	1180
Pass Creek	2.33	24	59	99	185	288	442	653	1080
Paymaster Gulch	0.58	8	21	38	76	122	194	295	506
Meadow Creek	0.64	5	13	24	51	84	135	207	358
Steven's Gulch	0.55	3	10	19	41	69	113	176	311
Qout	1.45	12	32	56	109	173	270	405	680

Topography and channel geometry

Detailed cross section geometries are necessary to predict flow characteristics in the wetland, and topographic land surveys were completed using a total station and a survey grade global positioning system (GPS) device. Variations in topography were also evaluated with an orthorectified aerial photo and aerial photographs. Using the Delunay triangulation method, an interpolated surface (TIN) was generated from land survey points and breaklines from the orthorectified aerial photo. The Delunay triangulation interpolation method had several advantages: 1) triangles created were as equi-angular as possible, 2) new node values were close to known observation points, and 3) interpolations were not affected by the sequence of input data (Hu 1995).

2.1 MODEL DESCRIPTION

The one-dimensional hydraulic model, HEC-RAS, incorporates several parameters to estimate water surface profiles for steady gradually varied flow. Discharge amounts for each flood event along contributing reaches and locations of flow changes are required for the analysis. Surveyed cross section geometries provide detailed topography of the channel and floodplain areas. The selection of roughness coefficients based on photographs, sediment samples, and topography transitions is a critical component when incorporating Manning's equation to estimate water surface profiles.

One-dimensional hydraulic models are widely used for flood mapping and are typically simpler to use with minimal amounts of input data in comparison to two- and three-dimensional models. The U.S. Army Corps of Engineers' River Analysis System, HEC-RAS, is a robust, public domain, internationally used hydraulic modeling program. Numerous studies in a variety of environments, including surface flow through wetlands, have demonstrated HEC-RAS's effectiveness in estimating peak discharge (Auble et al. 2005; Johnson et al. 1999). HEC-RAS calculates one-dimensional, energy-balanced water surface profiles for subcritical and supercritical conditions. Using an estimated downstream water surface elevation for subcritical flow, HEC-RAS iteratively determines upstream or downstream water surface profiles. Several equations are available for calculating channel flow using mass, energy, and momentum conservation. HEC-RAS has the ability to model an entire network of channels, in either looped or dendritic configurations.

The model supports several options for incorporating friction equations depending on the flow regime and profile type. For gradually varied, steady flow estimates, the energy equation is balanced between successive cross sections. The uniform flow equation, Manning's equation, is used to estimate the energy slope at each cross section. To estimate discharges, the Manning equation combines channel geometry, slope, and an estimate of resistance to flow (roughness coefficient) to determine stream velocity for turbulent flow on a rough surface. When the velocity head is rapidly varied (hydraulic jumps, junctions between reaches), the momentum equation is employed. Further, HEC-RAS offers the capability of entering a roughness coefficient for each topographic break in a cross-section rather than a single integrated value, thereby, producing a more accurate representation of spatial variability of roughness across channel and overbank environments.

Using the energy equation, the robust model estimates water surface profiles between successive cross sections using the standard step method (Chow 1959). Calculations of flow depth are carried upstream for subcritical flow and downstream for supercritical flow. An iterative solution calculates unknown water surface elevations at the cross section based on an assumed water surface elevation, the boundary condition. Total conveyance and velocity head are used to estimate the friction slope (S_f) and friction head loss (h_f).

The energy equation is given by:

$$y_1 + z_1 + \frac{\alpha_1 V_1^{\,2}}{2g} = y_2 + z_2 + \frac{\alpha_2 V_2^{\,2}}{2g} + h_e \qquad (1)$$

where; y = the thalweg flow depth,

z = the elevation of the channel invert,

α = the velocity head weighting coefficient,

V = the average cross section velocity,

g = the gravitational acceleration, and

h_e = the head loss.

The friction head loss is estimated through Manning's equation and accounts for boundary roughness conditions.

$$S_f \cdot \Delta x = \frac{\Delta x}{2}\left(\frac{V_1 n_1^{\ 2}}{K_n^{\ 2} R_1^{\ 4/3}} + \frac{V_2 n_2^{\ 2}}{K_n^{\ 2} R_2^{\ 4/3}}\right) \tag{2}$$

where; S_f = the friction slope between the cross sections,

Δx = the distance between cross sections,

n = Manning's n,

K_n = the unit correction factor for Manning's equation, and

R = the hydraulic radius.

Head loss due to velocity head changes between cross sections are calculated with the following:

$$K_{c/e}\left(\frac{\alpha_1 \mathrm{V}_1^{\ 2}}{2g} - \frac{\alpha_2 \mathrm{V}_2^{\ 2}}{2g}\right) \tag{3}$$

where; $K_{c/e}$ is the contraction or expansion coefficient. Contraction and expansion coefficients account for transitions in channel width and depth.

The standard step method has several advantages for modeling natural channels. Even if the water surface elevation is not known at the starting cross section, profile estimates converge closer to the correct elevation with every step. Therefore, if the elevation at the control section is unknown, estimates can be made for the initial elevation or computations can begin a few cross sections away from the desired location.

Manning's equation assumes uniform flow with consistent channel cross section and velocity where the energy gradient is equal to the slope of the water surface and stream bed (Chow 1959). Criticisms of the flow equation include Manning set the exponent of the wetted perimeter to 2/3 even though his and later research indicates that the value can range from 0.6175 to 0.8395. In addition, the flow equation is dimensionally inhomogeneous and represents uniform flow rather than non-uniform flow (Pappenberger et al. 2005). The square root of the slope tends to dampen the uncertainty from energy slopes based on water surface gradient surveyed in the field.

Selection of Manning's *n* Using a Component Method

The combination of calibrated roughness parameters and geometry affect the flood extent estimates as most hydraulic models are sensitive to these metrics (Marcus et al. 1992; Pappenberger et al. 2005). Uncertainty arises with approximations of geometry and selection of roughness values, and it is almost impossible to quantify every source of energy loss in a system. Roughness coefficients represent the resistance to flood flows in channels and floodplains. Flow resistance results from sediment size, sediment load, vegetation, sinuosity, contraction and expansion. Several methods have been developed to estimate values of n, including photographic comparisons, particle-size based techniques, combinations of roughness generating factors, direct measurement, and regime equations relating roughness to hydraulic variables (Chow 1959; Marcus et al. 1992; Pappenberger et al. 2005; Schneider and Arcement 1989).

Evaluations of methods for selecting roughness coefficients have been investigated as a primary factor affecting uncertainty in hydraulic modeling. Marcus and Roberts (1992) evaluated eleven techniques for estimating Manning's *n* in small mountain streams and concluded that ten of the techniques underestimate roughness coefficients up to an order of magnitude. These discrepancies result from observer bias and development of techniques in streams with smaller sediment, lower gradients, and lower ratios of mean sediment size to flow depth. For estimating a roughness coefficient in small mountain streams, Marcus and Roberts (1992) recommend measuring discharge at cross sections, directly calculating Manning's *n*, or using Jarrett's (1984) regime approach.

Roughness coefficients were estimated using the method described by Arcement and Schneider (1989) for the stream channels and by Cowan (1956) for floodplains. We collected data for the following parameters: depth of water, sediment size, channel irregularities, changes in size of channel, channel meanders, obstructions, and vegetation density. Depth and velocity are two critical factors that will affect the evaluation of flow through the wetland (Kadlec 1990) and should be considered when selecting a roughness coefficient. Roughness coefficients are larger if flow depths are small in comparison to the sediment size and decrease with increasing flow depth if channel banks are not rougher than the bed or if dense vegetation does not intercept flow in the channel (Schneider and Arcement 1989). The Arcement and Schneider procedure incorporates the effects of several factors to estimate a roughness coefficient for channel and floodplain areas. The value of total roughness factor, *n*, may be computed by the following:

$$n = (n_b + n_1 + n_2 + n_3 + n_4)m \tag{4}$$

where; n_b = a base value of *n*,

n_1 = a correction factor for the effect of surface irregularities,

n_2 = a value for variations in shape and size of the channel cross section,

n_3 = a value for obstructions,

n_4 = a value for vegetation and flow conditions, and

m = a correction factor for channel meandering.

Parameters n_1 through n_4 are determined through visual observations. Base roughness values (n_b) combine values from Chow (1959), Benson and Dalrymple (1967), and Aldridge and Garrett (1973). Selecting a base n_b value for a channel involves determining if the channel is a stable or sand channel. If the bed consists of firm soil, gravel, cobbles, boulders, or bedrock, it is classified as stable, while an unlimited supply of sand characterizes a sand channel with grain sizes ranging from 0.062 to 2mm. Sand bed channel material is transported easily and creates a resistance to flow with varying bed forms. The movement of sand and the creation of different configurations is a result of flow velocity, sediment size, bed shear, and temperature.

Floodplain roughness coefficients are estimated with the Cowen method using a similar procedure for estimating channel roughness. The base roughness value (n_b) is selected for the underlying sediment composition. Adjustment factors for surface irregularities (n_1), obstructions (n_3), and vegetation density (n_4) are then incorporated into the floodplain roughness coefficient.

The n values for the floodplains are estimated where abrupt changes in resistivity occur, including topographic breaks, vegetation density, and sediment size changes.

2.2 EROSION

Mine impacted natural wetlands exist in overbank areas throughout Montana, and evaluating floods for ecosystem impacts aids with making water resource management decisions (August et al. 2002). Because the mechanism for sediment resuspension in a wetland is erosion, the dominant controlling factors must be addressed in a model. Soil physical properties, vegetation, and geomorphology influence friction; therefore, shear stress differs across the wetland channel and overbank areas (Bendoricchio 2000; Kadlec and Knight 1996).

An essential step for mine-impacted wetland risk assessment is the capability to predict the impacts of flood events on wetlands (Thompson et al. 2004a). Erosion is a result of increased forces on soil particles within the channel bed and overbank surfaces and is a function of the magnitude of resisting channel forces and the hydraulic forces over time (Fischenich et al. 2001). Predictions of sediment transport and erosion potential depend on empirical equations for natural channels. Erosion characterization involves predictions of critical shear stress or critical velocity and is affected by the following parameters: flow properties, sediment composition, climate, subsurface conditions, channel geometry, biology, and anthropogenic factors. Velocity is a parameter measured within channel flow; while shear stress is calculated from flow parameters as a force per unit area. Metals that are resuspended, adsorbed to sediments, or precipitated, behave as any other sediment in a fluvial environment (Gibbs 1973); therefore, identifying erosion potential for channel and overbank areas for several flood magnitudes may be a valuable tool to assist in remediation efforts of mine impacted wetlands.

Evaluating the threshold condition or incipient motion reached between erosion and sedimentation as the forces resisting motion become balanced with the forces acting on particles provides a critical parameter for evaluation of resuspension potential (Fischenich et al. 2001; Julien 1995b). Under uniform steady flow, the forces acting on a noncohesive particle are a resisting force, hydrodynamic drag force, hydrodynamic lift, and submerged weight. The resultant of each of these forces is zero at the threshold condition, and the initial movement of soil particles can be evaluated with either critical shear stress (λ_{cr}) or critical velocity (V_c).

The maximum unit tractive force a surface can withstand without eroding is termed the critical shear stress and is a measure of fluid force on a channel. This includes the flow-generated shear and gravitational forces acting on soil particles. Shear stress is a widely used method to quantify the potential for transport of material. Average bed shear stress estimates incorporate variations in roughness and velocity caused by fluctuations in turbulence and is defined by the following:

$$\lambda = \gamma R S_f \tag{5}$$

where; λ = the fluid shear stress,

γ = the specific gravity of water,

R = the hydraulic radius, and

S_f = the frictional slope.

A particle's size relative to surrounding particle sizes, its orientation, and the degree it is embedded determine the amount of shear stress that particle will experience. By equating resisting forces to applied forces, critical shear stress estimates can be made. Approximations of critical shear stress can be made with widely used equations estimated by Shields (Brunner 2002), Lane, Julien (Julien 1995a), and Andrews (Andrews 1983). By equating resisting forces to applied forces, critical shear stress estimates can be made. Shields developed the following equation for critical shear stress (λ_{cr}) (at incipient motion) from flume experiments.

$$\lambda_{cr} = K_s(\gamma_s - \gamma)D \tag{6}$$

where; K_s = Shield's coefficient,

γ_s = the specific weight of sediment, and

D = the particle size.

The hydraulic model estimated average shear stress values for each cross section. Flow was modeled as subcritical using the normal depth as a boundary condition. Segmented roughness values across the cross sections in the wetland region and contributing tributaries were assigned based on sediment size, vegetation coverage, obstructions, and channel meanders. Shear values were a function of frictional slope, hydraulic radius, and the weight of water and, therefore, dependent on cross sectional area. Shear stress estimated in the one-dimensional model is an average shear stress; however, shear stress can also be calculated using log velocity profiles. The hydraulic radius, a ratio of area to wetted perimeter, heavily influences shear stress estimates in the hydraulic model. The von Karmen-Prandtl law of velocity distribution (Bergeron and Abrahams) is another method for estimating shear stress based on log-velocity profiles plotted as a function of velocity near the channel bed and the natural log of depth over roughness. Estimating the roughness parameter incorporates uncertainty into shear stress calculations, but with detailed vertical velocity profiles, the method provides another calibration estimate for the model.

Critical Velocity

The maximum velocity or critical velocity is the channel velocity that will not permit erosion, and surpassing the critical velocity results in the initiation of particle motion. An estimate for critical velocity, developed by Laursen (Akan 2006) is obtained by equating shear stress to critical shear stress and is based on the concept of tractive force:

$$V_c = \frac{K_n}{n}\sqrt{K_s(s-1)}\,y^{1/6}D^{1/2} \tag{7}$$

where: s is the specific gravity of particles (γ_s/γ). Typical values include 0.039 for K_s and median diameter (D_{50}) for particle size.

Empirical methods for evaluating velocity and shear stress were developed in flumes. Natural channels experience high levels of variability and may not experience uniform or steady flow. The amount of sediment in suspension minimizes turbulence and is not accounted for in the given estimates of velocity and shear stress. Variation in particle size influences stress in channels. Larger particles often inhibit smaller particles from motion until significant flows and higher stress are experienced. Application of this method to our data required the assumption that flow is steady and the use of an interpolated median particle size distribution.

Velocity distributions were calculated along each cross section in each hydraulic model. Dynamic segmentation provided a tool for assigning parameter values for velocity, depth, and roughness coefficients (*n*) across a cross section within segments. Continuous critical velocity data surfaces were created using Delaunay Triangulation to interpolate values between cross sections.

Soil Physical Properties

Sediment properties, particularly grain size and consolidation state, determine the incipient motion threshold of a soil. While predicting critical shear stress for erosion of mine tailings for future tailings disposal, Haneef-Mian et al. (2007) observed that the cohesive nature of mine tailings may contribute to the concentration of resuspended solids in water. The critical shear stress of tailing sediments is influenced by a number of physical and geological factors, including turbulent stress at the sediment-water interface, water content of the deposited sediments, mineralogical composition (for example different clay minerals), and the compositions of pore water and eroding fluid (saline or brackish). During critical shear stress analysis on mine tailing sediments, Haneef-Mian and others (2007) created a “deposited bed” within testing columns. The deposited bed was analogous to the bed formed in lakes after contaminated sediments resuspended by storms were redeposited in the bed. Sulfide-bearing materials, like those found in mine tailings, tend to oxidize during resuspension, which can change particle size distribution and lead to flocculation. Their results verify the similar physiochemical nature of tailings samples from this and other studies and a power-law relation between erosion rate and excess shear stress was determined for mine tailings. Aberle and others (2004) completed experiments on sediment erosion and found that erosion rate is dependent on bed material properties, such as dry bulk density, water content, organic content, and sand content. Since tailings have similar structures, cohesive natures, and, therefore, erosion rates upon consolidation, an evaluation of resuspension thresholds of tailings within the wetland contributes to further understanding of their behavior.

Field investigations provided several of the metrics required for the hydraulic model and for the velocity and critical velocity distribution analysis. Sediment size distributions were evaluated with samples extracted along each cross section (channel and floodplain) where sediment sizes varied. At each of these transition points, thirty sediment grain samples were selected from within a one square meter area and measured with a gravelometer. Additional samples with an abundance of fine material (less than 2mm) were analyzed with sediment sieves in the lab. Each sampled location was recorded, and sediment size distributions (e.g. D_{50}) were used in the selection of appropriate roughness coefficients. We used inverse distance weighting to spatially interpolate sediment sizes across the study site. Through this method, the value at an unknown point is estimated by surrounding known-point values which are weighted according to their respective distances. Therefore, the closer a point is to the center of the estimated cell, the more influence it has on the estimated value. For example, sediment sample points in the steep terrain beyond the floodplain did not significantly influence interpolated sediment size cells within the channel. Sediment particle distributions in the study area resulted from erosion and deposition and varied significantly between the channel and floodplain areas.

The MT DEQ provided the metal concentration levels sampled along a 250 foot square grid and some intermittent points within and surrounding the wetland area. Concentrations of aluminum (Al), arsenic (As), cadmium (Cd), copper (Cu), iron (Fe), lead (Pb), manganese (Mn), mercury (Hg), and zinc (Zn) within 0-2, 2-6, and 6-12 inches of the surface were sampled. We selected a subset of this data for analysis. Concentrations in the top two inches of soil were deemed most relevant to our analysis and were therefore used exclusively. Distribution surfaces were not interpolated for aluminum, manganese, and mercury due to lower concentration levels and an insufficient data set for spatial interpolation.

Kriging was selected as the spatial interpolation method for metal contamination and involved preliminary investigations of the spatial correlation of data. Each known point for individual parameter data sets was employed in the spatial interpolation to distribute values to unknown cells in the raster data set. The kriging interpolation involved a weighted moving average method derived from regionalized variable theory where similar patterns of variation occur at every location on the surface. These patterns were observed in a semivariogram, which measured the degree of spatial correlation among the metals concentration data points in the grid as a function of the distance and direction between observational data points (Hu 1995; Kitanidis 1997; Marx 1987; McCoy and Johnston 2001). The model fit to the semivariogram controlled kriging weights assigned to the interpolated data points. Kriging resulted in the creation of continuous data surfaces for metal concentrations across the study site. Metal distributions resulted from resuspension and deposition during larger storm events and did not display abrupt spatial changes or spikes. Higher concentrations were observed in the entrance to the wetland and decreased toward the outlet.

Vegetation

The presence of barriers, including vegetation and litter mats, inhibits wetland sediment resuspension. A greater force is required to displace particles within vegetated areas. After a storm event, Hicks and others (2005) observed that overbank areas with vegetation and shallow flow depths were less eroded because the surface resistance reduced the shear stress. Vegetation offers resistance to erosion but does not eliminate resuspension (Aberle et al. 2004; Kadlec and Knight 1996). Hydrodynamic drag and lift forces on soil particles in a channel are minimized with the presence of vegetation as flow resistance increases and velocity profiles migrate upwards with a higher effective roughness height. Within the first meter of depth, resistance due to vegetation drops exponentially at a rate of about factor 10 for each 30-40 cm increase in depth (Kadlec 1990). At higher flood depths, therefore, the roughness effects of vegetation diminish those of flow hydraulics and geomorphology dominates. Kadlec and Knight (1996) discuss how overland flow in wetlands can be determined with a suitable friction rule that is a power law for velocity in terms of depth and friction slope, which account for vertical vegetation stem density gradient and bottom elevation distribution. The condition, health, and robustness of a vegetation community influences friction in fluvial environments. Sediment transport through healthy wetland vegetation varies from that in an acid mine drainage wetland, where the individual plants have lower biomass and elasticity (Wong et al. 1998). With the presence of vegetation, the probability of erosion is dampened as the velocity decreases and the forces that initiate movement diminish.

Along each cross section, locations where changes in vegetation density and type occurred were recorded with a GPS. Obstructions, vegetation density, and vegetation species were documented and photographed. This assessment assisted with the selection of appropriate roughness coefficients during hydraulic model parameterization.

2.3 HAZARD MAPPING

Hazard potential maps were created by analyzing sediment characteristics, metals distributions, and hydraulic metrics, such as velocity distributions and inundation surfaces for the 10, 25 and 100 year flood events. The flow chart in Figure 2.1 summarizes the processes for the hazard probability map analysis completed for each flood event. Using water surface elevations and locations of the water surface extents generated from each hydraulic model, an inundation surface was mapped in the GIS. Terrain elevations subtracted from the water surface created the spatial extent of flood inundation and flood depth, and this layer provided a bounding layer for the data sets investigated in the hazard analysis. Using equation (7) continuous data surfaces for water depth, flow velocity, and sediment size for each of the flood events of interest were combined to produce spatially continuous critical velocity layers. These layers were then overlaid by modeled velocity distributions to obtain a percent exceedance value. For any given cell on the hazard potential map, percent exceedance was calculated as follows:

$$(V_m / V_c)*100 \tag{8}$$

where; V_m = modeled velocity

V_c = critical velocity

Results of the percent exceedance map suggest areas where the modeled flood velocity is likely to exceed the threshold condition at which sediment is mobilized. Combining the percent exceedance data with data surfaces for contaminant distributions of arsenic (As), copper (Cu), cadmium (Cd), lead (Pb), and zinc (Zn) allows for the creation of hazard potential maps. These maps provide a qualitative visual tool for assessing the spatial distribution of sediment contamination and the estimated percent velocity exceedance simultaneously.

2.4 SENSITIVITY ANALYSIS AND ERROR CHECKING

Evaluation of the hydrologic and hydraulic performance of the model within a dynamic wetland situation was conducted by testing the accuracy and stability of the output in a sensitivity analysis. In particular, alterations to roughness coefficients, contraction/expansion coefficients, and spacing of cross-sections addressed the dependence of the output on specific input variables communicates the model’s limitations. Manning’s roughness coefficients were globally altered by 10%, -10%, 25%, and -25%. Contraction/expansion coefficients were adjusted from 0.1/0.3 to 0/0.5, 0/0, and 0.3/0.7. By adjusting the spacing of cross-sections through interpolation or removal, shortcomings in our topographic survey were identified. Velocity distribution results from the hydraulic model for selected cross sections were compared to field velocity measurements.

Metal concentration distributions were spatially interpolated with ordinary kriging and spherical models. The spherical models were fit using a Monte Carlo analysis which provided parameter sets that minimized the sum of squared errors. Kriging provides estimates of error variance for the interpolated contamination levels within the wetland.

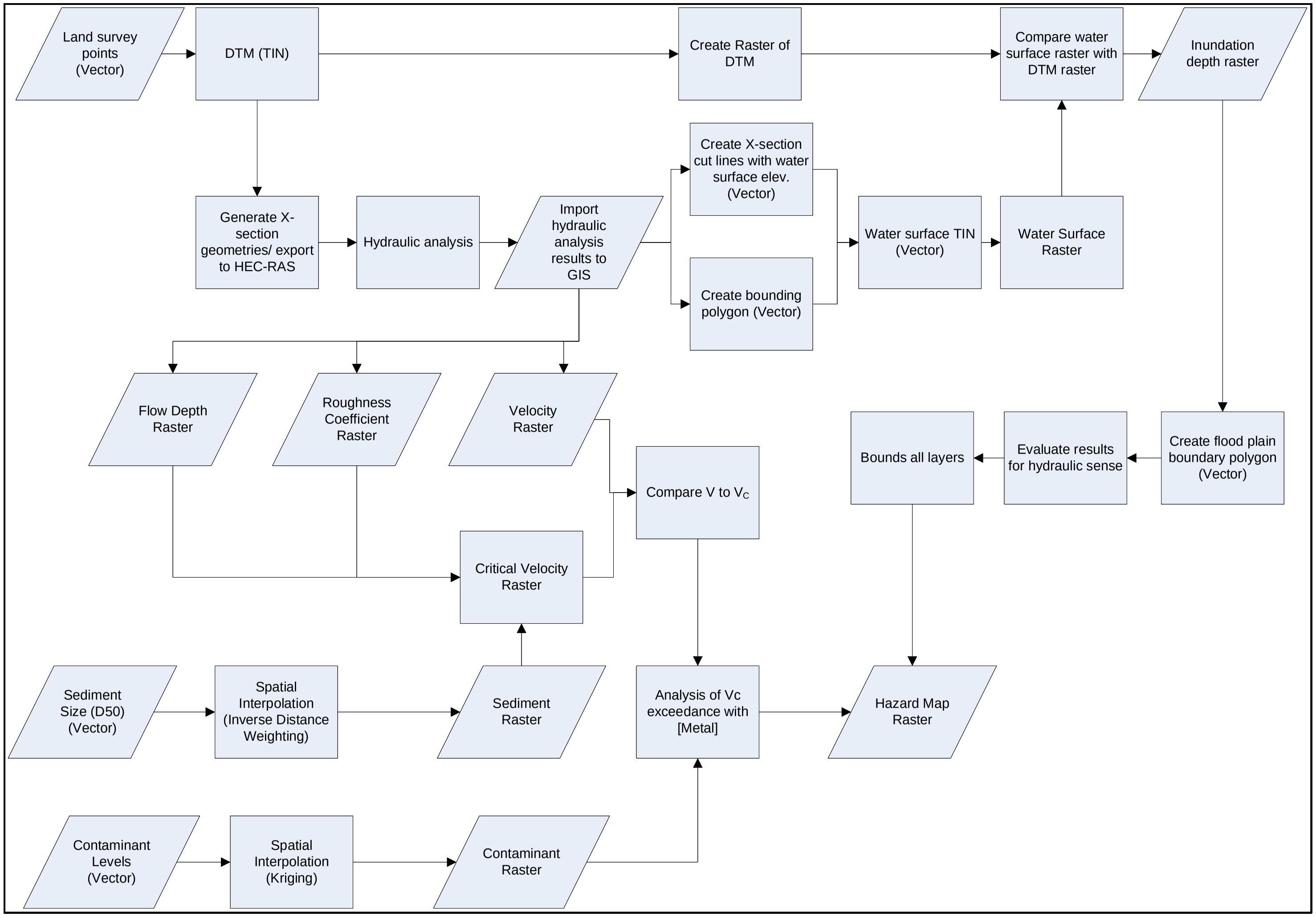

Figure 2.1. The hazard probability map flow chart describes the processes and data sets required for analysis in the GIS and hydraulic model.

3.0 Results and Discussion

3.1 HYDRAULIC ANALYSIS

The one-dimensional model estimated water surface elevations and hydraulic parameters for calculations of critical velocity. Detailed roughness parameters based on sediment size and vegetation were used to estimate flow across cross sections and, therefore, water surface elevations and velocity distributions. Some cross sections required critical depth determination when the energy equation failed to balance within a specific number of iterations. Appendix A contains output from HEC-RAS for each flood model.

Estimates of water surface elevations within the natural channel in the one-dimensional hydraulic model involve several assumptions. Flow was assumed to be steady throughout the reach and to be gradually varied between cross sections as the energy equation is based on the theory of a hydrostatic pressure distribution across each cross section. Cross sections were located along a given reach and satisfied the gradually varied flow assumption. Flow was considered to be one-dimensional and in the dominant flow direction without considering velocity in any other direction. The total energy head was assumed to be the same at every point along a cross section. The energy slope was assumed to be uniform across any given cross section and between consecutive cross sections.

Table 3.1. Nine reaches within the study area were modeled with at least five cross sections to estimate water surface elevations.

Drainage Area ID	**Reach Length (ft)**	**Number of Cross Sections**
Anaconda Creek	2223	16
Blackfoot Reach 1 (MikeHorse/Bear Trap Creek)	3641	35
Blackfoot Reach 2	4993	70
Shaue Creek	1392	8
Blackfoot Reach 3	4724	28
Pass Creek	1563	8
Blackfoot Reach 4	4487	17
Meadow Creek	1878	5
Blackfoot Reach 5	2448	11

Velocity distributions in HEC-RAS calculated for a set number of divisions across a cross section are a function of conveyance and area for each subdivision. Velocity in a natural channel varies vertically and horizontally, and output from the one-dimensional model is an average velocity for each segmented area within the channel. Velocity distributions typically increase the conveyance within each segment. Therefore, the sum of the conveyances from the segments does not equal the total conveyance from the original modeling technique, and a ratio of the total conveyance to the segmented conveyance is applied to the segments before estimating the average velocity.

Velocities were compared for thirteen cross sections in the marsh area, and results from each comparison can be found in Appendix B. Table 3.2 notes the absolute relative error between the averaged measured velocity in the channel and the averaged HEC calculated velocity in the channel. Absolute relative error describes the difference between the measured velocity and the predicted velocity relative to the measured velocity. The averaged HEC velocity distributions create smooth velocity transitions between banks and do not capture variations in velocity due to eddies and bed topography. The relative error for cross sections within a defined channel was lower than cross sections in wider flow areas. Velocity predictions within cross sections with defined channels closely matched the measured velocity values near the thalweg. Ground water interactions, vegetation, beaver dams, and mild gradients likely affected flow characteristics in the wetland and cannot be accounted for by one-dimensional models. These results suggest that in a low gradient wetland with large inundated areas and sinuous flow, our method may produce erroneous velocity estimates in near-bank or shallow over-bank zones. Future studies that include more extensive comparisons between modeled and observed velocity distributions on multiple cross sections over a variety of flow conditions may help quantify the degree and extent of this error. Assessment strategies similar to that outlined above may need to be implemented by practitioners on a case-by-case basis to determine the appropriateness of our method at a given site.

Table 3.2. Absolute relative error between average measured velocities and HEC average velocity output vary at thirteen locations in the wetland.

Cross Section	Absolute Relative Error (%)	Average Measured Velocity in Channel (ft/s)	Average HEC Calculated Velocity in Channel (ft/s)
11943	60	0.89	1.43
11633	386	0.40	1.96
10889	8	1.75	1.61
10184	24	1.15	0.87
9762	2	1.03	1.05
9566	151	0.59	1.49
9399	23	0.82	1.01
8594	6	0.74	0.79
7844	35	1.18	0.77
5674	412	0.41	2.12
5387	434	0.39	2.07
4463	13	0.69	0.60
2821	59	0.18	0.29

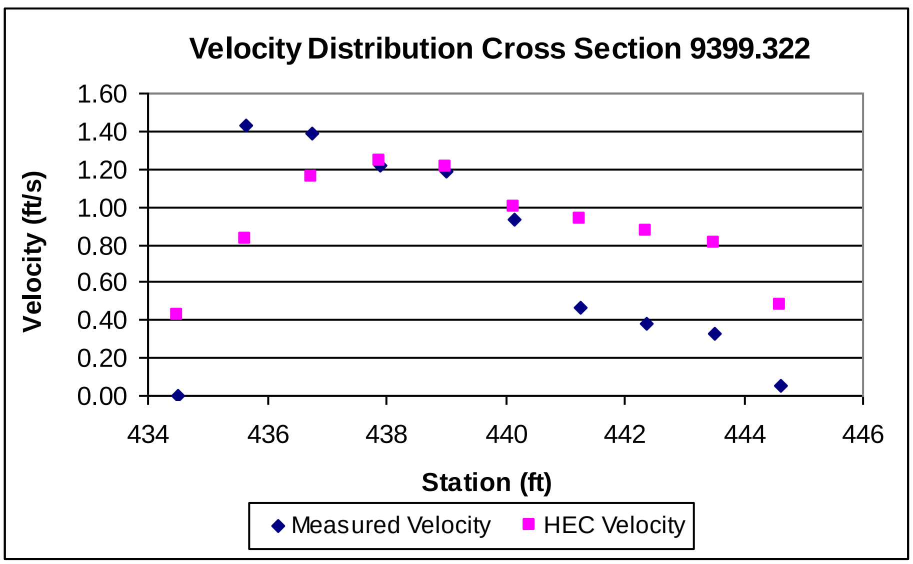

Figure 3.1. Velocity distributions at one foot increments across a defined cross section are similar near the thalweg (Station 438) but differ at the edges of the channel water surface.

Contraction and expansion coefficients and roughness coefficients were selected parameters for the sensitivity analysis, and comparison plots between predicted models and those with altered parameters indentified the significance of the selected parameters (see Appendix C). Changes in contraction and expansion coefficients had little effect on the performance of the one-dimensional model. Figure 3.2 is a representative example of changes in contraction and expansion coefficients where the initial velocity and shear stress values follow the linear 1:1 line in the graphs. Altering contraction and expansion coefficients to 0.3/0.7 respectively had the greatest effect on velocity and shear stress estimates. When the channel flowed from a wide area to a constricted section, such as the junction between Anaconda Creek and the Blackfoot River, shear stress values increased. Error estimates for the flood events indicate that larger flood events are less affected by changes in contraction and expansion coefficients.

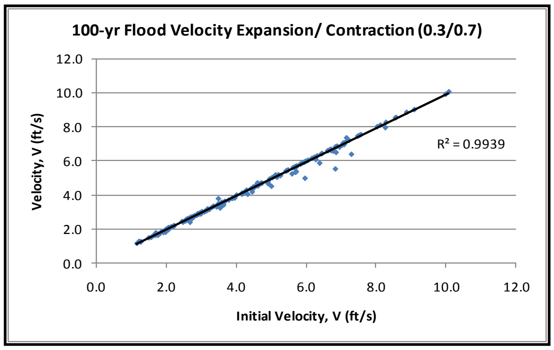

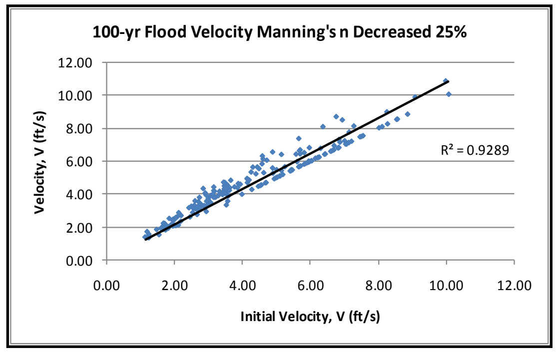

Figure 3.2. Changes in contraction and expansion coefficients from 0.1/0.3 to 0.3/0.7 had little effect on model velocity output. Decreasing the roughness coefficients by 25 percent caused an increase in velocity at cross sections that were near junctions and in constricted channel areas with steeper stream bed gradients.

Changes in velocity and shear stress were greater for global changes in Manning's n by 25% and -25% than those modified by 10% and -10%, shown in Tables 3.3 and 3.4. Evaluation of the results revealed a decrease in velocity and shear stress with increasing roughness and an increase in velocity and shear stress with decreasing roughness. We utilized root mean square error (RMSE) to assess how closely the velocity and shear stress values for models with altered parameters are to the original model output. Both velocity and shear stress estimates for the flood events indicate that smaller events (2-year through 50-year) were affected less by changes in roughness parameters than the larger events (100-year through 500-year). As the magnitude of the flood events increased, the error estimate increased. Roughness depends not only on vegetation, sediment size, and channel characteristics but on flow depth. The larger flow depth associated with larger flood events may require a change in roughness coefficient. Significant changes in velocity and shear stress were observed for cross section points that varied from the linear 1:1 line and were located at cross sections near junction locations, near flow change locations, and along reaches with significant bed slope changes. Cross sections upstream of culverts also displayed more error.

Table 3.3. The velocity root mean squared errors (ft/s) increase with higher magnitude flood events with changes in roughness and contraction and expansion coefficients.

Flood Event (year)	Increase Manning's n 10%	Decrease Manning's n 10%	Increase Manning's n 25%	Decrease Manning's n 25%	Contraction/ Expansion (0/0.5)	Contraction/ Expansion (0/0)	Contraction/ Expansion (0.3/0.7)
	RMSE (ft/s)	RMSE (ft/s)	RMSE (ft/s)	RMSE (ft/s)	RMSE (ft/s)	RMSE (ft/s)	RMSE (ft/s)
2	0.1226	0.1812	0.2676	0.3589	0.0361	0.0259	0.0909
10	0.2338	0.2695	0.4218	0.6242	0.1411	0.1555	0.1524
25	0.2173	0.2655	0.4874	0.6419	0.0800	0.0995	0.1213
50	0.2417	0.8297	0.5053	0.6688	0.0590	0.0888	0.1047
100	0.2734	0.2887	0.5914	0.6444	0.0755	0.1103	0.1674
200	0.5948	0.3145	0.5929	0.6942	0.0902	0.0947	0.1991
500	0.6478	0.2997	0.6428	0.7144	0.0870	0.1148	0.6478

Table 3.4. The shear stress root mean squared errors (lb/ft^2) increase with higher magnitude flood events with changes in roughness and contraction and expansion coefficients.

Flood Event (year)	Increase Manning's n 10%	Decrease Manning's n 10%	Increase Manning's n 25%	Decrease Manning's n 25%	Contraction/ Expansion (0/0.5)	Contraction/ Expansion (0/0)	Contraction/ Expansion (0.3/0.7)
	RMSE (lb/ft^2)	RMSE (lb/ft^2)	RMSE (lb/ft^2)	RMSE (lb/ft^2)	RMSE (lb/ft^2)	RMSE (lb/ft^2)	RMSE (lb/ft^2)
2	0.1578	0.1824	0.4064	0.3371	0.0165	0.0199	0.0753
10	0.3623	0.2742	0.6102	0.5259	0.2240	0.2388	0.2279
25	0.2564	0.2555	0.6390	0.5916	0.0725	0.1003	0.0937
50	0.3554	0.8774	0.8733	0.7622	0.0483	0.0825	0.0822
100	0.2960	0.2952	0.7019	0.7216	0.0812	0.1042	0.1721
200	1.0109	0.2683	0.6574	0.6213	0.0820	0.0905	0.1718
500	1.1335	0.2927	0.7127	0.6772	0.0688	0.0969	1.1335

From the sensitivity analysis, one dimensional modeling is dependent on the selection of Manning's n coefficients which account for energy losses associated with vegetation and sediment roughness. Therefore, erroneous estimates of these parameters negatively affect model output. The detailed roughness coefficient evaluation incorporated in our approach affords confidence in the model output.

The disconnected inundation surfaces in some areas of the study site result from cross section locations at junctions and areas of abrupt bed slope gradient change. Many of the reach junctions occurred in wide flat regions and restricted the number of cross sections that could be incorporated into the model. Balancing the momentum equation across large gaps with minimal cross sections is not recommended. The limited number of cross sections produced a disconnected inundation surface. A possible solution to the disconnected surface would be to model the Blackfoot network as a single reach with flow change locations where tributaries connect. The model also had difficulty creating an inundation surface at road intersections. Water surface elevations in the inundation map were based on interpolations between cross section water surface elevations. Changes in topography between cross sections were not accounted for in a one-dimensional model, which also could have produced error in the inundation surface. Smaller cell sizes in the inundation surface resulted in greater connectivity, but cell size selection was based on the accuracy of the survey data. These errors are acceptable because the inundation surface captured the critical areas of concern for the flood risk analysis.

Channel geometry was likely a source of error in the model output. The combination of several survey data sets to create a topographic TIN resulted in a highly variable elevation surface. Cross sections cut at locations with detailed survey data were located at elevations lower than those cut at interpolated locations without detailed survey data. The geometry of cross sections at interpolated locations was modified to fit the same slope as the surveyed cross sections while maintaining channel geometry across the cross section. However, this adjustment resulted in water surface elevations that did not match the TIN used to estimate the inundation surface and created gaps in the inundation surface. Future approaches should include a single detailed survey to avoid abrupt changes in geometry within the interpolated surface.

Initiation of motion using the Shields relation requires a dimensionless shear variable, which is dependent on the size and gradation of sediment, channel characteristics, and discharge. Even though the dimensionless shear varies, this parameter is often assumed to be constant for a range of sediment particle sizes (Simons and Sentürk 1992). Limitations exist with initiation of motion and sediment transport relations. Most transport relations, developed in sand-bed flumes and channels, rely on tests completed in flumes under steady and uniform conditions. The sediment transport relations also attribute measured variable deviations as errors in measurement and decrease the reliability of the estimates (Simons and Sentürk 1992).

Sediment sampled with a gravelometer provided data for sediment distributions across cross sections and provided parameters for roughness coefficient estimates and critical velocity calculations. Sediment distributions estimated with sieved samples introduces bias for smaller sediment sizes but provided data for fine sediment distributions which are generally mobilized first during a flood event. An in-depth investigation of sediment critical shear stress might involve flume tests with sediment samples but does not capture dynamic flow characteristics likely present in the system.

3.2 Model coupling and mapping

The analysis method presented here incorporates resuspension risk assessment variables with collected data and modeling techniques accepted within the practice. The topographic TIN generated from land surveys and an orthorectified aerial photo captured detailed topography for cross sections used in the hydraulic model. The velocity distribution TIN, generated from cross sections and associated velocity values, interpolated planar surfaces appropriate for the one-dimensional hydraulic model output. Since velocity values at cross sections vary significantly due to changes in channel slope, cross section geometry, and roughness factors, the planar surfaces of velocity values between the cross sections maintained velocity values along the cross sections.

Spatial interpolation of sample points is a common decision making tool for soil remediation and erosion and deposition studies. Soil properties and contaminant distributions are difficult to model and track even with a large number of sample points in such a heterogeneous system. The spatial interpolation tools in the GIS produce distribution surfaces that can be used for making cost-efficient decisions for remediation strategies, but the results of spatial analysis differ with interpolation techniques.

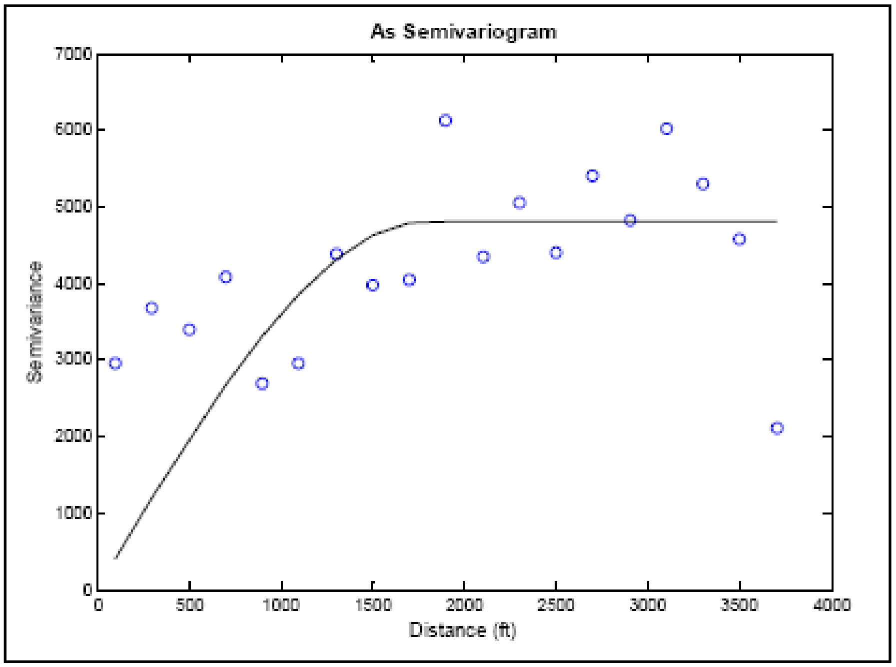

Figure 3.3. The semivariogram for sampled sediment containing arsenic, fit with a spherical model, demonstrates the decreasing similarity of data points (blue dots) with increasing distance from known points.

Spatial interpolation introduces uncertainty to modeling. Attempts to minimize uncertainty included selecting interpolation methods appropriate for the data type. Kriging of contamination sample points attempted to reduce interpolation bias by assigning weights to observational points dependent on distances between the points and estimation locations as well as mutual distances among observational points. Semivariograms helped to assess the spatial dependency of observational data points in which a functional relationship between the spatial pattern of the sampled points and their observed values was defined. Semivariograms for arsenic, cadmium, copper, zinc, and lead concentrations were fit with a spherical model (see Figure 3.3), and parameters from the model were used to interpolate a kriged contamination surface. The error variance for each kriged surface indicates higher variance further from known points. In particular, the error variance was high at the edges of the surface where fewer points were used to interpolate values across the grid. However, most of these areas were beyond the bounding inundation surface and likely had little effect on our results. Appendix F contains semivariogram figures for each metal evaluated.

Table 3.5. The summary of EPA Region 9 Preliminary Remediation Goals for comparison with soil, mine waste, and tailings sample data assisted with identifying areas where metal concentration levels exceeded screening levels in the upper marsh study area.

a DEQ Action Level for Arsenic in Surface Soil (DEQ Remediation Division, 2005).

b EPA Region 9 Preliminary Remediation Goals (PRGs) for residential soil (October 2004).

Metal	Aluminum (mg/kg)	Arsenic (mg/kg)	Cadmium (mg/kg)	Copper (mg/kg)	Lead (mg/kg)	Mercury (mg/kg)	Manganese (mg/kg)	Zinc (mg/kg)
Residential PRG	77,000	40[a]	37[b]	3,100[b]	400[b]	230[b]	1.800[b]	23,000[b]
TEL[c]	--	5.9	0.596	35.7	35	0.174	--	123
PAET[c]	--	19	97.5	340	240	0.16	1,400	500
SEL[c]	--	33	10	110	250	2	1,100	820

For the 10, 25, and 100 year flood events, the combination of distribution maps for velocity, critical velocity, sediment size, flood extents, and metal contamination (As, Cu, Cd, Pb, and Zn) help identify areas of potential concern in the wetland. Appendix D provides a list of input data sets collected for the hazard probability analysis. An analysis of the metals of potential concern identified areas where specific metals exceeded preliminary remediation goals for residential screening levels and ecological screening levels (see Appendix E). Table 3.5 lists the DEQ and Environmental Protection Agency (EPA) remediation goals for the site.

The velocity surface was compared to the critical velocity surface, and areas where the velocity exceeded the critical velocity were identified. Percentages of velocity exceeding critical velocity were high within the wetland study area and were indicated with a three-dimension elevation map. Spikes in Figure 3.4 indicate areas where velocities exceed critical velocities. Figure 3.4 demonstrates the hazardous areas for the 100 year flood event along with arsenic concentration distributions. For the 10, 25, and 100 year events, estimated velocities exceed critical velocity by 97 percent, 99 percent, and 76 percent, respectively, in the study area (see Table 3.6). Appendix G contains exceedance figures for each modeled event in addition to contaminant distribution surfaces. Results from the potential hazard analysis indicate increasing hazard regions with larger flood events. Metal concentrations are higher at the entrance of the wetland where tributaries intersect and where the flood wave from the 1975 breach event lost energy and deposited sediment.

Table 3.6. A comparison of the upper marsh area indicates areas where velocities for the 10, 25, and 100 year flood events exceed critical velocities.

Flood Event (year)	Total Area Inundated by 100yr flood in the Upper Marsh	Area Velocity Exceeds Critical Velocity	Percent of Total Marsh Area where $V>V_c$
	(acres)	(acres)	(%)
100	57	43	76
25	38	38	99
10	28	27	98

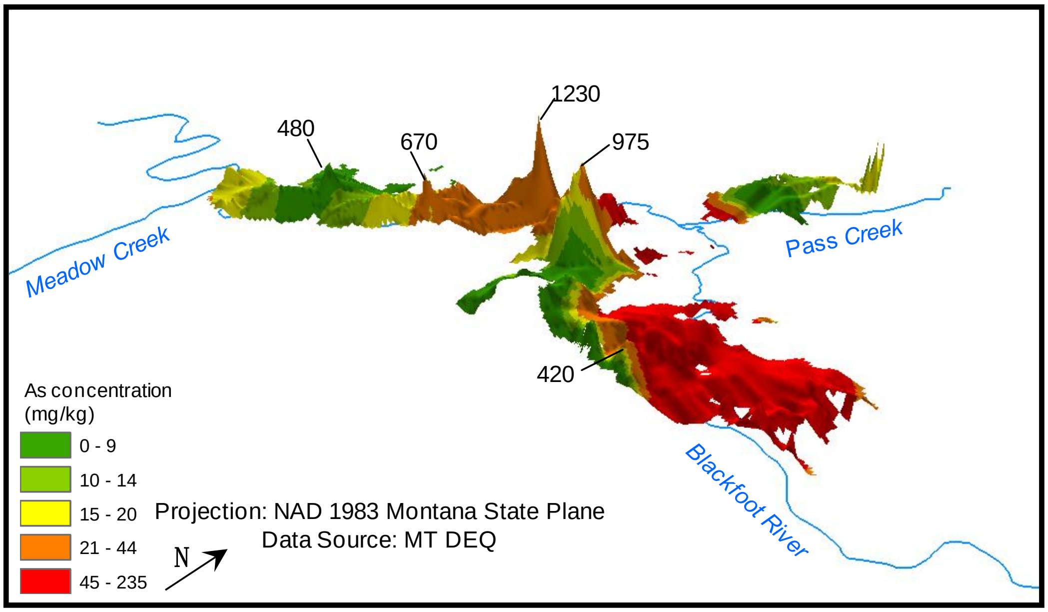

Figure 3.4. For a 100-year flood event, areas of potential concern include those where spikes occur in the surface identifying the magnitude of velocities exceeding critical velocities and those where contaminant sediment levels are significant.

4.0 CONCLUSION

Water resource problems, in particular, flood inundation mapping, rely on robust hydrologic and hydraulic models such as HEC-RAS. Intricate analysis and simulation capabilities are available with both hydrologic/hydraulic models and GIS, and the integration of the two provides a powerful tool for scientific researchers and policy makers. The widespread availability of spatially distributed data through GIS has made physically based hydrologic models more useable and spurred the development of hydrologic models that take advantage of these new data. This approach for evaluating the potential hazards of metals-trapping wetlands will aid the MT DEQ and the US Forest Service in prioritizing and implementing remediation action items for the UBMC and similar mine reclamation sites. In this study, the coupling of GIS and a hydraulic model through HEC-geoRAS produced an inundation surface only after numerous modeling iterations. The disconnected stream flow results resulted from cell size selection and were influenced by the wide shallow topography of the site. The inundation surface bounded resuspension parameters, critical velocity, sediment size, and metal contamination to model areas of possible resuspension risk. Providing agencies, consultants, and watershed groups with a viable, low cost, computationally efficient method with minimal data requirements for quantifying the risk associated with transport of contaminated sediments out of wetlands will aid these entities in prioritization of restoration efforts and help reduce mining impacts to downstream communities and environments.

Despite the complex nature of the wetland system, the one-dimensional hydraulic model proved to be a sufficient tool to estimate the water surface elevations and flow parameters. Sensitivity analysis showed the one-dimensional hydraulic model to be increasingly sensitive to roughness coefficients at larger discharges. This highlights the need for careful characterization and mapping of roughness values if large flood events are being modeled. Comparison of modeled stream velocity distributions to measured velocity distributions showed deviations from observed data in shallow near-bank and over-bank areas. Further investigation is needed in this area to quantify the effect of these deviations on model output for a variety of discharge events. Thorough investigation of differences between modeled and measured velocity distributions at a range of flows and across several transects at a given site will help practitioners decide whether or not this approach will be useful and may improve confidence in modeled output. We conclude that, if carefully applied, this approach may be a valuable tool for coarse assessments of contaminated sediment mobilization risk in areas where data is limited and/or development of more data/computationally intensive sediment transport, 2D or 3D models is not feasible.

REFERENCES

Aberle, J., Nikora, V., and Walters, R. (2004). "Effects of bed material properties on cohesive sediment erosion." *Marine Geology*, 207(1-4), 83-93.

Akan, A. O. (2006). *Open Channel Hydraulics*, Elsevier, Burlington, MA.

Aldridge, B. N., Garrett, J. M., and Highway, D. (1973). *Roughness Coefficients for Stream Channels in Arizona*, US Dept. of the Interior, US Geological Survey.

Andrews, E. D. (1983). "Entrainment of gravel from naturally sorted riverbed material." *Bulletin of the Geological Society of America*, 94(10), 1225-1231.

Auble, G. T., Scott, M. L., and Friedman, J. M. (2005). "Use of individualistic streamflow-vegetation relations along the Fremont River, Utah, USA to assess impacts of flow alteration on wetland and riparian areas." *Wetlands*, 25(1), 143-154.

August, E. E., McKnight, D. M., Hrncir, D. C., and Garhart, K. S. (2002). "Seasonal variability of metals transport through a wetland impacted by mine drainage in the Rocky Mountains." *Environmental Science & Technology*, 36(17), 3779-3786.

Bendoricchio, G., Luigi Dal Cin, and Jesper Persson. (2000). "Guidelines for free water surface wetland design." *ECOSYSTEMS*, 8, 51-91.

Benson, M. A., and Dalrymple, T. (1967). "GENERAL FIELD AND OFFICE PROCEDURES FOR INDIRECT DISCHARGE MEASUREMENTS."

Bergeron, N. E., and Abrahams, A. D. "Estimating shear velocity and roughness length from velocity profiles." *WATER RESOUR RES*, 28(8).

Brunner, G. W. (2002). "HEC-RAS, River Analysis System Hydraulic Reference Manual, Version 3.1." In: *US Army Corps of Engineers, Hydrologic Engineering Center, CPD-69*, 1-377.

Chow, V. T. (1959). "Open-channel hydraulics." In: *New York/Tokyo*, McGraw-Hill, 680.

Cook, S. A. (2007). "Characterization of riparian wetland soils and associated metal concentrations at the headwaters of the Stillwater River, Montana," Montana State University, Bozeman, MT.

Dollhopf, D. J., Goering, J. D., Rennick, R. B., Morton, R. B., Gauger, W. K., Guckert, J. B., Jones, P. B., Cooksey, K. C., Bucklin, K. E., Weed, R., and Lehman, M. M. (1988). "Hydrochemical, vegetational and microbiological effects of a natural and constructed wetland on the control of acid mine drainage." *RRU 8804*, Montana Abandoned Mine Reclamation Bureau, Helena, MT.

Fischenich, C., Engineer, R., and Development Center Vicksburg Ms Environmental, L. A. B. (2001). "Stability Thresholds for Stream Restoration Materials." ENGINEER RESEARCH AND DEVELOPMENT CENTER VICKSBURG MS ENVIRONMENTAL LAB.

Furniss, G., Hinman, N. W., Doyle, G. A., and Runnells, D. D. (1999). "Radiocarbon-dated ferricrete provides a record of natural acid rock drainage and paleoclimatic changes." *Environmental Geology*, 37(1), 102-106.

Gibbs, R. J. (1973). "Mechanisms of Trace Metal Transport in Rivers." *Science*, 180(4081), 71-73.

Gurrieri, J. T. (1998). "Distribution of metals in water and sediment and effects on aquatic biota in the upper Stillwater River basin, Montana." *Journal of Geochemical Exploration*, 64(1-3), 83-100.

Haag, I., Kern, U., and Westrich, B. (2001). "Erosion investigation and sediment quality measurements for a comprehensive risk assessment of contaminated aquatic sediments." *Science of the Total Environment, The*, 266(1-3), 249-257.

Haneef-Mian, M., Yanful, E. K., and Martinuzzi, R. (2007). "Measuring the onset of mine tailings erosion." *Canadian Geotechnical Journal*, 44(4), 473-489.

Hicks, N. S., Smith, J. A., Miller, A. J., and Nelson, P. A. (2005). "Catastrophic flooding from an orographic thunderstorm in the central Appalachians." *Water Resource Research*, 41(W12428), doi:10.1029/2005WR004129.

Hu, J. (Year). "Methods of Generating Surfaces In Environmental GIS Applications." 22-26.11.

Jarrett, R. D. (1984). "Hydraulics of high-gradient streams." *Journal of hydraulic engineering*, 110(11), 1519-1539.

Johnson, G. D., Strickland, M. D., Buyok, J. P., Derby, C. E., and Young, D. P. (1999). " Quantifying impacts to riparian wetlands associated with reduced flows along the Greybull River, Wyoming " *Wetlands*, 19(1), 71-77.

Julien, P. Y. (1995a). *Erosion and Sedimentation*, Cambridge University Press.

Julien, P. Y. (1995b). *Erosion and Sedimentation*, Cambridge University Press.

Kadlec, R. H. (1990). "Overland Flow in Wetlands: Vegetation Resistance." *Journal of Hydraulic Engineering*, 116(5), 691-706.

Kadlec, R. H., and Knight, R. L. (1996). *Treatment Wetlands*, CRC Press, Boca Raton, Fla.

Kitanidis, P. K. (1997). *Introduction to Geostatistics: Applications to Hydrogeology*, Cambridge University Press, Cambridge.

Marcus, W. A., Roberts, K., Harvey, L., and Tackman, G. (1992). "An evaluation of methods for estimating Manning's n in small mountain streams." *Mountain Research and Development*, 12(3), 227-239.

Marx, D. a. K. T. (1987). *Practical Aspects of Agricultural Kriging*, Arkansas Agricultural Experiment Station, Fayettville.

McCoy, J., and Johnston, K. (2001). *Using ArcGIS spatial analyst*, Environmental Systems Research Institute, Redlands.

Merwade, V., Cook, A., and Coonrod, J. (2008). "GIS techniques for creating river terrain models for hydrodynamic modeling and flood inundation mapping." *Environmental Modelling and Software*, 23(10-11), 1300-1311.

Moore, J. N. (1992). "Mine effluent effects on non-point source contaminants in the Blackfoot River, Montana." Prepared for Lewis and Clark City-County Health Department. University of Montana, Geology Department, Missoula, MT.

Ogden, F. L., Garbrecht, J., DeBarry, P. A., and Johnson, L. E. (2001). "GIS and Distributed Watershed Models. II: Modules, Interfaces, and Models." *Journal of Hydrologic Engineering*, 6(6), 515-523.

Pappenberger, F., Beven, K., Horritt, M., and Blazkova, S. (2005). "Uncertainty in the calibration of effective roughness parameters in HEC-RAS using inundation and downstream level observations." *Journal of Hydrology*, 302(1-4), 46-69.

Parrett, C., Johnson, D. R. C. A. G. S., United States, and Bureau of Indian Affairs. (2004). *Methods for estimating flood frequency in Montana based on data through water year 1998*, U.S. Dept. of the Interior U.S. Geological Survey ; Denver CO : U.S. Geological Survey Information Services distributor, Reston, Va.

Schneider, V. R., and Arcement, G. J. (1989). "Guide for Selecting Manning's Roughness Coefficients for Natural Channels and Flood Plains." *Available from the US Geological Survey, Books and Open-File Reports Section, Box 25425, Federal Center, Denver, CO 80225-0425. Water-Supply Paper 2339, 1989. 38 p, 22 fig, 4 tab, 23 ref.*

Simons, D. B., and Sentürk, F. (1992). *Sediment transport technology: water and sediment dynamics*, Water Resources Publication.

Spence, L. E. (1975). "Upper Blackfoot River Study, A Preliminary Inventory of Aquatic and Wildlife Resources." Montana Department of Fish and Game, Missoula, Montana.

Sui, D. Z., and Maggio, R. C. (1999). "Integrating GIS with hydrological modeling: practices, problems, and prospects." *Computers, Environment and Urban Systems*, 23(1), 33-51.

Tate, E. C., Maidment, D. R., Olivera, F., and Pe, D. J. A. (2002). "Creating a Terrain Model for Floodplain Mapping." *Journal of Hydrologic Engineering*, 7, 100.

TetraTech. (2007). "Final sampling and analysis plan. 2007 fall sampling event. Remedial investigation. Upper Blackfoot Mining Complex." Montana Department of Environmental Quality, Helena, MT.

Thompson, J. R., Soerenson, H. R., Gavin, H., and Refsgaard, A. (2004a). "Application of the coupled MIKE SHE/MIKE 11 modelling system to a lowland wet grassland in southeast England." *Journal of Hydrology*, 293(1), 151-179.

Thompson, J. R., Sørenson, H. R., Gavin, H., and Refsgaard, A. (2004b). "Application of the coupled MIKE SHE/MIKE 11 modelling system to a lowland wet grassland in southeast England." *Journal of Hydrology*, 293(1-4), 151-179.

Werner, M. G. F. (2001). "Impact of grid size in GIS based flood extent mapping using a 1D flow model." *Physics and Chemistry of the Earth, Part B*, 26(7-8), 517-522.

Wong, J. W. C., Ip, C. M., and Wong, M. H. (1998). "Acid-forming capacity of lead–zinc mine tailings and its implications for mine rehabilitation." *Environmental Geochemistry and Health*, 20(3), 149-155.

Appendix B

Watershed Variables

Table 11. Watershed variables for each transect of the study area.

XSID	REACH	DA	EARAVG	EARMED	SELEV	SNEAVG	SNEMED	UBEAVG	UBEMED	UBGAVG	UBGMED	SUBAVG
		m2	m	m	m	m	M	m	m			m2
4	BT	4761700	1907	1892	1653	1709	1702	1901	1886	49.41	50.03	800
5	BT	4779800	1906	1891	1651	1708	1701	1900	1885	49.37	50.03	800
6	BT	4781900	1906	1891	1650	1707	1701	1900	1885	49.36	50.03	800
7	BT	4794700	1905	1891	1645	1707	1701	1899	1884	49.36	50.03	800
8	BT	5011500	1900	1883	1641	1705	1700	1894	1876	49.17	50.00	800
9	BT	5081600	1897	1879	1637	1703	1698	1891	1873	49.09	50.00	800
10	BT	5125100	1896	1878	1633	1701	1697	1890	1871	49.03	50.00	800
11	BT	5170600	1894	1876	1631	1700	1696	1888	1869	48.95	49.91	800
12	AN	7469200	1923	1921	1630	1730	1718	1918	1916	49.37	49.53	1000
13	AN	7433300	1923	1922	1633	1731	1719	1919	1917	49.39	49.53	1000
14	AN	7368300	1925	1923	1637	1733	1722	1920	1919	49.42	49.62	1000
15	UB	12799900	1909	1901	1621	1714	1703	1903	1895	49.09	49.62	900
16	UB	12880900	1908	1900	1617	1713	1702	1901	1894	49.04	49.53	900
17	UB	12882400	1908	1900	1617	1713	1702	1901	1894	49.04	49.53	900
18	UB	13537200	1902	1892	1613	1712	1701	1896	1886	48.72	49.24	900
19	UB	13586900	1901	1891	1611	1711	1701	1895	1885	48.67	49.24	900
20	UB	13696200	1900	1889	1608	1710	1700	1894	1883	48.60	49.24	900
21	UB	13723900	1899	1889	1606	1709	1700	1893	1883	48.59	49.24	900
22	UB	13781500	1898	1888	1604	1708	1700	1892	1882	48.56	49.15	900
23	UB	13853800	1897	1887	1602	1708	1699	1891	1881	48.52	49.15	900
24	UB	13891100	1897	1887	1600	1707	1699	1890	1880	48.47	49.12	900
25	UB	14109600	1895	1884	1599	1706	1697	1889	1877	48.37	48.89	900
26	UB	14177700	1894	1883	1597	1707	1698	1888	1876	48.28	48.89	900
27	UB	14225800	1893	1882	1597	1706	1698	1887	1876	48.23	48.77	900

Appendix C
Watershed Variable Selection
Correlation Tables

Table 12. Watershed variables explored for use in the regression analysis.

Variable	Description
Drainage Area at Site (DA)	area draining in to stream at the site
Elevation above Riparian Area (EARAVG, EARMED)	the average and median difference in elevation between grid cells in the upslope drainage area and grid cells in the riparian zone
Site Elevation (SELEV)	elevation of the most downstream point in a site
Stream Network Elevation (SNEAVG, SNEMED)	the average and median elevation of all stream grid cells upstream of the site
Subcatchment Size (SUBAVG)	the average contributing area of all grid cells draining into the site
Upslope Basin Elevation (UBEAVG, UBEMED)	the average and median elevation of all grid cells draining into the riparian zone, including stream cells
Upslope Basin Gradient (UBGAVG, UBGMED)	the average and median slope of all grid cells draining into the riparian zone, including stream cells

Table 13. Correlation table of watershed variables for the Anaconda reach.

	DA	EARAVG	EARMED	SELEV	SUBAVG	SNEAVG	SNEMED	UBEAVG	UBEMED	UBGAVG	UBGMED
DA	1.000	-0.928	-0.986	-0.996	1.000	-1.000	-0.993	-0.986	-1.000	-0.999	-0.928
EARAVG	-0.928	1.000	0.854	0.894	-0.928	0.938	0.966	0.854	0.938	0.908	1.000
EARMED	-0.986	0.854	1.000	0.997	-0.986	0.982	0.959	1.000	0.982	0.993	0.854
SELEV	-0.996	0.894	0.997	1.000	-0.996	0.994	0.979	0.997	0.994	0.999	0.894
SUBAVG	1.000	-0.928	-0.986	-0.996	1.000	-1.000	-0.993	-0.986	-1.000	-0.999	-0.928
SNEAVG	-1.000	0.938	0.982	0.994	-1.000	1.000	0.996	0.982	1.000	0.997	0.938
SNEMED	-0.993	0.966	0.959	0.979	-0.993	0.996	1.000	0.959	0.996	0.985	0.966
UBEAVG	-0.986	0.854	1.000	0.997	-0.986	0.982	0.959	1.000	0.982	0.993	0.854
UBEMED	-1.000	0.938	0.982	0.994	-1.000	1.000	0.996	0.982	1.000	0.997	0.938
UBGAVG	-0.999	0.908	0.993	0.999	-0.999	0.997	0.985	0.993	0.997	1.000	0.908
UBGMED	-0.928	1.000	0.854	0.894	-0.928	0.938	0.966	0.854	0.938	0.908	1.000

Table 14. Correlation table of watershed variables for the Beartrap reach.

	DA	EARAVG	EARMED	SELEV	SUBAVG	SNEAVG	SNEMED	UBEAVG	UBEMED	UBGAVG	UBGMED
DA	1.000	-0.997	-0.999	-0.972	1.000	-0.974	-0.962	-0.997	-0.999	-0.995	-0.837
EARAVG	-0.997	1.000	0.997	0.984	-0.997	0.985	0.977	1.000	0.999	0.998	0.855
EARMED	-0.999	0.997	1.000	0.969	-0.999	0.976	0.969	0.997	0.998	0.996	0.840
SELEV	-0.972	0.984	0.969	1.000	-0.972	0.985	0.967	0.984	0.979	0.978	0.826
SUBAVG	1.000	-0.997	-0.999	-0.972	1.000	-0.974	-0.962	-0.997	-0.999	-0.995	-0.837
SNEAVG	-0.974	0.985	0.976	0.985	-0.974	1.000	0.992	0.985	0.979	0.988	0.856
SNEMED	-0.962	0.977	0.969	0.967	-0.962	0.992	1.000	0.977	0.968	0.982	0.874
UBEAVG	-0.997	1.000	0.997	0.984	-0.997	0.985	0.977	1.000	0.999	0.998	0.855
UBEMED	-0.999	0.999	0.998	0.979	-0.999	0.979	0.968	0.999	1.000	0.997	0.843
UBGAVG	-0.995	0.998	0.996	0.978	-0.995	0.988	0.982	0.998	0.997	1.000	0.873
UBGMED	-0.837	0.855	0.840	0.826	-0.837	0.856	0.874	0.855	0.843	0.873	1.000

Table 15. Correlation table of watershed variables for the Upper Blackfoot reach.

	DA	EARAVG	EARMED	SELEV	SUBAVG	SNEAVG	SNEMED	UBEAVG	UBEMED	UBGAVG	UBGMED
DA	1.000	-0.997	-0.999	-0.967	1.000	-0.952	-0.941	-0.992	-0.999	-0.996	-0.971
EARAVG	-0.997	1.000	0.998	0.980	-0.997	0.966	0.945	0.997	0.997	0.996	0.970
EARMED	-0.999	0.998	1.000	0.970	-0.999	0.955	0.941	0.992	0.998	0.997	0.970
SELEV	-0.967	0.980	0.970	1.000	-0.967	0.988	0.959	0.990	0.976	0.975	0.948
SUBAVG	1.000	-0.997	-0.999	-0.967	1.000	-0.952	-0.941	-0.992	-0.999	-0.996	-0.971
SNEAVG	-0.952	0.966	0.955	0.988	-0.952	1.000	0.962	0.975	0.961	0.955	0.935
SNEMED	-0.941	0.945	0.941	0.959	-0.941	0.962	1.000	0.950	0.952	0.943	0.953
UBEAVG	-0.992	0.997	0.992	0.990	-0.992	0.975	0.950	1.000	0.994	0.994	0.967
UBEMED	-0.999	0.997	0.998	0.976	-0.999	0.961	0.952	0.994	1.000	0.997	0.972
UBGAVG	-0.996	0.996	0.997	0.975	-0.996	0.955	0.943	0.994	0.997	1.000	0.979
UBGMED	-0.971	0.970	0.970	0.948	-0.971	0.935	0.953	0.967	0.972	0.979	1.000

Appendix D

Watershed Variable Selection

Distribution Among Canopy Types

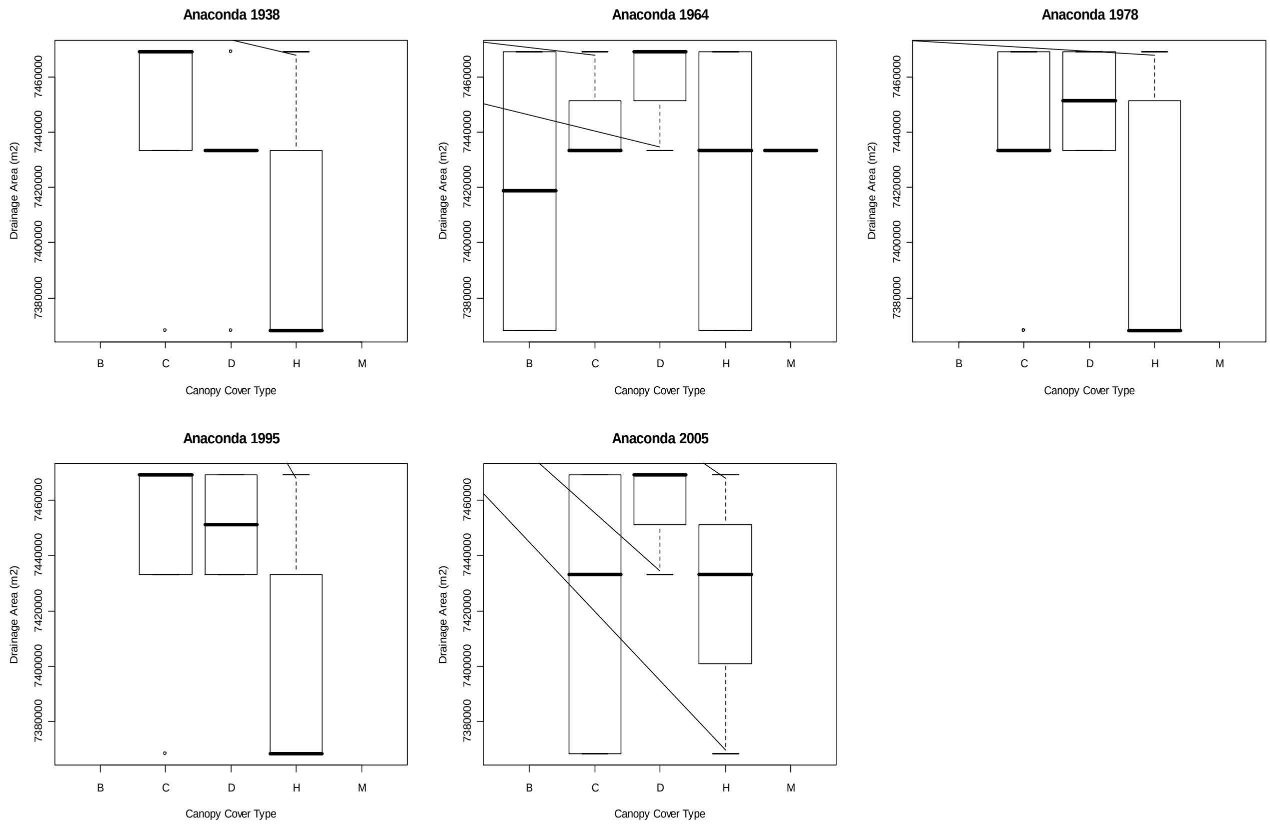

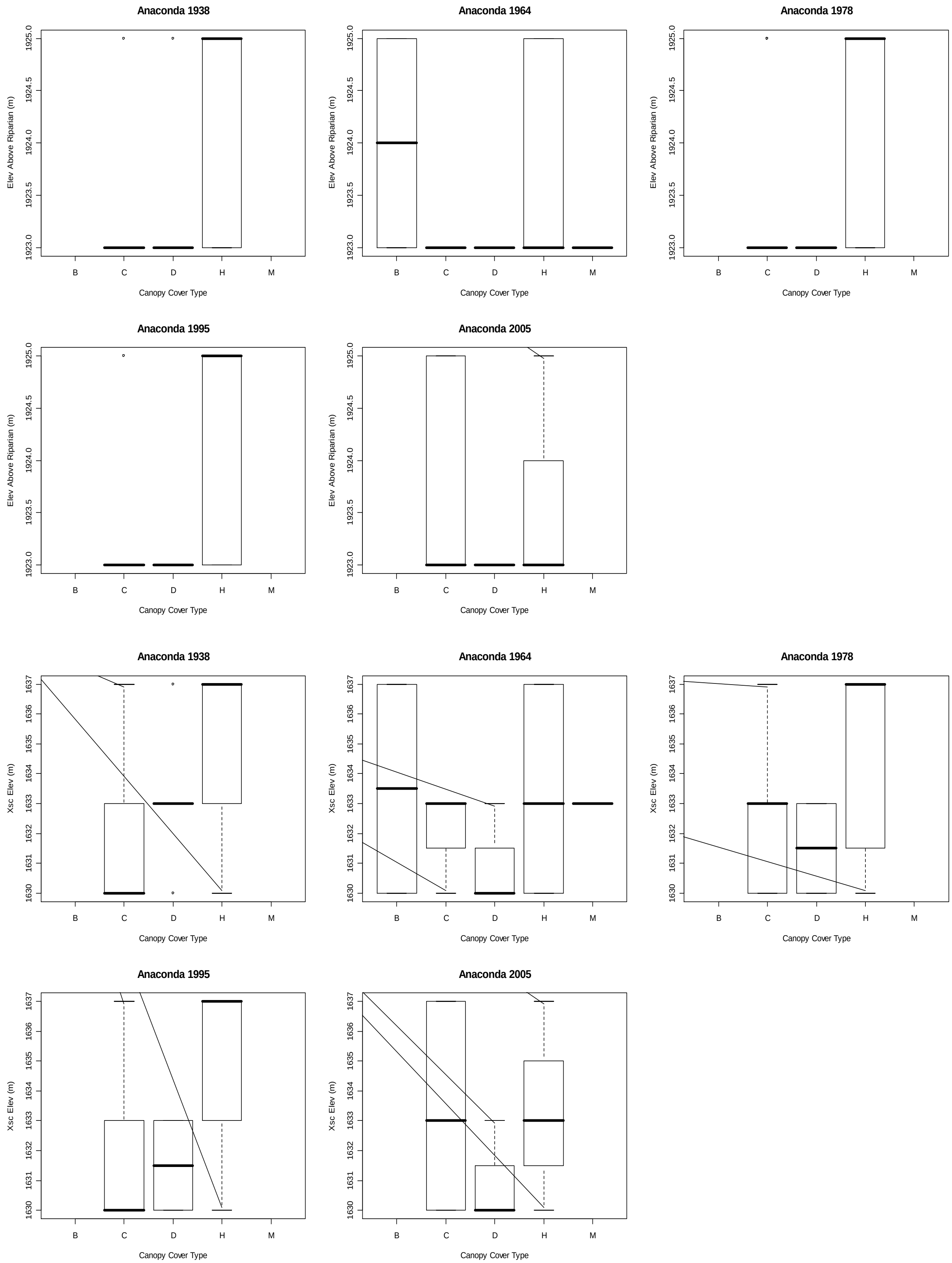
Anaconda 1938
Anaconda 1964
Anaconda 1978
Anaconda 1995
Anaconda 2005
Elev Above Riparian (m)
Xsc Elev (m)
Canopy Cover Type
B C D H M

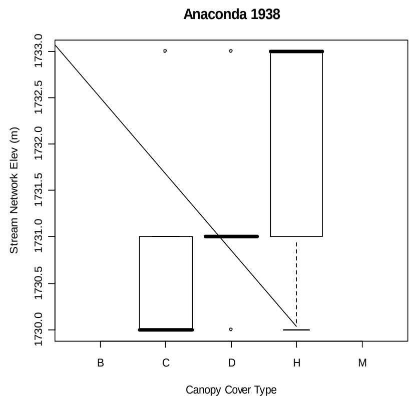
Anaconda 1938
Stream Network Elev (m)
1730.0 1730.5 1731.0 1731.5 1732.0 1732.5 1733.0
B C D H M
Canopy Cover Type

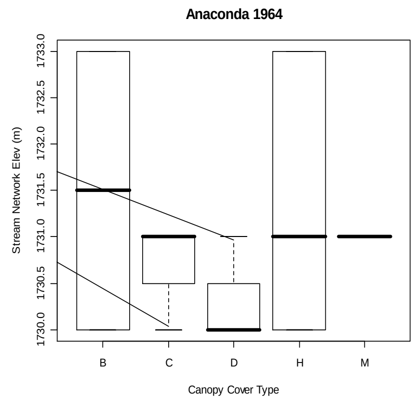
Anaconda 1964
Stream Network Elev (m)
1730.0 1730.5 1731.0 1731.5 1732.0 1732.5 1733.0
B C D H M
Canopy Cover Type

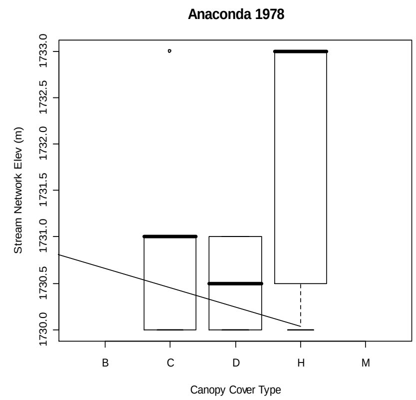
Anaconda 1978
Stream Network Elev (m)
1730.0 1730.5 1731.0 1731.5 1732.0 1732.5 1733.0
B C D H M
Canopy Cover Type

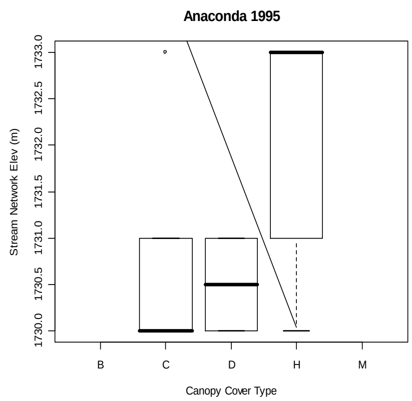
Anaconda 1995
Stream Network Elev (m)
1730.0 1730.5 1731.0 1731.5 1732.0 1732.5 1733.0
B C D H M
Canopy Cover Type

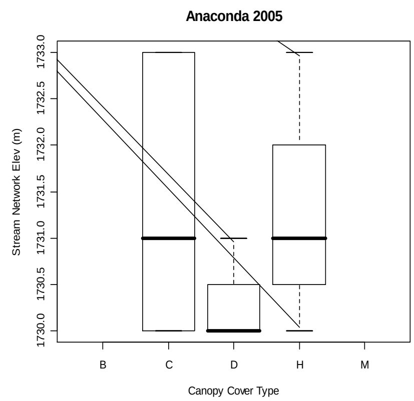
Anaconda 2005
Stream Network Elev (m)
1730.0 1730.5 1731.0 1731.5 1732.0 1732.5 1733.0
B C D H M
Canopy Cover Type

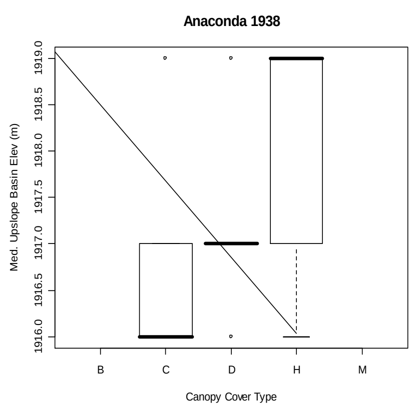
Anaconda 1938
Med. Upslope Basin Elev (m)
1916.0 1916.5 1917.0 1917.5 1918.0 1918.5 1919.0
B C D H M
Canopy Cover Type

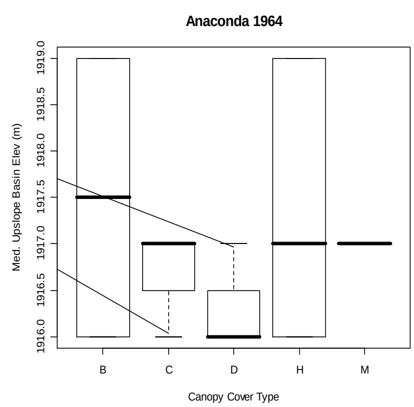
Anaconda 1964
Med. Upslope Basin Elev (m)
1916.0 1916.5 1917.0 1917.5 1918.0 1918.5 1919.0
B C D H M
Canopy Cover Type

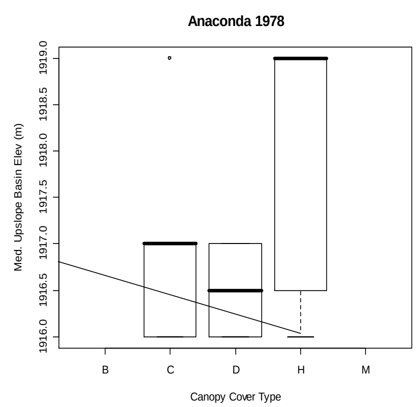
Anaconda 1978
Med. Upslope Basin Elev (m)
1916.0 1916.5 1917.0 1917.5 1918.0 1918.5 1919.0
B C D H M
Canopy Cover Type

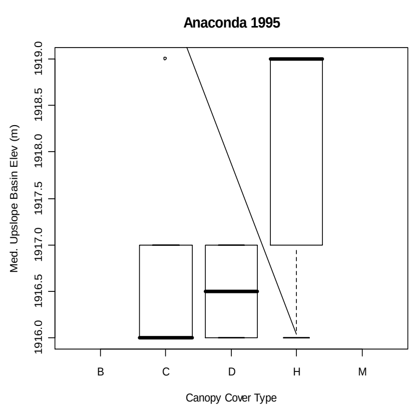
Anaconda 1995
Med. Upslope Basin Elev (m)
1916.0 1916.5 1917.0 1917.5 1918.0 1918.5 1919.0
B C D H M
Canopy Cover Type

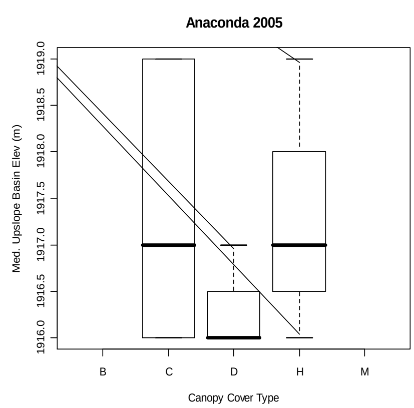
Anaconda 2005
Med. Upslope Basin Elev (m)
1916.0 1916.5 1917.0 1917.5 1918.0 1918.5 1919.0
B C D H M
Canopy Cover Type

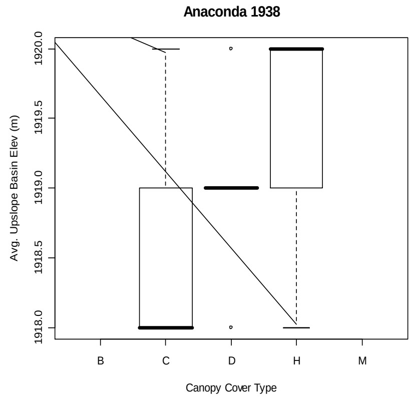
Anaconda 1938
Avg. Upslope Basin Elev (m)
1918.0
1918.5
1919.0
1919.5
1920.0
B
C
D
H
M
Canopy Cover Type

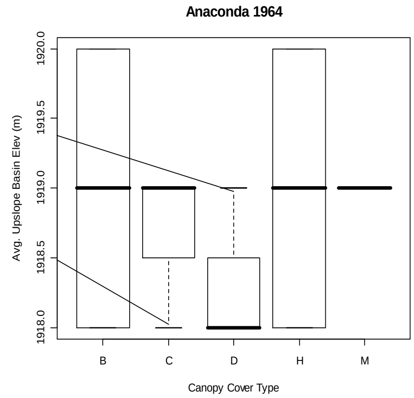
Anaconda 1964
Avg. Upslope Basin Elev (m)
1918.0
1918.5
1919.0
1919.5
1920.0
B
C
D
H
M
Canopy Cover Type

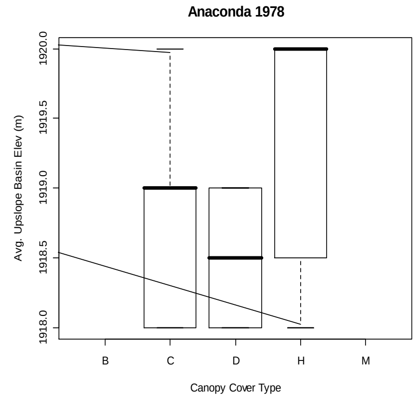
Anaconda 1978
Avg. Upslope Basin Elev (m)
1918.0
1918.5
1919.0
1919.5
1920.0
B
C
D
H
M
Canopy Cover Type

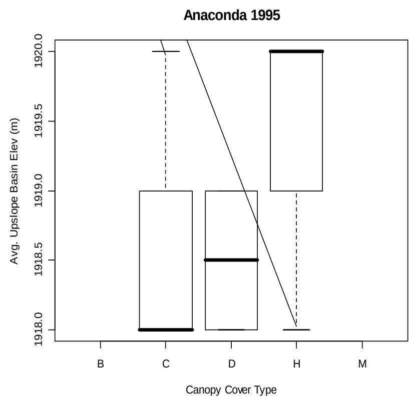
Anaconda 1995
Avg. Upslope Basin Elev (m)
1918.0
1918.5
1919.0
1919.5
1920.0
B
C
D
H
M
Canopy Cover Type

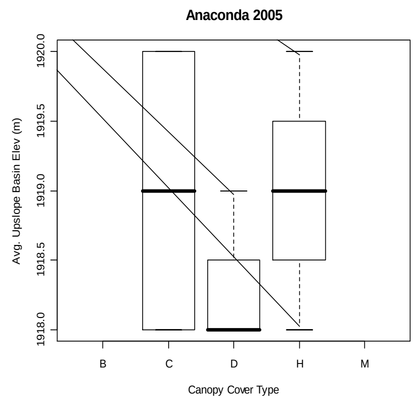
Anaconda 2005
Avg. Upslope Basin Elev (m)
1918.0
1918.5
1919.0
1919.5
1920.0
B
C
D
H
M
Canopy Cover Type

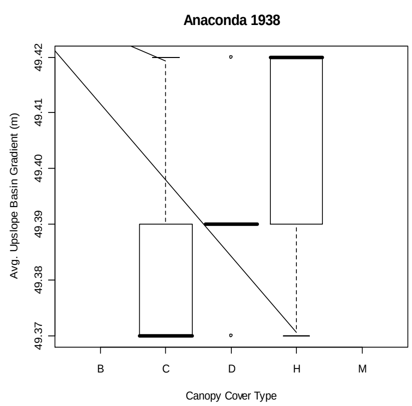
Anaconda 1938
Avg. Upslope Basin Gradient (m)
49.37
49.38
49.39
49.40
49.41
49.42
B
C
D
H
M
Canopy Cover Type

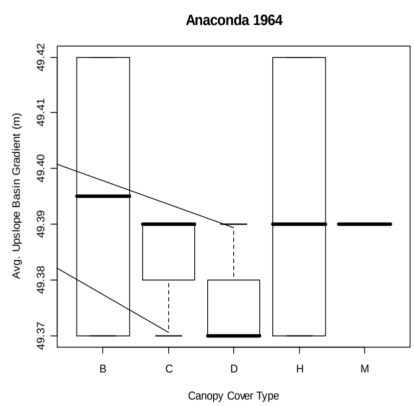
Anaconda 1964
Avg. Upslope Basin Gradient (m)
49.37
49.38
49.39
49.40
49.41
49.42
B
C
D
H
M
Canopy Cover Type

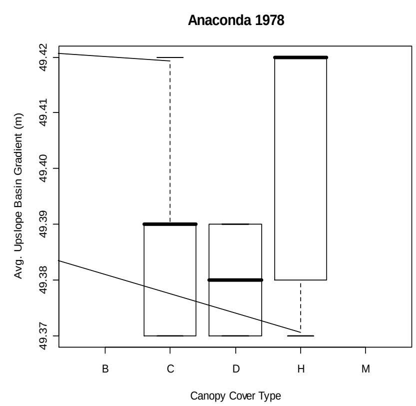
Anaconda 1978
Avg. Upslope Basin Gradient (m)
49.37
49.38
49.39
49.40
49.41
49.42
B
C
D
H
M
Canopy Cover Type

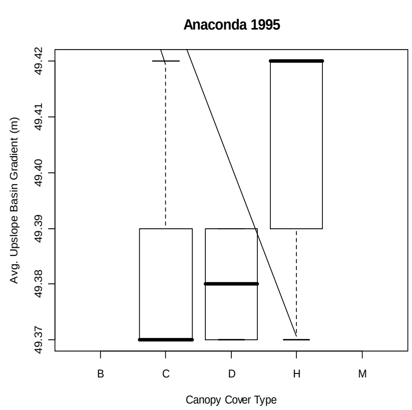
Anaconda 1995
Avg. Upslope Basin Gradient (m)
49.37
49.38
49.39
49.40
49.41
49.42
B
C
D
H
M
Canopy Cover Type

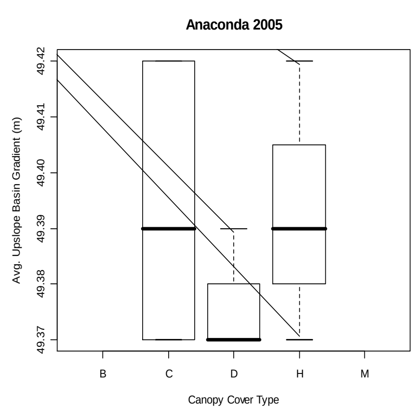
Anaconda 2005
Avg. Upslope Basin Gradient (m)
49.37
49.38
49.39
49.40
49.41
49.42
B
C
D
H
M
Canopy Cover Type

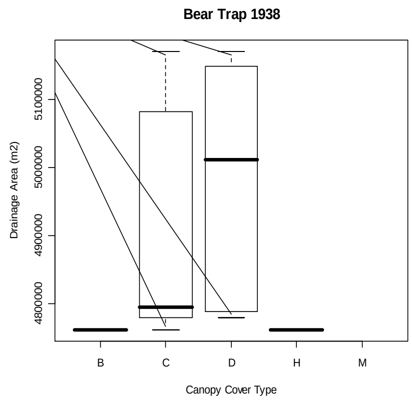
Bear Trap 1938
Drainage Area (m2)
4800000
4900000
5000000
5100000
B
C
D
H
M
Canopy Cover Type

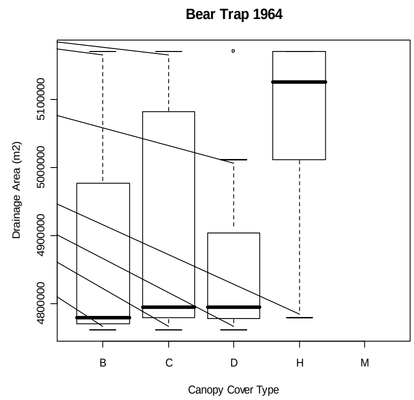
Bear Trap 1964
Drainage Area (m2)
4800000
4900000
5000000
5100000
B
C
D
H
M
Canopy Cover Type

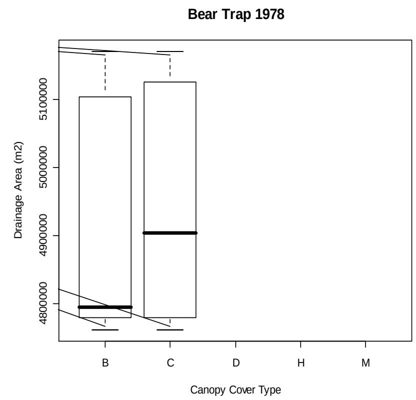
Bear Trap 1978
Drainage Area (m2)
4800000
4900000
5000000
5100000
B
C
D
H
M
Canopy Cover Type


Bear Trap 1995
Drainage Area (m2)
4800000
4900000
5000000
5100000
B
C
D
H
M
Canopy Cover Type

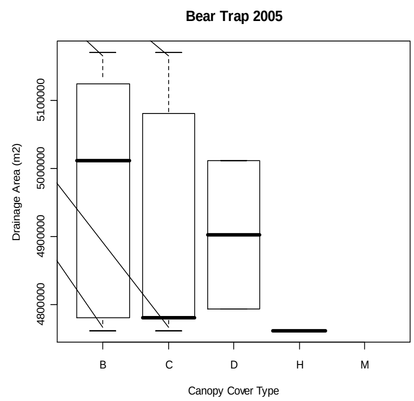
Bear Trap 2005
Drainage Area (m2)
4800000
4900000
5000000
5100000
B
C
D
H
M
Canopy Cover Type

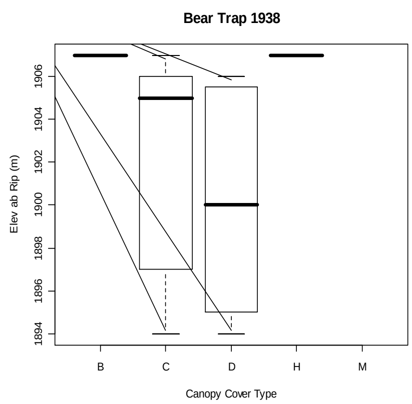
Bear Trap 1938
Elev ab Rip (m)
1894
1896
1898
1900
1902
1904
1906
B
C
D
H
M
Canopy Cover Type

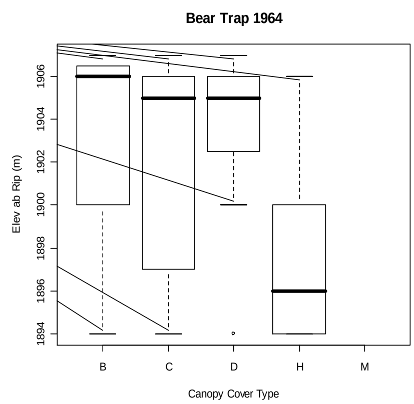
Bear Trap 1964
Elev ab Rip (m)
1894
1896
1898
1900
1902
1904
1906
B
C
D
H
M
Canopy Cover Type

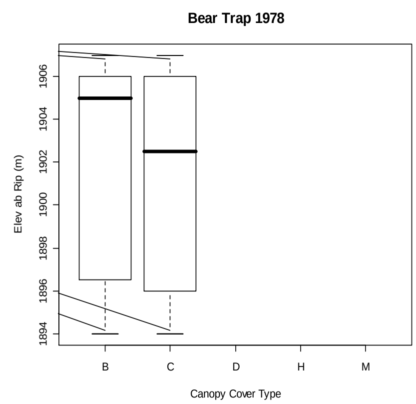
Bear Trap 1978
Elev ab Rip (m)
1894
1896
1898
1900
1902
1904
1906
B
C
D
H
M
Canopy Cover Type

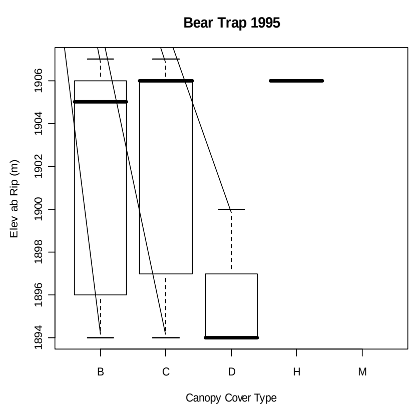
Bear Trap 1995
Elev ab Rip (m)
1894
1896
1898
1900
1902
1904
1906
B
C
D
H
M
Canopy Cover Type

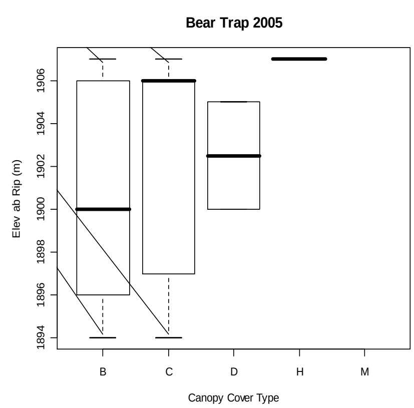
Bear Trap 2005
Elev ab Rip (m)
1894
1896
1898
1900
1902
1904
1906
B
C
D
H
M
Canopy Cover Type

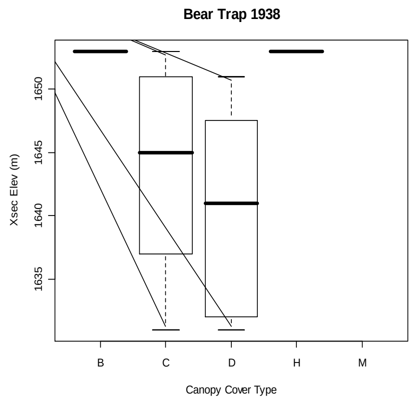
Bear Trap 1938
Xsec Elev (m)
1635 1640 1645 1650
B C D H M
Canopy Cover Type

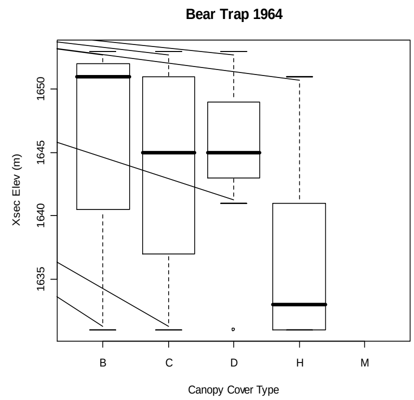
Bear Trap 1964
Xsec Elev (m)
1635 1640 1645 1650
B C D H M
Canopy Cover Type

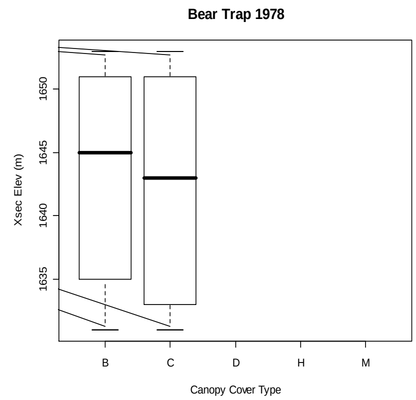
Bear Trap 1978
Xsec Elev (m)
1635 1640 1645 1650
B C D H M
Canopy Cover Type

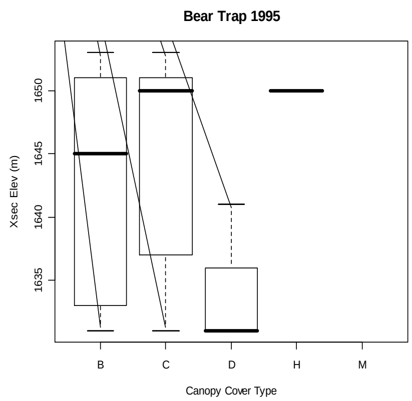
Bear Trap 1995
Xsec Elev (m)
1635 1640 1645 1650
B C D H M
Canopy Cover Type

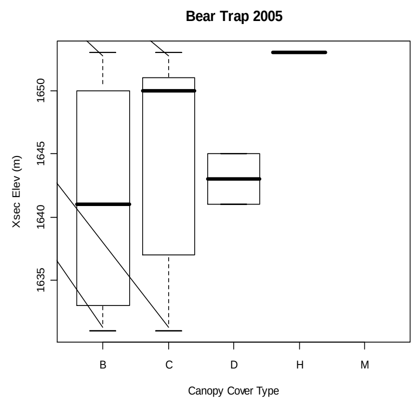
Bear Trap 2005
Xsec Elev (m)
1635 1640 1645 1650
B C D H M
Canopy Cover Type

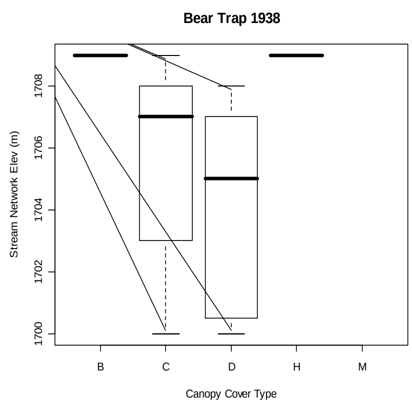
Bear Trap 1938
Stream Network Elev (m)
1700 1702 1704 1706 1708
B C D H M
Canopy Cover Type

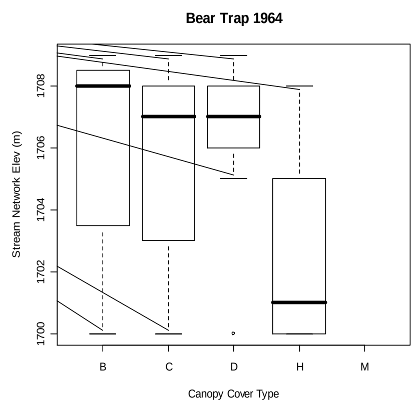
Bear Trap 1964
Stream Network Elev (m)
1700 1702 1704 1706 1708
B C D H M
Canopy Cover Type


Bear Trap 1978
Stream Network Elev (m)
1700 1702 1704 1706 1708
B C D H M
Canopy Cover Type


Bear Trap 1995
Stream Network Elev (m)
1700 1702 1704 1706 1708
B C D H M
Canopy Cover Type

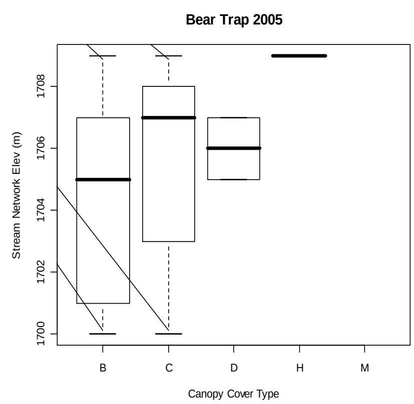
Bear Trap 2005
Stream Network Elev (m)
1700 1702 1704 1706 1708
B C D H M
Canopy Cover Type

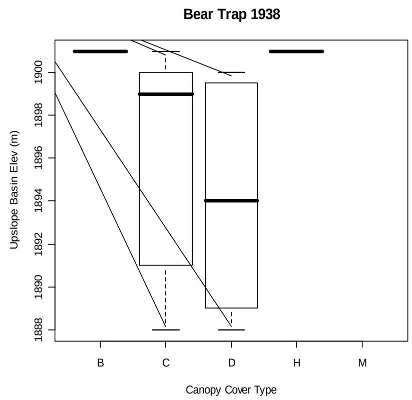
Bear Trap 1938
Upslope Basin Elev (m)
1888 1890 1892 1894 1896 1898 1900
B C D H M
Canopy Cover Type

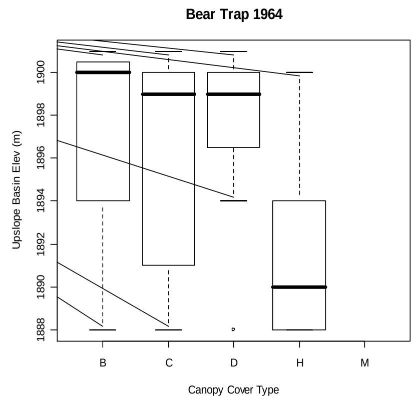
Bear Trap 1964
Upslope Basin Elev (m)
1888 1890 1892 1894 1896 1898 1900
B C D H M
Canopy Cover Type

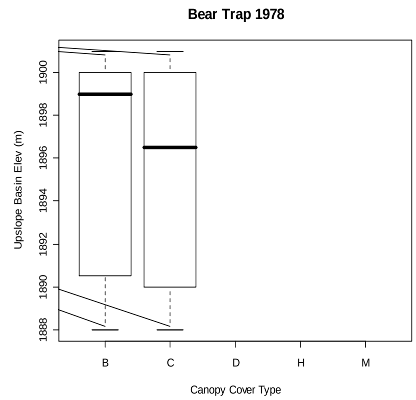
Bear Trap 1978
Upslope Basin Elev (m)
1888 1890 1892 1894 1896 1898 1900
B C D H M
Canopy Cover Type

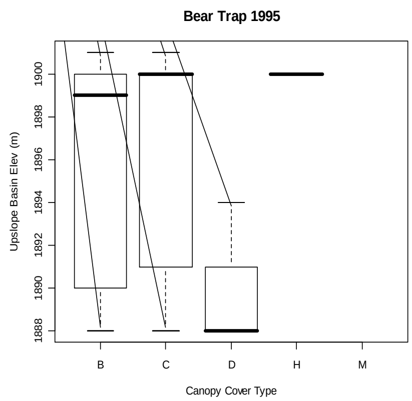
Bear Trap 1995
Upslope Basin Elev (m)
1888 1890 1892 1894 1896 1898 1900
B C D H M
Canopy Cover Type

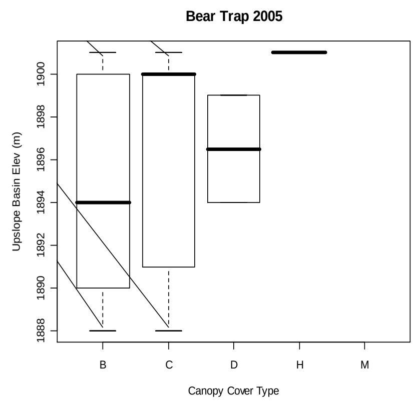
Bear Trap 2005
Upslope Basin Elev (m)
1888 1890 1892 1894 1896 1898 1900
B C D H M
Canopy Cover Type


Bear Trap 1938
Med. Upslope Basin Elev (m)
1870 1875 1880 1885
B C D H M
Canopy Cover Type

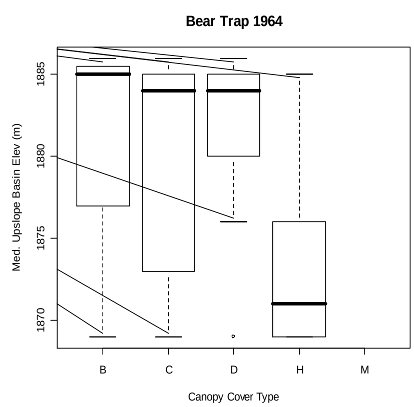
Bear Trap 1964
Med. Upslope Basin Elev (m)
1870 1875 1880 1885
B C D H M
Canopy Cover Type


Bear Trap 1978
Med. Upslope Basin Elev (m)
1870 1875 1880 1885
B C D H M
Canopy Cover Type

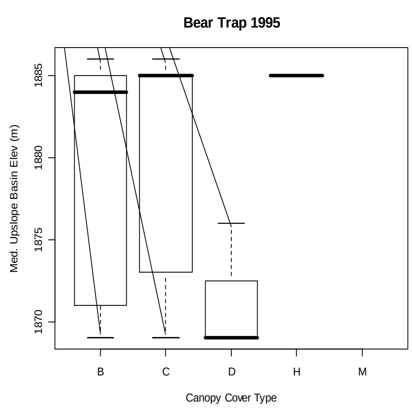
Bear Trap 1995
Med. Upslope Basin Elev (m)
1870 1875 1880 1885
B C D H M
Canopy Cover Type

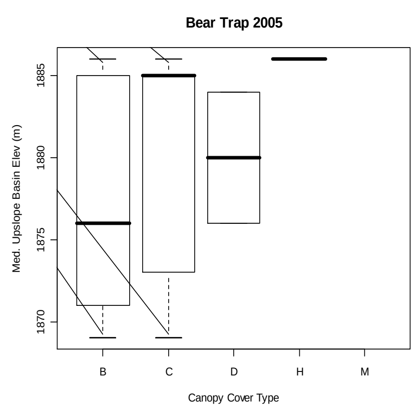
Bear Trap 2005
Med. Upslope Basin Elev (m)
1870 1875 1880 1885
B C D H M
Canopy Cover Type

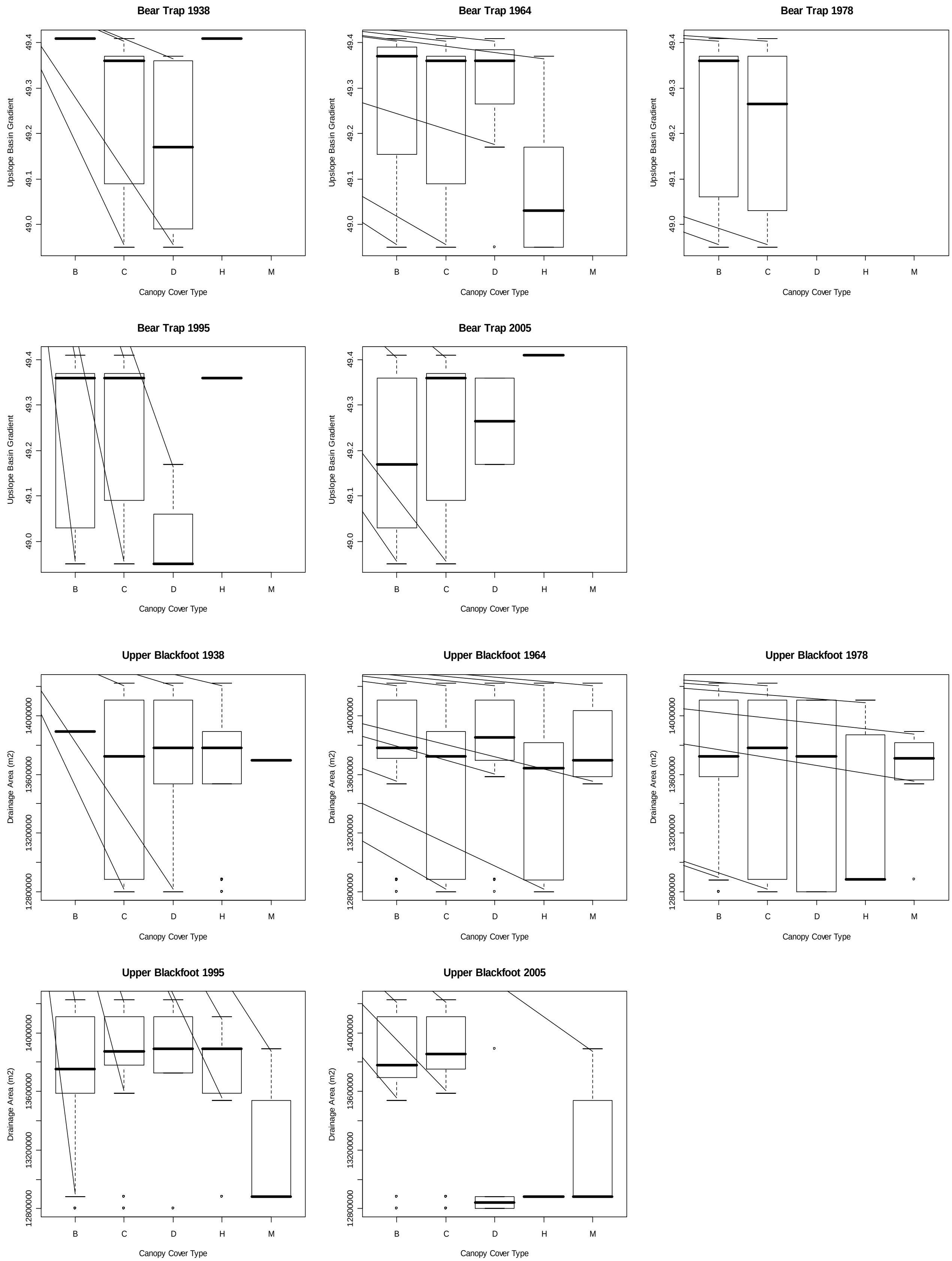
Bear Trap 1938
Bear Trap 1964
Bear Trap 1978
Bear Trap 1995
Bear Trap 2005
Upslope Basin Gradient
49.0
49.1
49.2
49.3
49.4
Upper Blackfoot 1938
Upper Blackfoot 1964
Upper Blackfoot 1978
Upper Blackfoot 1995
Upper Blackfoot 2005
Drainage Area (m2)
12800000
13200000
13600000
14000000
B C D H M
Canopy Cover Type

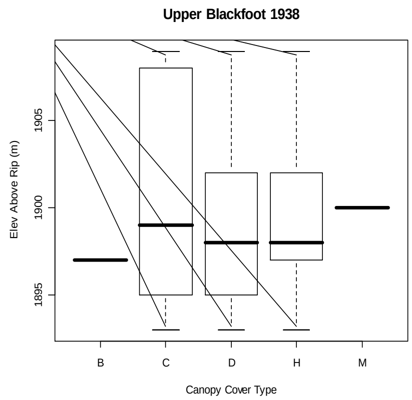
Upper Blackfoot 1938
Elev Above Rip (m)
1895
1900
1905
B
C
D
H
M
Canopy Cover Type

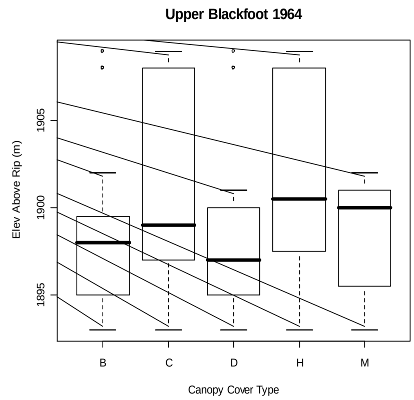
Upper Blackfoot 1964
Elev Above Rip (m)
1895
1900
1905
B
C
D
H
M
Canopy Cover Type

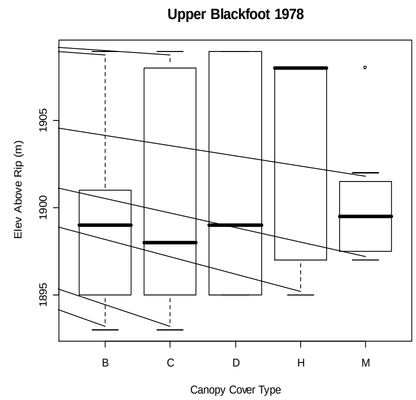
Upper Blackfoot 1978
Elev Above Rip (m)
1895
1900
1905
B
C
D
H
M
Canopy Cover Type

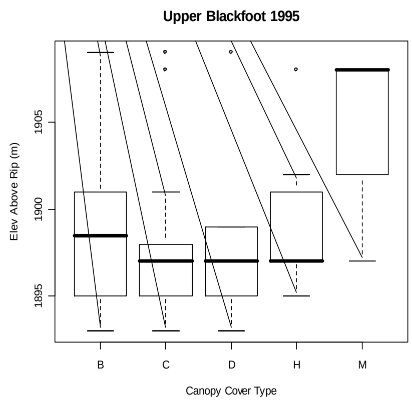
Upper Blackfoot 1995
Elev Above Rip (m)
1895
1900
1905
B
C
D
H
M
Canopy Cover Type

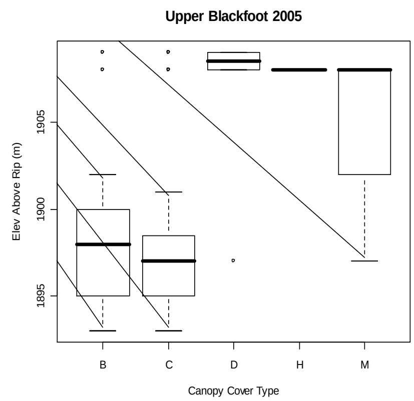
Upper Blackfoot 2005
Elev Above Rip (m)
1895
1900
1905
B
C
D
H
M
Canopy Cover Type

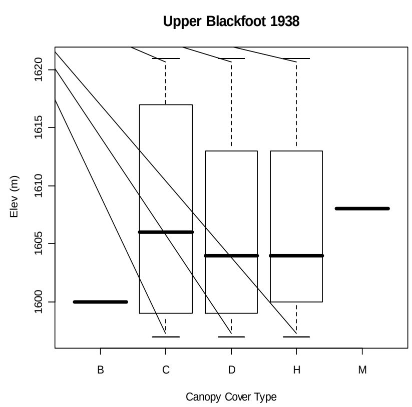
Upper Blackfoot 1938
Elev (m)
1600
1605
1610
1615
1620
B
C
D
H
M
Canopy Cover Type

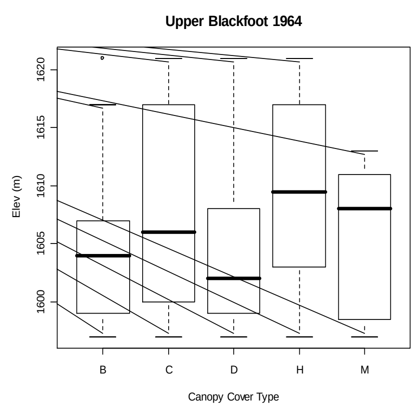
Upper Blackfoot 1964
Elev (m)
1600
1605
1610
1615
1620
B
C
D
H
M
Canopy Cover Type

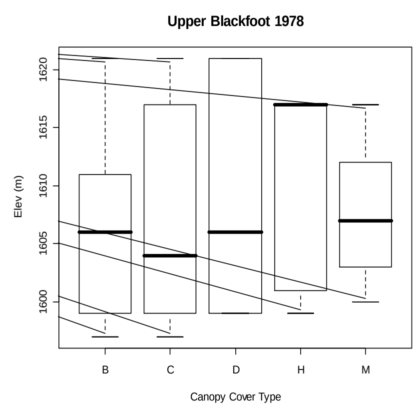
Upper Blackfoot 1978
Elev (m)
1600
1605
1610
1615
1620
B
C
D
H
M
Canopy Cover Type

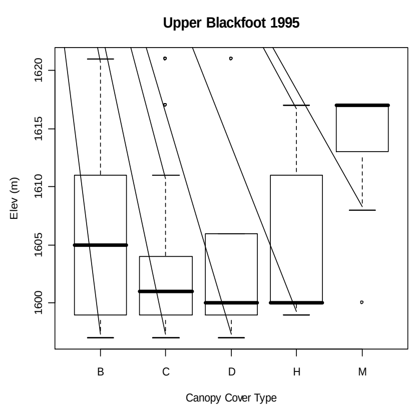
Upper Blackfoot 1995
Elev (m)
1600
1605
1610
1615
1620
B
C
D
H
M
Canopy Cover Type

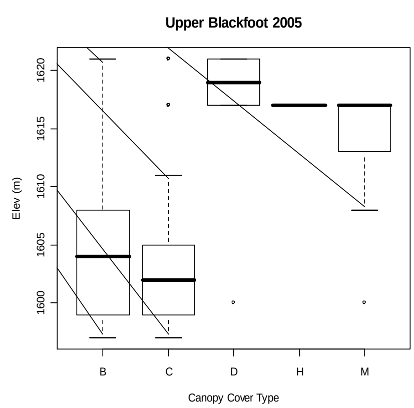
Upper Blackfoot 2005
Elev (m)
1600
1605
1610
1615
1620
B
C
D
H
M
Canopy Cover Type

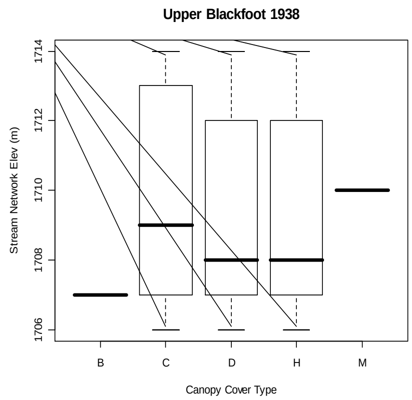
Upper Blackfoot 1938
Stream Network Elev (m)
1706 1708 1710 1712 1714
B C D H M
Canopy Cover Type

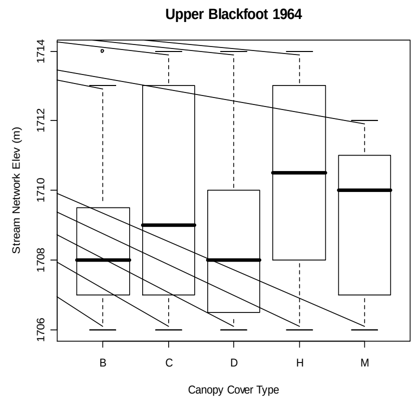
Upper Blackfoot 1964
Stream Network Elev (m)
1706 1708 1710 1712 1714
B C D H M
Canopy Cover Type

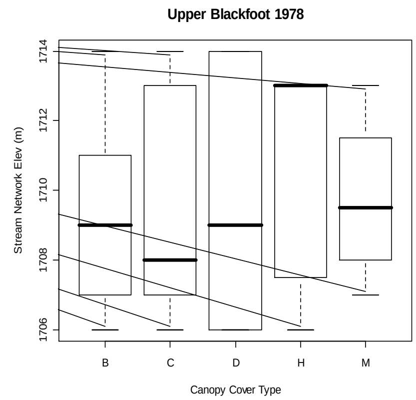
Upper Blackfoot 1978
Stream Network Elev (m)
1706 1708 1710 1712 1714
B C D H M
Canopy Cover Type

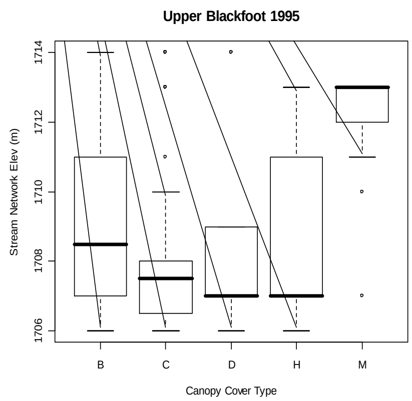
Upper Blackfoot 1995
Stream Network Elev (m)
1706 1708 1710 1712 1714
B C D H M
Canopy Cover Type

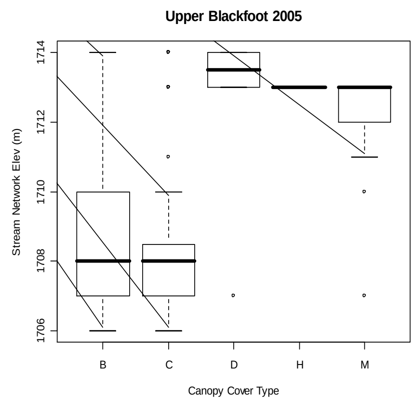
Upper Blackfoot 2005
Stream Network Elev (m)
1706 1708 1710 1712 1714
B C D H M
Canopy Cover Type

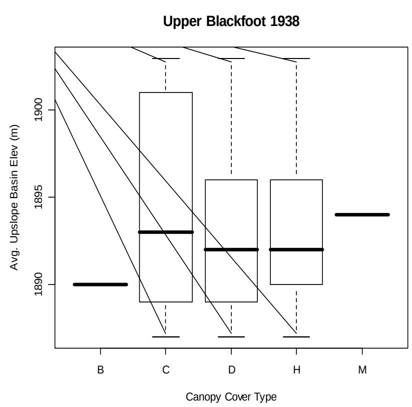
Upper Blackfoot 1938
Avg. Upslope Basin Elev (m)
1890 1895 1900
B C D H M
Canopy Cover Type

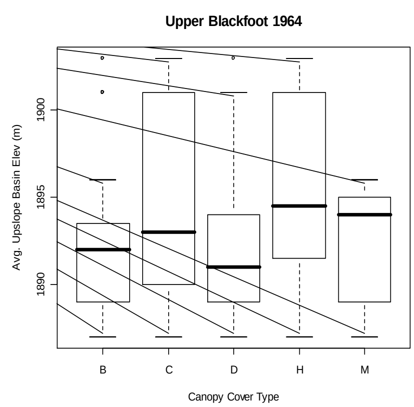
Upper Blackfoot 1964
Avg. Upslope Basin Elev (m)
1890 1895 1900
B C D H M
Canopy Cover Type

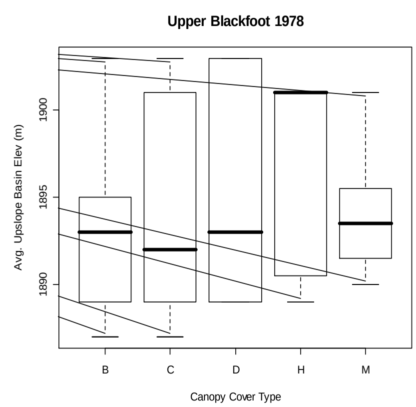
Upper Blackfoot 1978
Avg. Upslope Basin Elev (m)
1890 1895 1900
B C D H M
Canopy Cover Type

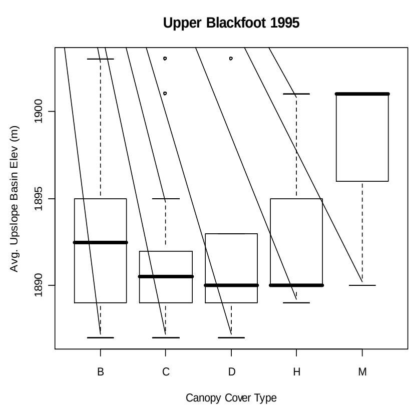
Upper Blackfoot 1995
Avg. Upslope Basin Elev (m)
1890 1895 1900
B C D H M
Canopy Cover Type

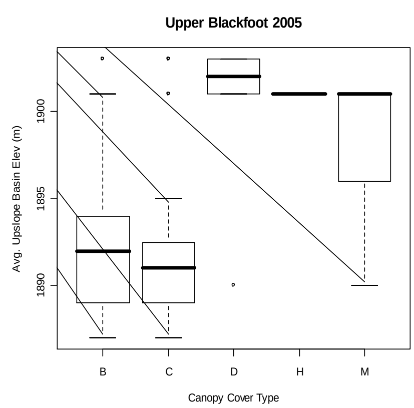
Upper Blackfoot 2005
Avg. Upslope Basin Elev (m)
1890 1895 1900
B C D H M
Canopy Cover Type

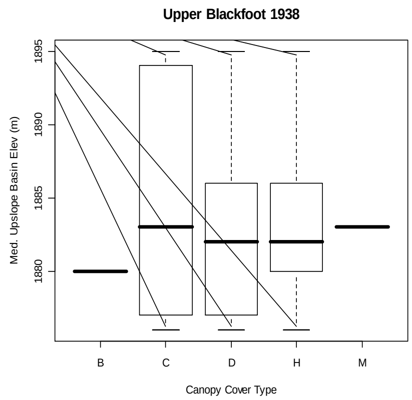
Upper Blackfoot 1938
Med. Upslope Basin Elev (m)
1880 1885 1890 1895
B C D H M
Canopy Cover Type

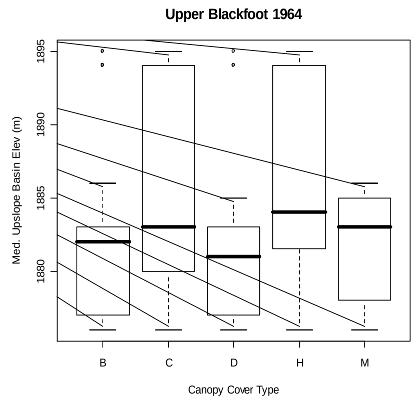
Upper Blackfoot 1964
Med. Upslope Basin Elev (m)
1880 1885 1890 1895
B C D H M
Canopy Cover Type

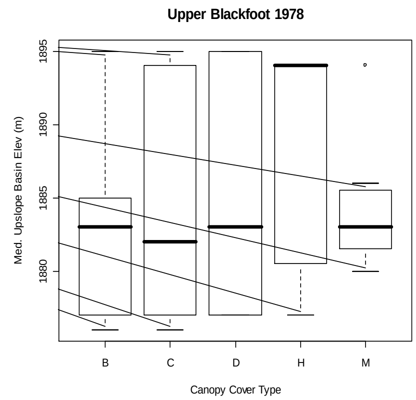
Upper Blackfoot 1978
Med. Upslope Basin Elev (m)
1880 1885 1890 1895
B C D H M
Canopy Cover Type

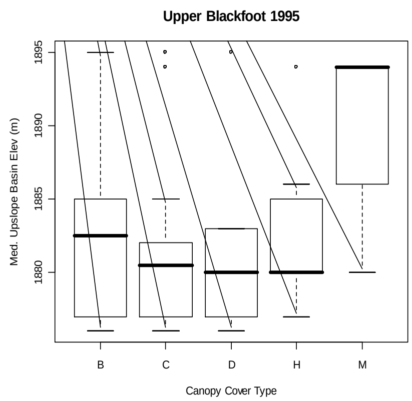
Upper Blackfoot 1995
Med. Upslope Basin Elev (m)
1880 1885 1890 1895
B C D H M
Canopy Cover Type

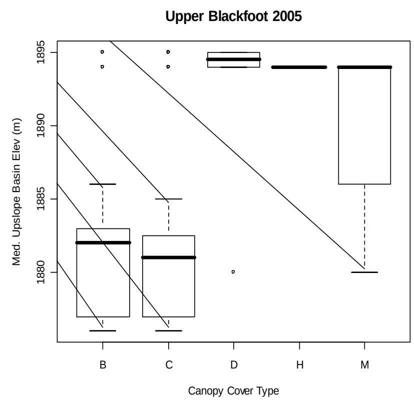
Upper Blackfoot 2005
Med. Upslope Basin Elev (m)
1880 1885 1890 1895
B C D H M
Canopy Cover Type

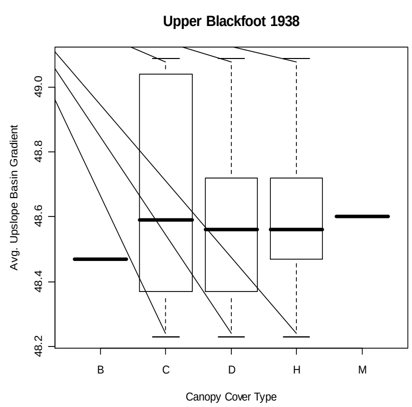
Upper Blackfoot 1938
Avg. Upslope Basin Gradient
48.2 48.4 48.6 48.8 49.0
B C D H M
Canopy Cover Type

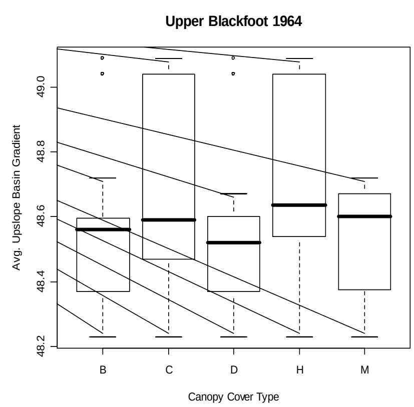
Upper Blackfoot 1964
Avg. Upslope Basin Gradient
48.2 48.4 48.6 48.8 49.0
B C D H M
Canopy Cover Type

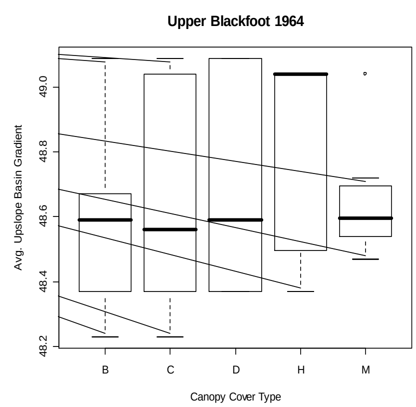
Upper Blackfoot 1964
Avg. Upslope Basin Gradient
48.2 48.4 48.6 48.8 49.0
B C D H M
Canopy Cover Type

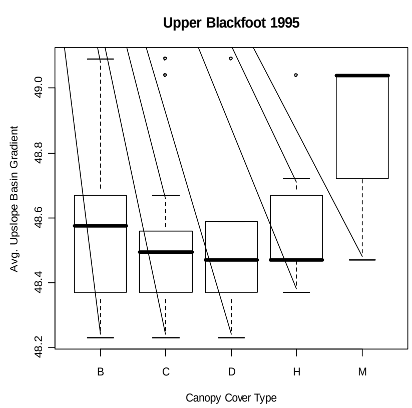
Upper Blackfoot 1995
Avg. Upslope Basin Gradient
48.2 48.4 48.6 48.8 49.0
B C D H M
Canopy Cover Type

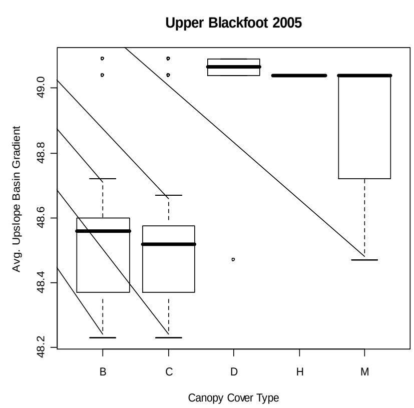
Upper Blackfoot 2005
Avg. Upslope Basin Gradient
48.2 48.4 48.6 48.8 49.0
B C D H M
Canopy Cover Type

Appendix E

Watershed Variable Selection

Distribution Among Canopy Type Change per Photo Period

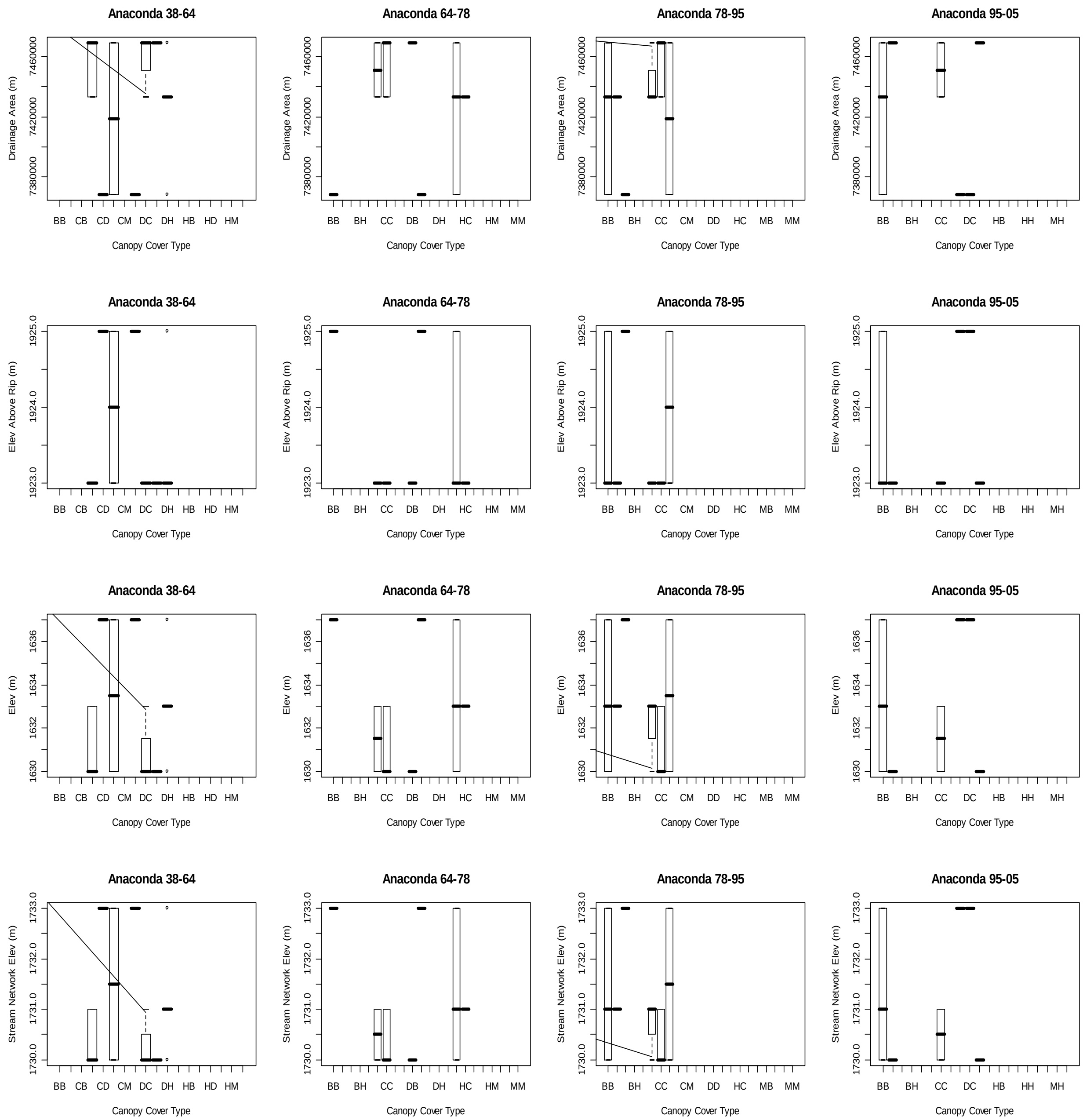

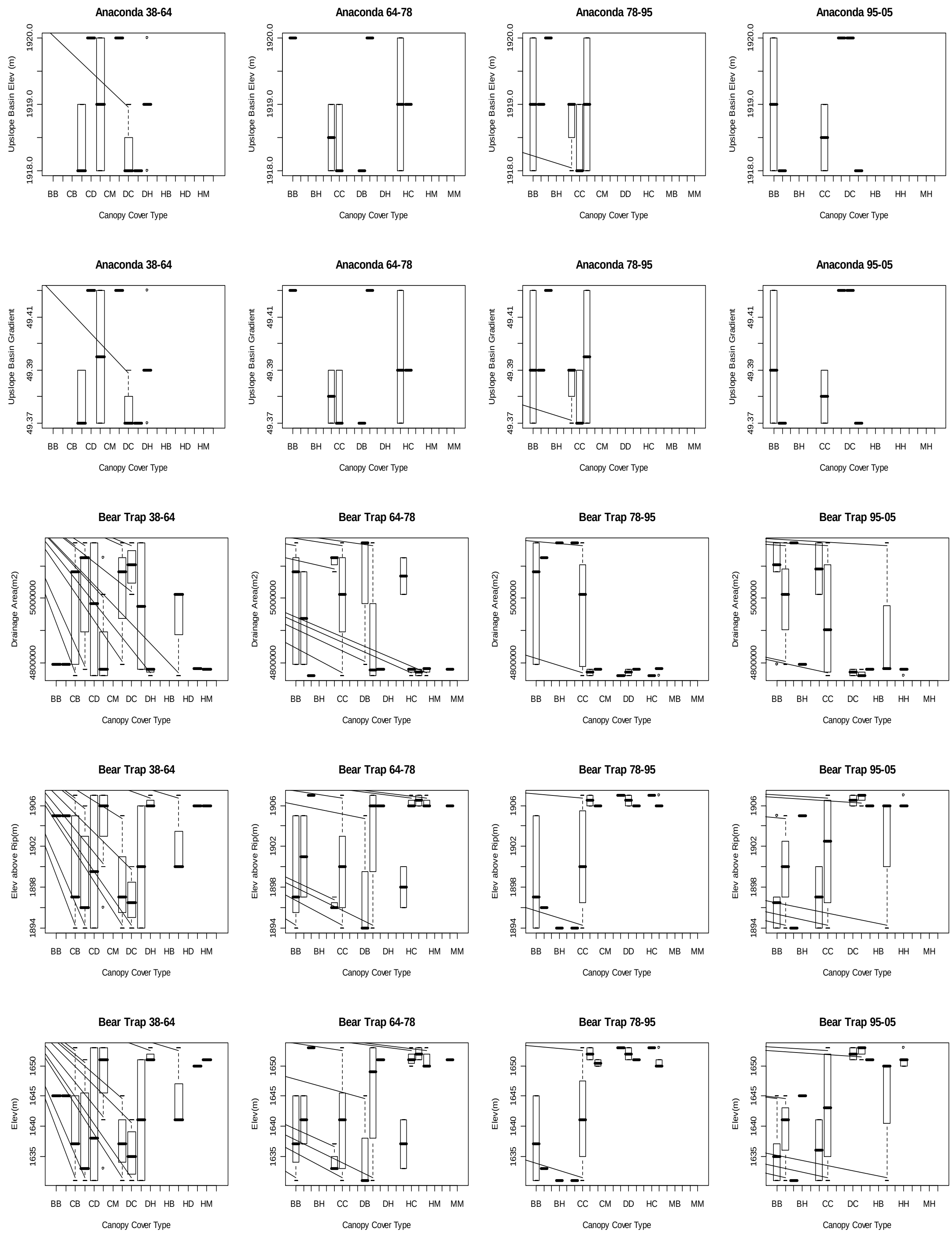
Anaconda 38-64
Upslope Basin Elev (m)
1918.0 1919.0 1920.0
BB CB CD CM DC DH HB HD HM
Canopy Cover Type
Anaconda 64-78
Upslope Basin Elev (m)
1918.0 1919.0 1920.0
BB BH CC DB DH HC HM MM
Canopy Cover Type
Anaconda 78-95
Upslope Basin Elev (m)
1918.0 1919.0 1920.0
BB BH CC CM DD HC MB MM
Canopy Cover Type
Anaconda 95-05
Upslope Basin Elev (m)
1918.0 1919.0 1920.0
BB BH CC DC HB HH MH
Canopy Cover Type
Anaconda 38-64
Upslope Basin Gradient
49.37 49.39 49.41
BB CB CD CM DC DH HB HD HM
Canopy Cover Type
Anaconda 64-78
Upslope Basin Gradient
49.37 49.39 49.41
BB BH CC DB DH HC HM MM
Canopy Cover Type
Anaconda 78-95
Upslope Basin Gradient
49.37 49.39 49.41
BB BH CC CM DD HC MB MM
Canopy Cover Type
Anaconda 95-05
Upslope Basin Gradient
49.37 49.39 49.41
BB BH CC DC HB HH MH
Canopy Cover Type
Bear Trap 38-64
Drainage Area(m2)
4800000 5000000
BB CB CD CM DC DH HB HD HM
Canopy Cover Type
Bear Trap 64-78
Drainage Area(m2)
4800000 5000000
BB BH CC DB DH HC HM MM
Canopy Cover Type
Bear Trap 78-95
Drainage Area(m2)
4800000 5000000
BB BH CC CM DD HC MB MM
Canopy Cover Type
Bear Trap 95-05
Drainage Area(m2)
4800000 5000000
BB BH CC DC HB HH MH
Canopy Cover Type
Bear Trap 38-64
Elev above Rip(m)
1894 1898 1902 1906
BB CB CD CM DC DH HB HD HM
Canopy Cover Type
Bear Trap 64-78
Elev above Rip(m)
1894 1898 1902 1906
BB BH CC DB DH HC HM MM
Canopy Cover Type
Bear Trap 78-95
Elev above Rip(m)
1894 1898 1902 1906
BB BH CC CM DD HC MB MM
Canopy Cover Type
Bear Trap 95-05
Elev above Rip(m)
1894 1898 1902 1906
BB BH CC DC HB HH MH
Canopy Cover Type
Bear Trap 38-64
Elev(m)
1635 1640 1645 1650
BB CB CD CM DC DH HB HD HM
Canopy Cover Type
Bear Trap 64-78
Elev(m)
1635 1640 1645 1650
BB BH CC DB DH HC HM MM
Canopy Cover Type
Bear Trap 78-95
Elev(m)
1635 1640 1645 1650
BB BH CC CM DD HC MB MM
Canopy Cover Type
Bear Trap 95-05
Elev(m)
1635 1640 1645 1650
BB BH CC DC HB HH MH
Canopy Cover Type

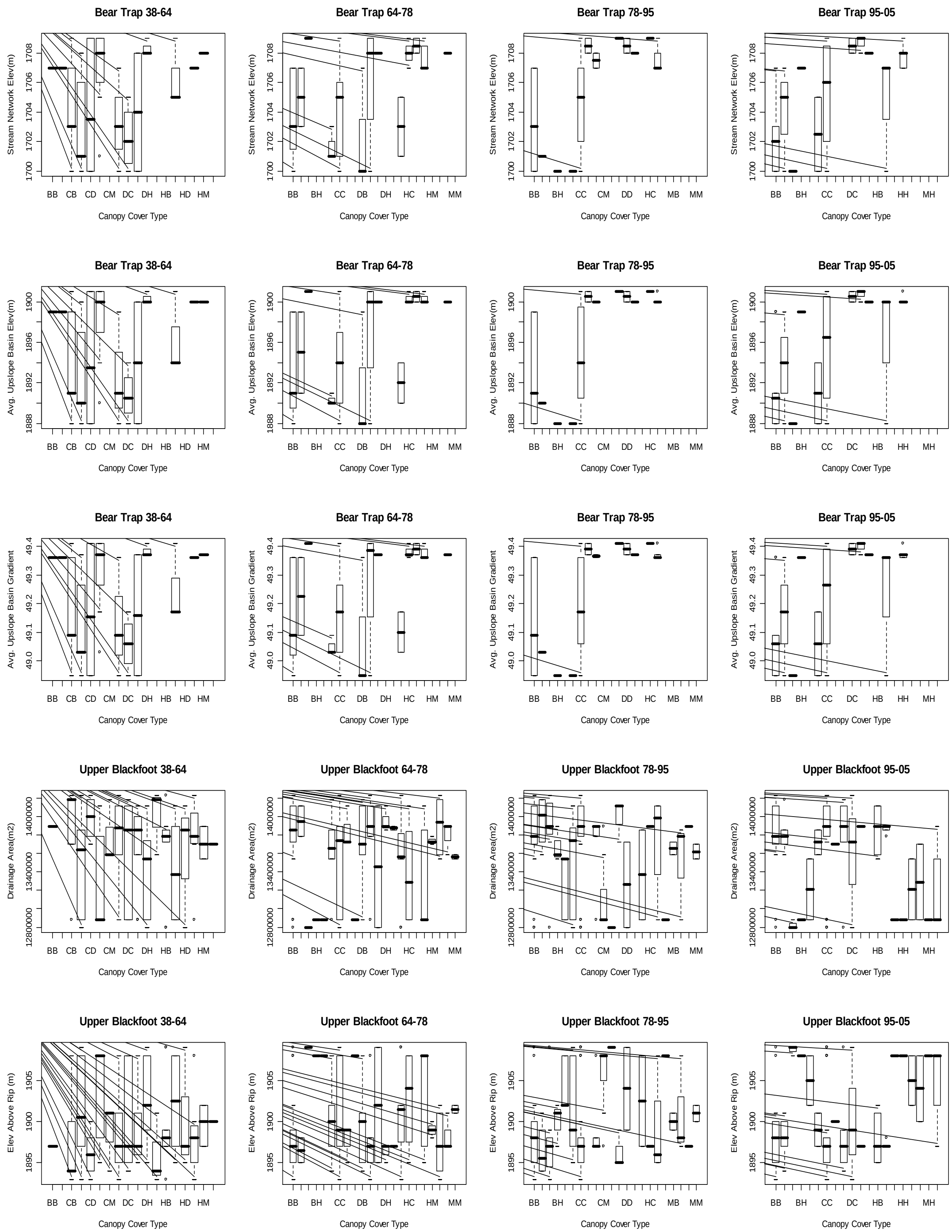
Bear Trap 38-64
Stream Network Elev(m)
1700 1702 1704 1706 1708
BB CB CD CM DC DH HB HD HM
Canopy Cover Type
Bear Trap 64-78
Stream Network Elev(m)
1700 1702 1704 1706 1708
BB BH CC DB DH HC HM MM
Canopy Cover Type
Bear Trap 78-95
Stream Network Elev(m)
1700 1702 1704 1706 1708
BB BH CC CM DD HC MB MM
Canopy Cover Type
Bear Trap 95-05
Stream Network Elev(m)
1700 1702 1704 1706 1708
BB BH CC DC HB HH MH
Canopy Cover Type
Bear Trap 38-64
Avg. Upslope Basin Elev(m)
1888 1892 1896 1900
BB CB CD CM DC DH HB HD HM
Canopy Cover Type
Bear Trap 64-78
Avg. Upslope Basin Elev(m)
1888 1892 1896 1900
BB BH CC DB DH HC HM MM
Canopy Cover Type
Bear Trap 78-95
Avg. Upslope Basin Elev(m)
1888 1892 1896 1900
BB BH CC CM DD HC MB MM
Canopy Cover Type
Bear Trap 95-05
Avg. Upslope Basin Elev(m)
1888 1892 1896 1900
BB BH CC DC HB HH MH
Canopy Cover Type
Bear Trap 38-64
Avg. Upslope Basin Gradient
49.0 49.1 49.2 49.3 49.4
BB CB CD CM DC DH HB HD HM
Canopy Cover Type
Bear Trap 64-78
Avg. Upslope Basin Gradient
49.0 49.1 49.2 49.3 49.4
BB BH CC DB DH HC HM MM
Canopy Cover Type
Bear Trap 78-95
Avg. Upslope Basin Gradient
49.0 49.1 49.2 49.3 49.4
BB BH CC CM DD HC MB MM
Canopy Cover Type
Bear Trap 95-05
Avg. Upslope Basin Gradient
49.0 49.1 49.2 49.3 49.4
BB BH CC DC HB HH MH
Canopy Cover Type
Upper Blackfoot 38-64
Drainage Area(m2)
12800000 13400000 14000000
BB CB CD CM DC DH HB HD HM
Canopy Cover Type
Upper Blackfoot 64-78
Drainage Area(m2)
12800000 13400000 14000000
BB BH CC DB DH HC HM MM
Canopy Cover Type
Upper Blackfoot 78-95
Drainage Area(m2)
12800000 13400000 14000000
BB BH CC CM DD HC MB MM
Canopy Cover Type
Upper Blackfoot 95-05
Drainage Area(m2)
12800000 13400000 14000000
BB BH CC DC HB HH MH
Canopy Cover Type
Upper Blackfoot 38-64
Elev Above Rip (m)
1895 1900 1905
BB CB CD CM DC DH HB HD HM
Canopy Cover Type
Upper Blackfoot 64-78
Elev Above Rip (m)
1895 1900 1905
BB BH CC DB DH HC HM MM
Canopy Cover Type
Upper Blackfoot 78-95
Elev Above Rip (m)
1895 1900 1905
BB BH CC CM DD HC MB MM
Canopy Cover Type
Upper Blackfoot 95-05
Elev Above Rip (m)
1895 1900 1905
BB BH CC DC HB HH MH
Canopy Cover Type

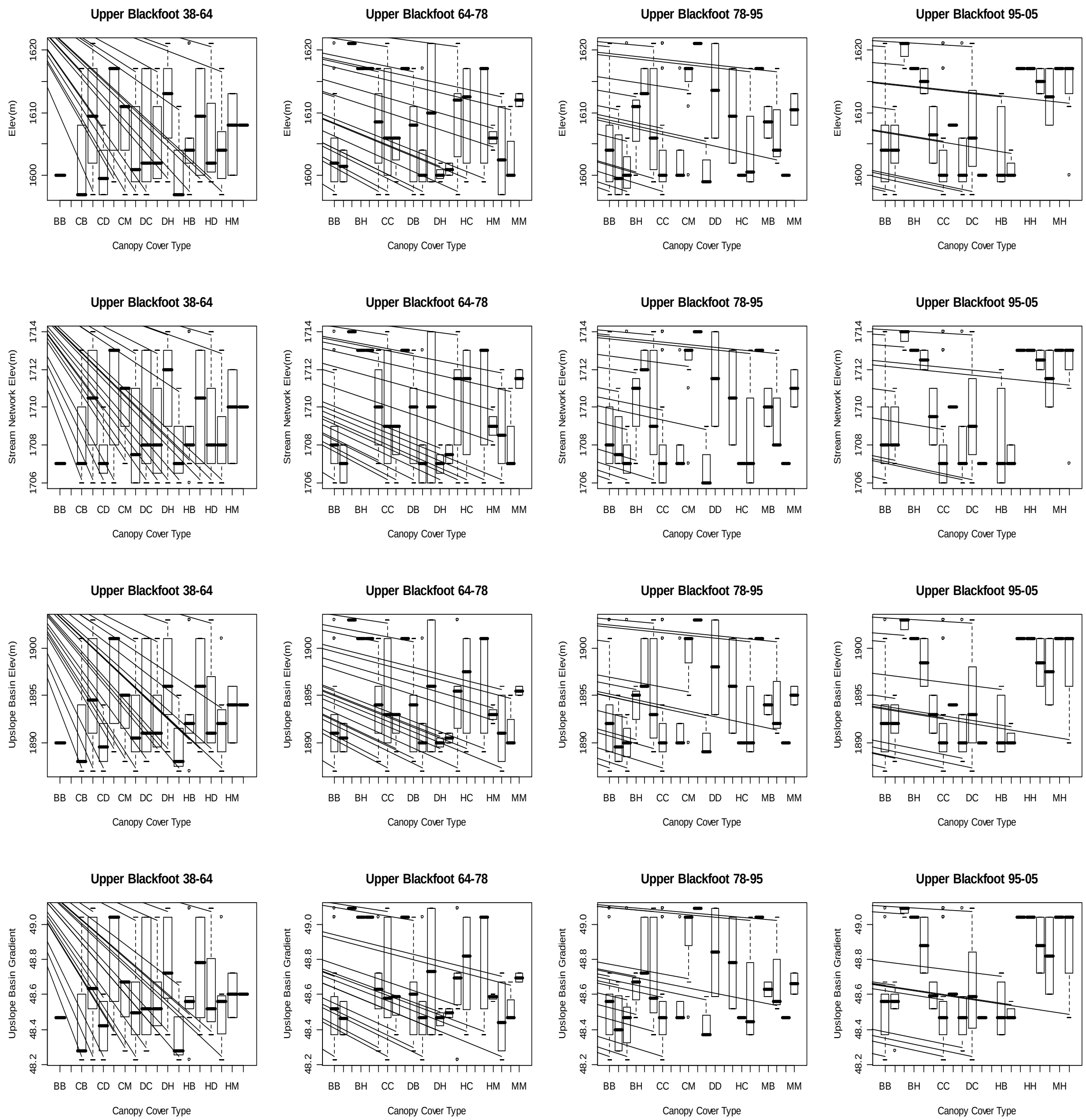
Upper Blackfoot 38-64
Upper Blackfoot 64-78
Upper Blackfoot 78-95
Upper Blackfoot 95-05
Elev(m)
1600
1610
1620
Stream Network Elev(m)
1706
1708
1710
1712
1714
Upslope Basin Elev(m)
1890
1895
1900
Upslope Basin Gradient
48.2
48.4
48.6
48.8
49.0
BB CB CD CM DC DH HB HD HM
BB BH CC DB DH HC HM MM
BB BH CC CM DD HC MB MM
BB BH CC DC HB HH MH
Canopy Cover Type

8. REFERENCES

Austin, M. P., A. O. Nicholls, et al. (1990). "Measurement of the realized qualitative niche: Environmental niches of five Eucalyptus species." Ecological Monographs **60**(2): 161-177.

Baker, W. L. and G. M. Walford (1995). "Multiple stable states and models of riparian vegetation succession on the Animas River, Colorado." Annals of Association of American Geographers **85**(2): 320-338.

Baker, V.R., (1987). "Paleoflood hydrology and extraordinary flood events." Journal of Hydrology **96** (1-4), 79-99.

Bednarek, A.T. (2001). "Undamming rivers: a review of the ecological impacts of dam removal. Environmental Management **27** (6): 803-814.

Bendix, J. (1994). "Scale, direction, and pattern in riparian vegetation-environment relationships." Annals of the Association of American Geographers **84**(4): 652-665.

Beven, K. J. and M. J. Kirkby (1979). "A physically-based variable contributing area model of basin hydrology." Hydrological Sciences Bulletin **24**: 43-69.

Burroughs, B.A. (2007). "Rehabilitation Potential of Dam Removal: Temporal Perspective from Michigan's Past Dam Removals." PhD thesis, Department of Fisheries and Wildlife, Michigan State University, East Landing, p. 27.

Catalano, M.J., Bozek, M.A., Pellet, T.D. (2001). "Fish-habitat relations and initial response of the Baraboo River fish community to dam removal." Bulletin of the North American Benthological Society **18**, 177.

Cenderelli, D.A., Wohl, E.E. (2001). "Peak discharge estimates of glacial-lake outburst floods and 'normal' climatic floods in the Mount Everest region, Nepal." Geomorphology **40** (1-2): 57-90.

Chow, V.T. (1959). Open-Channel Hydraulics. McGraw-Hill, New York.

Confluence Consulting Inc., DTM Consulting Inc., et al. (2004). Blackfoot Headwaters Planning Area water quality and habitat restoration plan and TMDL for sediment**:** 114.

Costa, J.E., Schuster, R.L. (1988). "The formation and failure of natural dams." Geologic Society of America Bulletin 100, 1054-1068.

Department of Urban and Regional Planning (DURP). (1996). The Removal of Small Dams: an Institutional Analysis of the Wisconsin Experience. University of Wisconsin-Madison/Extension, Madison, p. 52.

Doyle, M., Stanley, E., Harbor, J. (2003a). "Channel adjustments following two dam removals in Wisconsin." Water Resources Research **39** (1), 1101, doi:10.1029/2002WR001714.

Dukes, J., Mooney, H. (1999). "Does global change increase the success of biological invaders?" Trends in Ecology and Evolution **14** (4), 135-139.

Envirocon Inc. (1993). Flood plain analysis for the Blackfoot River and tributaries in the vicinity of the Upper Blackfoot Mining Complex.

ESRI. (2005). "ArcGIS 9.1 Documentation." 2005.

Grant,G. (2004). "The geomorphic response of rivers to dam removal" In: Assessing and Re-naturalizing Stream Impacted By Dams and Dam Removal, Missoula, Montana.

Greco, S. E. and R. E. Plant (2003). "Temporal mapping of riparian landscape change on the Sacramento River, mile 196–218, California, USA." Landscape Research **28**(4): 405-426.

Hansen, P. L., R. D. Pfister, et al. (1995). Classification and management of Montana's riparian and wetland sites. Missoula, Montana, Montana Forest and Conservation Experiment Station.

Hawkins, C. P., K. L. Bartz, et al. (1997). "Vulnerability of riparian vegetation to catastrophic flooding: Implications for riparian restoration." Restoration Ecology **5**(4s): 75-84.

Hughes, M. L., P. F. McDowell, et al. (2006). "Accuracy assessment of georectified aerial photographs: Implications for measuring lateral channel movement in a GIS." Geomorphology **74**(1-4): 1-16.

Hydrometrics Inc. and Blackfoot Challenge (2003). Water Quality restoration plan for metals in the Blackfoot headwaters TMDL planning area**:** 98.

Iversen, T.M., Kronvang, B., Madsen, B.L., Markmann, P., Nielsen, M.D. (1993). "Reestablishment of Danish streams: restoration and maintenance measures." Aquatic Conservation: Marine and Freshwater Ecosystems **3** (2): 73-92.

Jarrett, R.D. (1990). "Paleohydrologic techniques used to define the spatial occurrence of floods." Geomorphology **3** (2), 181-195.

Jarrett, R.D., Tomlinson, E.M. (2000). "Regional interdisciplinary paleoflood approach to assess extreme flood potential." Water Resources Research **36** (10): 2957-2984.

Junk, W.J., Bayley, P.B., Sparks, R.E. (1986). "The flood pulse concept in river-floodplain systems." In: Proceedings of the International Large River Symposium (LARS), Ontario, Canada. Canadian Special Publication of Fisheries and Aquatic Sciences.

Johnson, W. C. (1994). "Woodland expansion in the Platte River, Nebraska: patterns and causes." Ecological Monographs **64** (1): 45-84.

Kirkby, M. J. (1993). Network hydrology and geomorphology. Channel Network Hydrology. K. J. Beven and M. J. Kirkby. Chichester, John Wiley & Sons, Ltd.**:** 1-11.

Mahoney, J.M., Rood, S.B. (1998). "Streamflow requirements for cottonwood seedling recruitment - an interactive model." Wetlands **18** (4): 634-645.

McDonnell, J. J., B. L. McGlynn, et al. (1998). The role of near-stream riparian zones in the hydrology of steep upland catchments. HeadWater '98 Conference, Merano, Itally, IAHS.

McGlynn, B. L. and J. J. McDonnell (2003). "Quantifying the relative contributions of riparian and hillslope zones to catchment runoff." Water Resources Research **39** (11): 1310, doi:10.1029/2003WR002091.

McGlynn, B. L. and J. Seibert (2003). "Distributed assessment of contributing area and riparian buffering along stream networks." Water Resources Research **39** (4).

McGlynn, B. L., M. N. Gooseff, et al. (2003). Stream-upland connections and the effects of discharge on transient storage processes. Eos Trans. AGU, American Geophysical Union Fall Meeting, San Fransisco.

McGlynn, B. L., J. J. McDonnell, et al. (2003). "On the relationships between catchment scale and streamwater mean residence time." Hydrological Processes **17**: 175-181.

Middleton, B. (1999). Wetland Restoration: Flood Pulsing and Disturbance Dynamics. John Wiley and Sons, New York.

Moore, J. N. (1992). Mine effluent effects on non-point source contaminants in the Blackfoot River, Montana. Missoula, MT, Prepared for Lewis and Clark City-County Health Department. University of Montana, Geology Department.

Nilsson, C. (1987). "Distribution of stream-edge vegetation along gradient of current velocity." Journal of Ecology **75** (2): 513-522.

Nilsson, C. and M. Svedmark (2002). "Basic principles and ecological consequences of changing water regimes: Riparian plant communities." Environmental Management **30** (4): 468-480.

Parrett, C., and D.R. Johnson (2004). Methods for Estimating Flood Frequency in Montana Based on Data Through Water Year 1998. U.S. Department of the Interior, U.S. Geological Survey, Reston, VA. Denver, CO: U.S. Geological Survey Information Services Distributor.

Piegay, H., Bornette, G., Citterio, A., Herouin, E., Moulin, B., Satiotis, C., 2000. "Channel instability as a control on silting dynamics and vegetation patterns within perifluvial aquatic zones." Hydrological Processes **14** (16-17): 3011-3029.

Pizzuto, J. (2002). "Effects of dam removal on river form and process." Bioscience **52** (8): 683-691.

Pizzuto, J.E. (1994). "Channel adjustments to changing discharges, Powder River, Montana." Geologic Society of America Bulletin **106** (11): 1494-1501.

Pruess, J., Wohl, E.E., Jarrett, R.D. (1998). "Methodology and implications of maximum paleodischarge estimates for mountain channels, Upper Animas River basin, Colorado, USA." Arctic and Alpine Research 30 (1): 40-50.

Schmitz, D., M. Blank, et al. (2009). "Using historic aerial photography and paleohydrologic techniques to assess long-term ecological response to two Montana dam removals." Journal of Environmental Management **90**: S237-S248.

Schumm, S.A., Harvey, M.D., Watson, C.C. (1984). "Incised Channels: Morphology, Dynamics, and Control." Water Resources Publishing, Highlands Ranch, CO.

Shafroth, P.B., Freidman, J.M., Auble, G.T., Scott, M.L., Braatne, J.H. (2003). "Potential responses of riparian vegetation to dam removal." Bioscience **52** (8): 703-712.

Spence, L. E. (1977). Effects of the June 1975 Mike Horse mine tailings dam failure on water quality and aquatic resources of the Upper Blackfoot River. Helena, Montana, Montana Fish, Wildlife and Parks**:** 92.

Stanley, E.H., Catalano, M.J., Mercado-Silva, N., Orr, C.H. (2007). "Effects of dam removal on brook trout in a Wisconsin stream." River Research and Applications **23** (7): 792-798.

Stanley, E.H., Doyle, M.W. (2002). "A geomorphic perspective on nutrient retention following dam removal." Bioscience **52** (8): 693-701.

Steiger, J., Gurnell, A.M. (2003). "Spatial hydrogeomorphological influences on sediment and nutrient deposition in riparian zones: observations from the Garonne River, France." Geomorphology **49** (1-2): 1-23.

Stromberg, J.C., Tiller, R., Richter, B.D. (1996). "Effects of groundwater decline on riparian vegetation of semiarid regions: the San Pedro, Arizona." Ecological Applications **6** (1): 113-131.

Tarboton, D. G. (1997). "A new method for the determination of flow directions and upslope areas in grid digital elevation models." Water Resources Research **33**(2): 309-319.

Tarboton, D. G. (2008). "Terrain Analysis Using Digital Elevation Models (TauDEM)." 2009, from TauDEM (Terrain Analysis Using Digital Elevation Models) is a set of tools for the analysis of terrain using digital elevation models. It incorporates programs and digital elevation model (DEM) analysis functions developed over several years of research. TauDEM is currently packaged as an extendable component (toolbar plugin) to both ESRI ArcGIS (8.x and 9.0) and MapWindow Open Source GIS.

Treiste, D.J., Jarrett, R.D. (1987). "Roughness coefficients of large floods. In: Irrigation Systems for the 21st Century." Society of Civil Engineering, Portland, OR.

US Forest Service (2006). Draft concept alternatives technical memorandum for the Mike Horse Dam and Tailings Impoundment at the Upper Blackfoot Mining Complex. Helena, USFS.

US Forest Service (2007). Engineering evaluation/cost analysis for the Mike Horse Dam and impounded tailing, lower Mike Horse Creek, Beartrap Creek and the Upper Blackfoot River floodplain removal areas Upper Blackfoot Mining Complex. Helena, USFS.

Vaghti, M. G. (2003). Riparian vegetation classification in relation to environmental gradients, Sacramento River, California. Ecology. Davis, CA, University of California, Davis**:** 139.

Vandeberg, G. S. (2005). The distribution of trace elements in floodplain soils and sediments of the Upper Blackfoot River, Montana. Geography. Manhattan, Kansas, Kansas State University. **PhD:** 335.

Walford, G. M., G. Jones, et al. (2001). Riparian and wetland plant community types of the Shoshone National Forest. Ogden, Rocky Mountain Research Station**:** 122.

Wallace, J. S. and H. R. Oliver (1990). Vegetation and hydroclimate. Process Studies in Hillslope Hydrology. M. G. Anderson and T. P. Burt. Chichester, John Wiley & Sons, Ltd**:** 9-41.

Winter, B.D. (1990). A Brief Review of Dam Removal Efforts in Washington, Oregon, Idaho and California. US Department of Commerce, National Oceanic and Atmospheric Administration, National Marine Fisheries Service, Seattle, p. 13.

Wohl, E.E. (1995). "Estimating flood magnitude in ungauged mountain channels, Nepal." Mountain Research and Development **15** (1): 69-76.

Youngblood, A. P., W. G. Padgett, et al. (1985). Riparian community type classification of eastern Idaho-western Wyoming, USDA**:** 1-78.